MOLECULAR IMAGING OF AMYLOID-BETA PROTEINS BY POLYMERIC

NANOPARTICLES IN MOUSE MODELS OF ALZHEIMER'S DISEASE

APPROVED BY SUPERVISORY COMMITTEE

Frederick J. Bonte, M.D., Mentor

Peter Antich, Ph.D., Chairman

Padmakar Kulkarni, Ph.D.

Michael Bennett, M.D.

DEDICATION

I would like to thank the members of my Graduate Committee, my family, friends, and all

who have prayed with me through this journey called LIFE.

MOLECULAR IMAGING OF AMYLOID-BETA PROTEINS BY POLYMERIC

NANOPARTICLES IN MOUSE MODELS OF ALZHEIMER'S DISEASE

by

CELESTE ANITA RONEY, B.S.

DISSERTATION

Presented to the Faculty of the Graduate School of Biomedical Sciences

The University of Texas Southwestern Medical Center at Dallas

In Partial Fulfillment of the Requirements

For the Degree of

DOCTOR OF PHILOSOPHY

The University of Texas Southwestern Medical Center at Dallas

Dallas, Texas

December, 2006

MOLECULAR IMAGING OF AMYLOID BETA PROTEINS BY POLYMERIC NANOPARTICLES IN MOUSE MODELS OF ALZHEIMER'S DISEASE

Celeste Roney, Ph.D

The University of Texas Southwestern Medical Center at Dallas, 2006

Frederick J. Bonte, M.D.

Alzheimer's disease (AD) is the most common cause of dementia among the elderly, affecting 5% of Americans over age 65, and 20% over age 80. An excess of senile plaques (β-amyloid protein) and neurofibrillary tangles (tau protein), ventricular enlargement, and cortical atrophy characterizes it. *In vivo* detection of aggregated amyloid peptides (Aβ) (amyloid plaques) presents targets for development of biological markers for Alzheimer's disease. In an effort to fabricate *in vivo* probes, polymeric n-butyl-2-cyanoacrylate (BCA) nanoparticles (NPs) were encapsulated with the radiolabelled amyloid affinity drug ^{125}I-clioquinol (CQ, 5-chloro-7-iodo-8-hydroxyquinoline). [125]ICQ was initially selected as a tracer of interest because it chelates transition metals, crosses the BBB, and is easily labeled with radioisotopes of iodine (e.g. [123]I, [124]I and ^{125}I). Preliminary studies with [125]ICQ showed that the agent crossed the BBB, but was

retained too briefly for effective chelation. Therefore, a drug carrier is required to improve the extravascular retention of ^{125}ICQ; BCA NPs were chosen as the drug carrier. ^{125}I-CQ discriminately binds to AD post-mortem brain tissue homogenates, versus control. Additionally, ^{125}I-CQ-BCA NPs labeled the Aβ plaques from AD human post-mortem frontal cortical sections, on paraffin-fixed slides. Storage phosphor imaging verified preferential uptake by the AD brain sections, compared to cortical control sections. Additionally, ^{125}I-CQ-BCA NPs cross the BBB in the wild type mouse, with an enhanced brain uptake (%ID/g, significant with 95% confidence (p=0.05)), compared to ^{125}I-CQ. Moreover, brain uptake of ^{125}I-CQ-BCA NPs is enhanced in AD transgenic mice (APP/PS1 and APP/PS1/Tau), and in mice intracranially injected with the aggregated Aβ peptide, versus age-matched wild type controls. Thus, ^{125}I-CQ-BCA NPs act as targeted drug carriers with an affinity for amyloid plaques. Brain entry of ^{125}I-CQ-BCA NPs was rapid, demonstrating ideal *in vivo* imaging characteristics for small animal modalities; good clearance of free and non-specifically bound radioisotope affords high-quality temporal resolution, and good signal-to-noise. ^{125}I-CQ-BCA NPs have specificity for the Aβ plaques in post-mortem tissue, and have a rapid brain entry. This combination makes radioiodinated CQ-BCA NPs a promising candidate as an *in vivo* SPECT (^{123}I), or PET (^{124}I) amyloid imaging agent.

TABLE OF CONTENTS

Hypothesis: Nanoparticles can be polymerized with the appropriate size, surface and surfactant characteristics, which render them suitable for passage across the blood brain barrier

Hypothesis: Amyloid affinity drugs can be successfully radiolabelled, encapsulated within nanoparticles, and fully characterized *in vitro* and by *in vivo* biodistribution

Hypotheses: (1) Nanoparticles will act as drug carriers by delivering the desirable drugs to the brain tissue; (2) Amyloid proteins can be imaged using novel nanoparticles as drug carriers

Hypothesis: Amyloid plaques can be imaged with drugs that bind to them

PRIOR PUBLICATIONS

Original Reports:

1. Aminabhavi TM, Kulkarni AR, Kulkarni PV, Bonte FJ, Antich P, Bennett M, Arora V, **Roney C**., Polymers in Drug Delivery: Radioactive Iodine ^{125}I loaded Polymeric Nanoparticles for Biodistribution Study in Mice, Polymer News, 28 (3), 83, 2002.
2. Bonte FJ, Harris TS, **Roney CA,** Hynan LS. Differential Diagnosis Between Alzheimer's and Frontotemporal Disease by the Posterior Cingulate Sign, J Nucl Med 2004, 45(5):771-774
3. **Roney CA**, Kulkarni PV, Arora V, Bennett M, Antich P, Bonte F, Wu A, Mallikarjana NN, Manohar S, Sai Ram M, Aminabhavi T, Polymeric Nanoparticulate Drug Delivery Through the Blood Brain Barrier, Polymer News, 2005, Vol 30: 311-321.
4. **Roney CA,** Kulkarni PV, Arora V, Antich P, Bonte F, Wu A, Mallikarjuana NN, Manohar S, Liang H-F, Kulkarni AR, Sung H-S, Sai Ram, M, Aminabhavi T, Targeted Nanoparticles for Drug Delivery Through the Blood Brain Barrier, J Control Release. 2005 Nov 28;108(2-3):193-214
5. Chapman SB, Bonte FJ, Wong SBC, Zientz JN, Hynan LS, Harris TS, Gorman AR, **Roney CA**, Lipton AM. Convergence of Connected Language and SPECT in Variants of Frontotemporal Lobar Degeneration. Alzheimer Dis Assoc Disord. 2005 October/November/December; 19(4):202-213.
6. Kulkarni PV, Arora V, **Roney CA,** White C, Bennett M, Antich PP, Bonte FJ, Radiolabeled probes for imaging Alzheimer's plaques, Nucl. Instr. And Meth. In Phys. Res. B 241 (2005), 676-680

Abstracts:

1. Chiu S, Zientz J, Chapman SB, Harris TS, **Roney CA**, Bonte FJ. Correspondence Between SPECT and Cognitive-Linguistic Testing in Frontotemporal Dementia Variants, J Nucl Med 2003, 44:229P
2. Bonte FJ, Harris TS, Haley RW, **Roney CA**, Weiner MF. Role of Blood Flow Reduction in the Posterior Cingulate Cortex in Diagnosis of Alzheimer's Disease: Statistical Parametric Mapping of SPECT Scan Data, J Nucl Med 2003, 44:228P

3. **Roney CA**, Kulkarni PV, Arora V, Bennett M, Antich PP, Bonte FJ, Molecular Imaging of Amyloid-Beta Proteins in a Mouse Model of Alzheimer's Disease, Molecular Imaging, 4(3), July 2005, 302

LIST OF FIGURES

LIST OF TABLES

LIST OF APPENDICES

ABBREVIATIONS

AD	Alzheimer's Disease
APP	Amyloid Precursor Protein
Aβ	Amyloid Beta
BBB	Blood Brain Barrier
BCA	Butyl Cyanoacrylate
CMC	Critical Micellar Concentration
CNS	Central Nervous System
CQ	Clioquinol
CR	Congo Red
DLS	Dynamic Light Scattering
EC	Endothelial Cell
ECM	Extracellular Matrix
GPC	Gel Permeation Chromatography
NFT	Neurofibrillary Tangles
HRP	Horseradish Peroxidase
JAM	Junctional Adhesion Molecule
MRI	Magnetic Resonance Imaging
MS	Multiple Sclerosis
NMR	Nuclear Magnetic Resonance
NP	Nanoparticle
O/W	Oil-in-Water
OCA	Octyl Cyanoacrylate
PACA	Polyalkylcyanoacrylate
PBCA	Polybutylcyanoacrylate
PCS	Photon Correlation Spectroscopy
PET	Positron Emission Tomography
RES	Reticuloendothelial System
SEM	Scanning Electron Microscopy
SPECT	Single Photon Emission Computed Tomography
ThS	Thioflavin-S
ThT	Thioflavin-T
TJ	Tight Junction
TEM	Transmission Electron Microscopy
PI	Post Injection

PREFACE

Alzheimer's disease (AD), a neurodegenerative disorder of the elderly, is the most prevalent form of dementia. The cognitive decline associated with AD drastically affects the social and behavioral skills of people living with this disease. Notwithstanding the social impact, however, AD also imparts great financial burdens on patients, families, and the community as a whole. The National Institutes of Health (NIH) estimates that 4.5 million Americans are affected by AD, at an annual cost of $ 100 billion per year. Yet even more ominous is the estimate that by 2050, 13.2 million older Americans are expected to have AD if the current trends hold and no preventive treatment becomes available. These statistics are exacerbated by the fact that there are no current biological markers of AD, and therefore, definitive diagnoses are made upon autopsy and new treatment efficacy cannot be extended overtime. Furthermore, therapeutic strategies to probe the central nervous system (CNS) are limited by the restrictive tight junctions at the endothelial cells of the blood brain barrier (BBB). To overcome the impositions of the BBB, polymeric biocompatible drug carriers have been applied to the central nervous system for many applications such as cancers, but the field of drug carrier technology is not well developed in AD research [1]. However, polymeric nanoparticles are promising candidates in the investigation of AD because nanoparticles are capable of: opening tight

junctions [2] crossing the BBB [3], high drug loading capacities, and targeting the

mutant proteins of Alzheimer's [4, 5].

1. ALZHEIMER'S DISEASE

Alzheimer's disease is a heterogeneous neurodegenerative disorder that results from the deposition of the amyloid beta protein (senile plaques) into the extracellular synaptic spaces of the neocortex, particularly in the temporal and parietal lobes. Neurodegeneration affects cognition (learning, abstraction, judgment, etc.) and memory, with behavioral consequences such as aggression, depression, hallucination, delusion, anger and agitation [6]. Pathologically, ventricular enlargement and atrophy of the hippocampus (the limbic structure responsible for memory) and the cerebral cortex can be seen. At present, definitive diagnoses of AD are made upon histological verification of the Aß plaques (or the hyperphyosphorlyated tau protein) at autopsy. The tau protein is normally seen in microtubule formation, but causes neurofibrillary tangles (NFT) in AD.

1.1. PHENOTYPE of AD

Neuritic plaques contain deposits of extracellular amyloid beta protein, axons and injured dendrites. Such plaques usually occur as masses of amyloid fibrils with structural abnormalities, including dilated organelles, with large

lysosomes and abundant mitochondria [7]. Deposits of peptides with 40- and 42-amino acids co-localize within the fibrils, however, $A\beta_{40}$ is produced in greater mass by cells, and $A\beta_{42}$ is more hydrophobic and prone to aggregate.

Diffuse plaques are amorphous but lack the compacted fibrillar appearance of the neuritic plaques. Instead, diffuse plaques show a fine granular pattern upon immunohistochemical staining; they are formed of $A\beta_{42}$ and detected in many of the same regions (cerebral and limbic cortices) as the neuritic plaques. Nevertheless, diffuse plaques are also found in brain regions where neuritic plaques are not detected (e.g. cerebellum, striatum, thalamus), and so represent immature forms, or precursors, of the mature lesion. In fact, evidence supports diffuse plaques as precursors (transgenic mice expressing human APP have been shown to develop diffuse plaques before developing fibrils [7]). Neurofibrillary tangles are also found in neurons that occupy brain regions common to AD. The microtubule protein tau is common to the tangles, which are large abnormal bundles of nonmembrane-bound paired helical filaments. Within the neurons, the tangles are primarily found in the perinuclear cytoplasm, and are insoluble to dephosphorylating detergents and solvents [7]. Although it is not yet clear how many different kinases are capable of phosphorylating tau, it is understood that the hyperphosphorylated protein dissociates from the microtubule and aggregates into the insoluble paired helical filaments of AD [8].

Tau is also found in less common neurodegenerative diseases, in forms biochemically similar to the tau of AD. However, these diseases (e.g. Kuf's disease, progressive supranuclear palsy) do not show neuritic plaques, suggesting that plaques and tangles can occur independently of each other. Respectively, "plaques only" can be found in healthy human brains, and AD brains have been shown with an abundance of Aβ deposits and few neurofibrillary tangles [9]. Finally, in the Lewy body variant of AD, the α-synuclein protein, which is found near the nuclear cytoplasm of cortical pyramidal neurons, aggregates into infrequent tangles in the neocortex, and is associated with the Aβ plaques [10].

1.2. Aβ PROTEIN is DERIVED FROM the AMYLOID PRECURSOR PROTEIN

The amyloid precursor protein (APP) is a transmembrane polypeptide that undergoes proteolytic cleavage and posttranslational modifications (e.g. sulfation, phosphorylation, sugar modifications) to yield Aβ [11, 12]. The APP itself is from a larger family of proteins called the amyloid precursor-like proteins (APLPs) [13]. APP exists as three major isoforms of 695, 751, and 770 amino acids, and between 110-140 kDa [14]. Typically, neurons express the 695 amino acid isoform, although the 751- and 770- residue isoforms are found in neuronal and nonneuronal cells [15].

APP, which is proteolytically cleaved along the course of its secretory pathway, releases derivatives into the extracellular space. It has been shown that these cleavages occur by α-, β- and γ- secretase enzymes [16-18]. Alpha cleavages release large soluble fragments into the extracellular space and result in the membrane retention of an 83-residue carboxy-terminal fragment [19], while beta cleavages release smaller derivatives into the extracellular space and retain a 99- residue carboxy-terminal fragment in the membrane [20]. The C-terminal 99- and 83- residue fragments are subject to γ-secretase cleavage; the result of the processing, post-translational modifications and secretory trafficking of APP is the generation of $A\beta_{40}$ and $A\beta_{42}$ [21], which can be chemically detected in extracellular fluids, such as plasma [22] and cerebrospinal fluid (CSF) [23]. Finally, APP is located in the axon terminus of the neuron and travels against the grade, and up the axon to the cell body and the cellular surface to deposit the protein into the extracellular space [24]. In addition to neurons, and other cells such as microglia, astrocytes, and endothelial or smooth muscle cells also express Aβ, and may collectively contribute to the extracellular deposition of the peptide [18].

1.3. GENOMICS and PROTEOMICS of AD

Autosomal dominance inheritance of AD, called familial AD, is linked to 4 major genes including the gene that codes for APP, located on chromosome 21;

the other three genes are located on chromosomes 1, 14 and 19. Sporadic, or nonfamilial AD, is phenotypically and clinically similar to familial AD. The two sometimes only differ by the age of onset, whereby autosomal dominant AD is associated with early onset. The missense mutations in APP are located in close proximity to the α-, β- and γ-secretase cleavage sites, and are responsible for the enzymatic activity that accounts for the abnormal proteolytic processing of APP. No other mutations have been found in this polypeptide that cause AD [7], however, trisomy 21 can lead to the overexpression of structurally normal APP, and result in early onset (adult middle years) AD neuropathology in affected individuals (e.g. Down's syndrome patients). In such cases, chromosome 21 is duplicated, and overproduction of $A\beta_{40}$ and $A\beta_{42}$ peptides can occur from birth. In fact, individuals have been documented with pathology as early as age 12 [25].

Although APP produces the Aβ peptide, many families do not link to chromosome 21. In fact, missense mutations of APP are a very rare cause of AD. However, *the* most common cause of autosomal dominant AD is missense mutations of the presenilin proteins on chromosomes 12 and 1. Mutations on presenilin 1, located on chromosome 14 cause clinical onset of AD in the 40s and 50s [26]. Other cases of early onset AD are linked to presenilin 2, which is located on chromosome 1 [27]. There are at least 75 mutations identified in presenilin 1, and 3 identified in presenilin 2 that are responsible for early onset AD [28].

Genetic mutations in the APP gene and in the presenilins are responsible for early onset AD. However, it has been shown that a risk factor for late onset AD is a defect in the €4 allele of apolipoprotein E (ApoE), which has been linked to chromosome 19q [29]. Late onset AD, which is associated with genetic mutations in the €4 allele of ApoE, usually occurs in subjects who are in their 60s and 70s. The €4 allele is more pathogenic than the €2 or the €3 allele of ApoE; it is more prevalent in the general population of AD patients, and individuals who inherit one or both copies of €4 have an increased likelihood of developing AD. On the other hand, patients with the €2 allele have shown conferred protections against AD [30]. Finally, whereas genetic mutations on chromosome 19 predispose to AD via the €2, 3-, and 4- alleles of ApoE, predisposing loci on chromosomes 10q and 12- have also been found to be responsible for forms of late-onset AD [31-33].

1.3.1. APP Mutations

Nine missense mutations in APP work by different pathways to increase Aβ production. For example, at a site 2 amino acids upstream of β-secretase cleavage, there exists a double mutation (called the "Swedish" APP mutation) that induces the β-secretase to cleave APP and increase the production of $A\beta_{40}$ and $A\beta_{42}$. However, at the γ-secretase cleavage site, 5 mutations occurring carboxy-terminal to the site of cleavage, only yield the production of $A\beta_{42}$; the final 2

mutations are internal to the Aβ species and function by enhancing Aβ aggregation [7].

1.3.2. Presenilin Mutations

Humans with the presenilin mutation have at least a two-fold increase in the plasma concentration of Aβ$_{42}$ [25]; these findings have been substantiated in cell culture [34] and in transgenic mice [35]. Holcomb *et al* experimented with a duel transgenic strain for APP and PS1 [36]. The AD phenotype (diffuse and neuritic plaques) was greatly accelerated in the offspring of the mutant mice [36]. Furthermore, the presenilin mutation was responsible for the elevation of Aβ$_{42}$. Quantitative image analyses have also verified Aβ$_{42}$ plaques in the brains of patients with presenilin mutations [37]. In these studies, the plaques were identified using Aβ$_{40}$- and Aβ$_{42}$- specific antibodies, and it was shown that the presenilin mutation led to an average 2-fold increase of Aβ$_{42}$, compared to plaques containing Aβ$_{42}$ in sporadic AD cases [37].

1.3.3. APOE E4 Mutations

Inheritance of the E4 allele significantly increases plaque burden compared to patients who lack ApoE4 [38], and immunohistochemistry is a common technique widely used to correlate increased levels of apolipoprotein in

Aβ deposits of AD brain tissue [39]. In fact, Polvikoski *et al* have demonstrated that nondemented elderly subjects without AD show increased levels of ApoE and Aβ$_{42}$ deposition, thereby suggesting that Aβ$_{42}$ elevation caused by enhanced ApoE production, may be "presymptom" of AD development [40]. Gearing *et al* suggests that ApoE4 decreases the brain clearance of Aβ$_{40}$ [38]; it has also been surmised that the E4 lipoprotein increases Aβ fibrillogenesis, compared to ApoE3 [41]. Moreover, when mice transgenic for human APP were crossed with mice with deleted endogenous mouse ApoE genes, the resultant offspring had decreased plaque burdens compared to the transgenic parent APP line [42]. Finally, Holtzman *et al* demonstrated decreased Aβ deposits in mice with deleted ApoE but expressing human ApoE3 or E4 plus mutant human APP, as compared with mice expressing no ApoE [43].

1.4. THE NEUROTOXIC CASCADE of ALZHEIMER'S DISEASE

The neuropathological process that occurs in Down's syndrome is highly indistinguishable from that which occurs in AD. Down's syndrome patients develop diffuse plaques (Aβ$_{42}$) by the first or second decade. Consequently, Down's patients develop full AD pathology and die by their third or fourth decade. Since brain tissue can only be studied at the end of a patient's life, and the histopathology is similar in the two disease processes, Down's benefits AD research because the pathology can be studied in middle aged adults [25].

Furthermore, Gouras *et al* have shown that the neurons of young Down's patients display intraneuronal immunoreactivity for diffuse plaques, which preclude their older, fibrillized counterparts ($A\beta_{40}$) [44]. Additionally, $A\beta_{42}$ aggregates [45] and more readily fibrilizes [46] than $A\beta_{40}$. Thus, $A\beta_{42}$ is the species found in the diffuse plaques, which are the lesions that are morphologically detected before the accumulation of $A\beta_{40}$. Hsia *et al* have shown structural changes of synapes in transgenic mice expressing human APP even before the accumulation of the diffuse plaques. This suggests that cellular dysfunction may occur before plaque formation [47]. However, some plaque formation may be necessary to initiate cell injury. And, since $A\beta_{40}$ is highly resistant to fibrillogenesis, it must first co-deposit onto pre-existing $A\beta_{42}$ [7]. Of course, in the case of Down's syndrome, the interval between $A\beta_{40}$ deposition, and $A\beta_{42}$ co-deposition, can be as lengthy as years to a decade or more [25].

Activated microglia, which are derived from monocytes and macrophages, are one example of brain inflammatory changes in the limbic and association cortices of AD patients. Microglia display cell surface markers within or surrounding mature amyloid plaques, and are early respondents to the extracellular accumulations, or "foreign" deposits and fibrils of $A\beta$; they also function to initiate the cascade of neurotoxic events leading to dementia [48]. Rogers *et al* have shown that $A\beta$ binds to the C1q component of the C1 complement protein *in vitro*, an initial component of the classical complement

pathway of inflammation [49], and Griffin *et al* implicates interleukin-1β as a pro-inflammatory cytokine in the AD cascade of neuronal injury [50]. Likewise, other mediators, including astrocytes, associate with fibrillar-rich plaques [51].

In addition to the inflammatory response, Aβ accumulation causes perioxidative injury to the cell by generating excessive free radicals. Specifically, the production of peroxides results in the oxidation of macromolecules such as lipids and proteins [52, 53]. Metabolically, Aβ accumulation has been shown to alter ionic homeostasis. For example, at maximal calcium uptake, aggregated Aβ in culture has deleterious effects on neurons. Excess calcium may also activate kinases that play a role in the hyperphosphorylation of the paired helical filaments of the tau protein [54]. The cumulative effects of oxidative, inflammatory and ionic impairment to the AD neocortex occur gradually from preclinical to clinical progression, and include neuritic dystrophy, synaptic loss, neuronal perikarya shrinkage and selective neuronal loss. Eventually, neuromodulator systems and cholinergic enzymes degenerate as synaptic transmission is compromised [7]. Meanwhile, patients show increasing difficulty with storing and retrieving information.

1.5. THE METALLOCHEMISTRY of AD

As previously stated [45], $A\beta_{42}$ more readily self-aggregates than does $A\beta_{40}$. Bush [55] implies that there is inhibition of $A\beta_{42}$ self-aggregation in the

absence of metal ion binding. Aβ has a high affinity for metal-ion binding in neutral buffers. This affinity is lost if the peptide is removed from the metal ions, in buffer solution, by high-affinity chelators. In fact, Atwood *et al* have shown that the high metal binding affinity (attomolar for Cu^{2+}) of $A\beta_{42}$ enhances self-aggregation (in the presence of Cu^{2+}, Zn^{2+}, Fe^{3+}), which is eradicated by high affinity chelators [56]. To trace the metallochemistry of AD, it was shown that APP was selective for Zn^{2+} and Cu^{2+} [57, 58]; such selectivity moderates the physicochemical behavior of the peptide. Additionally, Zn^{2+} rapidly precipitates Aβ at physiological pH [59], while Cu^{2+} and Fe^{3+} account for the precipitation of the peptide under mild acidosis [56], a state which resembles conditions in the AD brain (e.g. pH 6.6 [60]). Cu^{2+} induction of Aβ precipitation leads to the greatest fibrillization of the peptide [61]; likewise, $A\beta_{42}$ has a higher affinity for Cu^{2+} than does $A\beta_{40}$. In addition, the Aβ metal ion binding sites are bridged by the amino acid histidine [62]. This amino acid, which is missing in rodents, is essential to the disease process because of the histidine bridge. Vaughn and Peters [63] suggest the histidine substitution as a possible explanation of why rats and mice don't inherently develop Alzheimer's.

Zn^{2+} precipitates Aβ at low-affinity (5μM) binding, and this concentration mediates the peptide's resistance to tryptic (similar to α-secretase) cleavage [64]. Thus, Zn^{2+} both precipitates the peptide and protects it from secretase activity. Zn^{2+} also contains high affinity binding sites for Aβ. At physiological pH, Aβ

binds Zn^{2+} and Cu^{2+} at equimolar concentrations, however under acidosis Zn^{2+} is completely displaced by Cu^{2+} [62]. As well, Cu^{2+} possesses high- and low-affinity binding sites for Aβ, and in addition, the high-affinity binding site on Cu^{2+} is greater for $Aβ_{42}$ than for $Aβ_{40}$. This may be due to greater precipitation of $Aβ_{42}$ by Cu^{2+} [62], or because the longer peptide may enhance coordination of oligimerization and cooperativity between Cu^{2+} [65]. Huang *et al* have shown that Zn/Cu-selective chelators can completely reverse the ions' inductive precipitating effect on the Aβ peptide [4]. In this way, the chelation is mediated by the peptide's α-helical conformation. Additionally, Cherney *et al* found enhanced resolubilization of extractable deposits of Aβ (from post-mortem human AD brain samples) with Zn/Cu-selective chelators [66]. The authors correlate extractable Aβ from post-mortem AD brain specimens, with depletions in the concentrations of zinc and copper [66].

Aβ accumulation causes perioxidative injury to the cell by generating free radicals. In particular, Aβ binds Cu^{2+} or Fe^{3+} and reduces H_2O_2 to O_2 by double electron transfer [67]. The role of H_2O_2 in oxidative stress is widely supported in the literature [68]. Namely, it serves as a pro-oxidant and as a substrate in the Fenton reaction. In addition, H_2O_2 generates deadly reactive hydroxyl radicals $(OH^{\bullet})$ that permeate cell boundaries and modify nucleic acids, proteins, and lipids. Cyto-modifications such as these are typical in AD neuropathology [69-71]. In

Alzheimer's disease, the cerebral defense mechanisms against H_2O_2 cellular mutation (e.g. catalase, glutathione peroxidase), eventually become overwhelmed.

The most prevalent reactions involved in AD neurochemistry (i.e. metal ion reduction, and $OH^{\bullet}$ and H_2O_2 generation), are mediated by the $A\beta$ metalloprotein, and are redox active. Redox activity follows the trend where $A\beta_{42human} > A\beta_{40human} >> A\beta_{40mouse} \approx 0$ [55]; this is an appropriate relationship when one considers $A\beta_{42}$ as the causative mutation in familial AD. Furthermore, redox activity also correlates with the neurotoxicity of neurons in culture [5], which is largely mediated by the interaction of $A\beta_{42}$ and Cu^{2+}. The product of the copper-amyloid reaction is, of course, the generation of H_2O_2 [5]. Moreover, Cuajungco *et al* present compelling evidence of Zn^{2+} as a redox-silencer of the $A\beta$ peptide. Therefore, in this case, zinc functions to suppress H_2O_2 production [72]. However, Opazo *et al* have shown that the amyloid plaques are insufficiently loaded with enough Zn^{2+} to completely overcome the ion's protective effects [73].

It is clear that zinc's responsibility in amyloid pathophysiology is multifaceted. As aforementioned [64], Zn^{2+} induces $A\beta$ precipitation, and inhibits secretase activity upon the peptide to prevent extracellular deposition. During neurotransmission, the ion is released from corticofugal glutamatergic fibers in the neocortex, where it appears to be the dominant neurochemical in the plaque histopathology [74] (extracellular $Zn^{2+} \approx 300$ µM [75]; $Cu^{2+} \approx 15$ µM [76, 77]). In fact, the zinc released during neurotransmission represents the largest labile

pool of brain zinc, and it parallels the distribution of amyloid deposition in the neocortex [78]. Extracellular zinc is packaged into synaptic vesicles by ZnT3 membrane protein receptors. Cole *et al* have found an $\approx$ 25% reduction in the hippocampus of the concentration of Zn^{2+} when the ZnT3 receptor is knocked out in experimental mice [79]. When ZnT3 knockout mice were crossed with AD transgenic mice, Aβ deposition was found to significantly decrease [74]. Furthermore, Bush *et al* have shown that zinc's induced precipitation may inhibit Aβ clearance and catabolism [64]. In addition, Cherney *et al* found the Zn/Cu-selective chelator clioquinol (CQ) was successful in rapidly reducing β-amyloid accumulation in AD transgenic mice [80]. In summary, Zn^{2+} acts to clear Aβ production, while Cu^{2+} and Fe^{3+} induce H_2O_2 production. Therefore, CQ may represent a useful therapeutic strategy in the treatment of AD.

1.6. CLIOQUINOL (CQ) as a METAL-COMPLEXING AGENT

Markedly elevated concentrations of zinc, copper, and iron in Aβ deposits of the AD brain are well documented in the literature [81, 82]. Cherney *et al* have employed the use of the antibiotic and Cu/Zn-selective metal chelator, CQ, to inhibit Aβ accumulations in AD APP2576 transgenic (Tg) mice. Oral treatments with CQ reduced Aβ deposition by $\approx$ 49%, and produced no neurotoxicity in a blinded study. Furthermore, the authors [80] speculate that CQ's action on the

peptide may facilitate metal-induced dissagregation and/or H_2O_2 inhibition [80]. Interestingly, the general health and body weight parameters of the treated animals improved after only 16 days. This may have been due to the rapid effect of CQ, in part to the quick decline in cerebral H_2O_2 concentration caused by the inhibition of Aβ [55]. Moreover, the authors validated the selectivity of CQ since systemic metal depletion was not found [80]; hence, CQ does not deplete brain tissue of metals, but rather binds to the Aβ-metal complex itself.

Clioquinol is a weak chelator. However, in *in vitro* assays, CQ blocked the production of H_2O_2, prevented the precipitation of synthetic Aβ by Cu^{2+} and Zn^{2+}, and extracted Aβ from AD post-mortem brain tissue [80]. Cherney *et al* found CQ as effective in precipitating and extracting Aβ (and preventing the precipitation of H_2O_2), as other high affinity Cu/Zn standard chelators such as EDTA or TETA [80]. In essence, CQ may operate by dissolving pre-existing Aβ aggregates or by inhibiting Aβ precipitation, and CQ removes Cu^{2+} and Zn^{2+} from both neuritic and diffuse deposits of Aβ [55]. Furthermore, it is well established that metal-precipitated Aβ aggregates are fully reversible by chelation [66, 83]. Wu *et al* proved metal-mediated protein aggregation that subsequently results in perioxidative brain injury may also inhibit clearing mechanisms such as the scavenging system known as the LDL receptor-related protein, LRP [84]. Therefore, CQ modifies the equilibrium between the dissolution and the deposition of the peptide. This action liberates the soluble Aβ, which can then be

cleared by LRP or by proteolysis. Finally, DeMattos *et al* demonstrated that resolubilized Aβ may either be removed into the vascular system, or uploaded into cells by hydrolysis [85].

In *in vivo* experiments of non-transgenic animals treated with CQ, Yassin *et al* confirmed significant decreases in the cerebral concentrations of Cu, Zn and Fe metal ions [86]. Ironically, however, in Cherney's studies of the APP2576 Tg mice, the inhibition of Aβ deposition by CQ caused significant *increases* in the cerebral concentrations of Cu and Zn [80]. This is because APP transgene expression reduces Cu and Zn levels *in vivo*, while the Aβ concentration steadily rises [55]. There are a few possibilities for the decrease. For example, the metal ions may be effluxed by Aβ; the APP may be secreted; or, APP/ Aβ may prevent re-uptake of the ions [87]. Despite the mechanism, CQ prevents uptake of the metals by the protein. This action affords metallic access to peripheral brain tissue, hence, the metal ion concentration increases. Since AD is a syndrome of metal dyshomeostasis, CQ may be able to restore the metal metabolism.

1.7. TRANSGENIC MOUSE MODELS of AD

There are several advantages to studying transgenic mouse models in AD research. Namely, mouse models allow for fundamental understandings of the underlying disease mechanisms, as well as pathological developments and

progression(s). Mouse models also provide *in vivo* vehicles for testing therapeutics, thereby aiding in the identification of potential targets for clinical treatments in human subjects. However, in AD research, no single mouse model has been developed to completely replicate all of the disease pathology. This fact constrains the progress of the field to a relevant degree. For example, experimental mice mutated to develop amyloid plaques do not acquire neurofibrillary tangles. And, likewise, tau transgenic mice don't produce senile plaques [88]. Nevertheless, rodents form more relevant pathology than do aged primates or dogs, which show AD neuropathology [89], or guinea pigs, which possess human APP [90].

However, mice show resistance to some neurotoxins, and this is a major drawback to developing mouse models for AD research. Specifically, "mice overexpressing mutant APP have to make at least 8-fold over endogenous levels of APP to develop amyloid plaques, whereas humans with only a 50 percent increase in APP (those with Down's syndrome) develop AD rapidly" [88]. Other problems associated with mouse models of AD include sub-species variability and regional susceptibility (i.e. transgene expression in the mouse is different from that seen in the human, based on the type of heterologous promoter used), both of which are crucial factors in identifying true pathology and risk factors [88].

Furthermore, AD is a compound disease; in order to replicate as many of the disease facets as possible, most mouse models generated to date are double or

triple transgenics created to overexpress mutant APP, presenilin, or tau. Of particular note, Duff and Suleman provide a comprehensive review of Tg mouse models of AD [88]. Most AD Tg mice are created by microinjecting the mutated complementary DNA (cDNA) transgene, although it has also been possible to create transgenics with the whole wild-type human gene, including the promoter region, the introns and the flanking sequence. For instance, mice have been created with the whole APP gene [91], the whole PS-1 gene [92], or the whole tau gene [93]. Unfortunately, because of the various mouse strains and techniques employed, standardized results have become difficult to achieve. For example, of the mice who overexpress APP, many don't develop pathology, or don't display the same pathology or disease progression as other APP-bearing mice [88].

1.7.1. APP Mice Form Amyloid Plaques

The commercially developed PD-APP (cDNA construct using the platelet-derived growth factor, PDGF, and a human APP mini-gene) mouse was created in 1995 by Exemplar-Athena Neuroscience. This mouse line was the first such generated with AD neuropathology, and was shown to exhibit both diffuse and progressive fibrillar amyloid pathology in cortical and hippocampal neuronal cells [94]. Additionally, this pioneer PD-APP mouse exhibited ~ 10-fold higher levels of human APP than endogenous mouse APP, with observed $A\beta$ deposition at age eight months [94]. Furthermore, PD-APP mice have been proven to show

cognitive-related deficits, which correlate with Aβ deposition and impaired spatial memory, on behavioral tasks [95].

Hsiao *et al* demonstrated the APP Tg2576 mouse (based on the 695 amino acid isoform of APP) with amyloidsis had cognitive deficits; no cell loss was shown in this animal model. The Tg2576 mouse had an ~ 5.5-fold higher transgene APP than did the endogenous mouse APP, and with observable Aβ deposition at age 9-11 months [96]. Although no cell loss was found in the Tg2576 mouse, hippocampal CA1 cell loss has been shown in the APP-23 mouse model (based on the 751 amino acid isoform of APP) [97]. The TgAPP-23 mouse developed an ~ 7-fold higher transgene expression of human APP compared to the endogenous mouse APP; additionally, the animals exhibited both parenchymal and vascular Aβ deposition at age 6 months [97]. Finally, APP mouse models with cognitive impairment are well documented [36, 96, 98, 99] in the literature, thereby validating the hypothesis of neurodegeneration in these mutant mice. In addition, vaccination of Tg2576 mice with $A\beta_{42}$ reduces the amyloid burden and sustains the spatial memory [100].

The APP 695-isoform cDNA transgenic mouse created by Borchelt *et al*, called TgC3-3, expressed human APP twofold higher than endogenous APP and developed Aβ deposits at age 18 months [101, 102]. Another cDNA APP mouse model, called TgCRND8 (based on the 695 APP isoform), developed Aβ deposits at 3 months of age, with 5-fold higher transgene expression than endogenous APP,

and showed a decreased plaque burden with cognitive impairment upon $A\beta_{42}$ immunization [103]. Lastly, the TgAPP/Ld/2 line developed by Moechars *et al* demonstrated a 25-fold higher transgene expression compared with endogenous mouse APP; the mice also exhibited fibrillar $A\beta$ deposits (at age 13 months), premature deaths (at age 6 months), memory deficits and aggressiveness [104, 105].

1.7.2. Presenilin Mice Overexpress $A\beta_{42}$

Duff *et al* have created mice expressing mutant PS-1 to increase $A\beta_{42}$ production [35]. This essentially confirms the gene's effects on the proteolytic processing of $A\beta$. Additionally, $A\beta$ aggregation into amyloid plaques is greatly enhanced when PS-1 mutant mice are crossed with APP mutant mice [36]. As further validation of the role of PS-1 on APP processing, Dewachter *et al* established a PS-1 knockout (KO) model with decreased cerebral $A\beta$ [106]. Furthermore, current speculation implicates PS-1 as the APP-cleaving enzyme better known as γ-secretase [107].

1.7.3. APOE Mice

Bales *et al* signified the role of ApoE in $A\beta$ deposition in their studies on the progeny of ApoE KO mice crossed with PD-APP mice [42]. The authors

found significant reductions in the deposition of the Aβ metallopeptide, and as further confirmation, Holtzman *et al* verified the protective role of the E2 isoform (and the destruction of the E4 variant) when they found increased amyloid concentrations in the progeny of an ApoE4/PD-APP cross, compared with an ApoE2/PD-APP cross [108]. Finally, the ApoE pathway in Alzheimer's disease has not been elucidated, although it has been linked with cholesterol [109].

1.7.4. Tau Transgenic Mice Form Neurofibrillary Tangles

Neurofibrillary lesions consist of neurofibrillary tangles, formed of paired helical filaments (PHF), which are generated from the CNS microtubule protein tau. Post-translational protein modifications characterize the variety of tau implicated in AD. In the AD brain, tau is in a constant state of phosphorylation [110]. An imbalance between kinases (responsible for the phosphorylation) and phosphatases (responsible for dephosphorylation) result in a hyperphosphorylated tau protein that is prone to insolubule aggregation. In fact, it is the hyperphosphorylated tau that dissociates from the microtubule, and aggregates within the neurons of the AD brain.

In addition to phosphorylation, several other factors promote the aggregation of tau, including the association with metal ions such as Fe^{3+} and $Cu^{2+.}$ Yamamoto *et al* have demonstrated, by *in vitro* assay, that Fe^{3+} induces the

aggregation of hyperphosphorylated tau; furthermore, the reduction of Fe^{3+} to Fe^{2+} reverses hyperphosphorylated tau aggregation [110]. Lastly, Ma et al have used spectroscopy (NMR and MALDI-TOF MS, matrix assisted laser desprption/ionization time of flight mass spectrometry) to show Cu^{2+} binding to an Alzheimer's tau peptide [111].

Gotz *et al* created the first tau Tg mouse in 1995 with somatodendritic localization and hyperphosphosphorylation of tau, however they found little neurofibrillary pathology [112]. Nevertheless, Lewis *et al* have inserted tau cDNA transgenes with mutations along chromosome 17 (tauopathy related to fronto-temporal lobe dementia linked to chromosome 17, FTD-17) to create mice with the neurofibrillary tangles of AD and motor deficits [113]. Furthermore, tau Tg mice have also been produced from human wildtype genome, to express abundant loads of aggregated hyperphosphorylated tangles [114]. Most mice created with tauopathies by cDNA transfer have had cell loss in the neuronal motor spinal cord and brain stem; subsequent cognitive and memory evaluations have proven inconclusive, as they are derived from motor skills. However, recent developments have lead to creations of tauopathy models with tangles and related cell loss in the hippocampus and cortex [88].

Even though tau-bearing mice do not form amyloid plaques, there does seem to be a relationship between the two proteins. For example, when tau Tg mice are crossed with experimental mice bearing the amyloid protein, the tau

pathology increases; this phenomenon is true when tau Tg mice are crossed with APP mice [115], and when Aβ is directly injected into the brains of tau mice [116]. In fact, Aβ has been implicated as the signal which upregulates tau, the subsequent action of which leads to the phosphorylation and aggregation of the tau protein [117]. Finally, Oddo *et al* have created a triple transgenic model that expresses mutant APP, PS-1, and tau [118]. These mice form both plaques and tangles; the initial pathology is plaque deposition. Additionally, synaptic dysfunction was proven [118].

1.7.5. Triple Transgenic Mouse Models of Alzheimer's Disease Exhibit Plaques and Tangles

A novel triple transgenic mouse model (3xTg-AD) was developed in the laboratory of Frank LaFerla (and S. Oddo) at the University of California, Irvine, composed of the AD transgenes $PS1_{M146V}$, APP_{Swe}, and tau_{P301L} [118]. This transgenic version was derived by coinjecting two additional transgenes (human APP_{Swe} and tau_{P301L}) into an embryo harvested from a mouse whose genetic background had been previously modified (mutant homozygous $PS1_{M146V}$ knockin). The motive behind the 3xTg-AD design was to establish a model which more closely resembles AD pathology, since previous literature accounts have speculated that mice with multiple transgenes display pathology closer in form to the human type of disease [116]. For example, synaptic disfunction and

loss of long-term potentiation is expressed in triple transgenic variants, whereas these characteristics are not found in mice with only two mutant genes. Similarly, 3xTg-AD mice show extracellular deposits of Aβ and intraneuronal immunoreactivity to Aβ, whereas the same is not true of double transgenic mice [118].

Otto *et al* found that intraneuronal Aβ immunoreactivity precedes Aβ deposition, which occurs previous to tau manifestations [119]. This finding supports the amyloid cascade hypothesis, which suggests that Aβ deposition underlies AD neuropathology [120]. Furthermore, immunoreactivity and protein deposition are region specific (e.g. neocortex, hippocampal CA1) symptoms that increase with age in the 3xTg-AD mouse. Although tau was also found to be region specific and age-dependant, its manifestation was not apparent until 12-15 months of age. Age related tau expression contrasts with the findings of Aβ deposition, at 6 months of age, and with immunoreactivity, which was apparent at 3-4 months of age. These data were despite comparable brain expression of both transgenes, which more importantly, were of the same genetic background.

Lastly, it is well established that synaptic loss correlates with memory decline in humans [121]. Consequently, Otto *et al* have also demonstrated this phenomenon in the 3xTg-AD mouse model, noting impaired synaptic transmission by 6 months of age. Moreover, the plasticity underlying memory, or long-term potentiation (LTP), was reduced in the transgenic mice, versus non-

transgenic controls. In addition, the authors showed that LTP and synaptic dysfunction were precipitated by intracellular amyloid expression. Synaptic dysfunction was more greatly impacted by APP expression, compared to tau expression; LTP deficits were shown in the triple transgenic model, but were not observed in a double transgenic model that lacked the APP transgene, which again, suggests that intraneuronal accumulation of Aβ, which leads to extracellular deposition, is most likely accountable for triggering the "cascade" of AD pathology.

1.8. *IN VIVO* DETECTION of ALZHEIMER'S PATHOLOGY in TRANSGENIC MICE

In vivo detection of amyloid plaques for the early diagnosis of AD is desirable. Presently, histological confirmation of the plaques, and of the neurofibrillary tangles, is the only definitive mode of diagnosis. This is true despite the fact that patients typically receive clinical diagnoses based on cognitive tests, medical histories, etc. Non-invasive *in vivo* detection affords patients the opportunity to receive the most astute patient care as early as possible. Likewise, it would allow clinicians the prospect of tracking disease progression, thus, more specifically defining diagnostic criteria along the disease course. Hence, healthcare professionals would be able to design appropriate therapeutic

strategies. However, the greatest benefit, perhaps, would come in the possibility of decreasing the life of the disease, thereby extending the patient's life, and improving their quality of life, by early detection. Successful plaque labeling, and subsequent imaging, in the animal model precipitates non-invasive imaging in the intact, living human brain.

1.8.1. Fluorescence imaging

Skovronsky *et al* developed BSB, or [(trans, trans),-1-bromo-2,5-bis-(3-hydroxycarbonyl-4-hydroxy)styrylbenzene, as an *in vivo* imaging probe to detect Aβ by intrahippocampal, intraventricular, or intravenous injection of the probe [122]. Staining intensity was most for intraventricular injection, and least for intravenous injection. Although the authors proved *in vivo* staining of the plaques, the imaging was done by *ex vivo* fluorescence microscopy. While this method represents a valid staining technique (rapid plaque labeling in transgenic mice, versus non-specific labeling of parenchyma in wild type controls), it does not represent *in vivo* detection.

The fluorescence imaging method of Okamura *et al,* using the amyloid probe BF-168 (6-(2-Fluoroethoxy)-2-[2-(4-methylaminophenil)ethenyl]benzoxazole), also represents *in vivo* labeling, and *ex vivo* detection [123]. Additionally, Okamura *et al* radiolabelled BF-168 with ^{18}F,

and also administered this compound by intravenous injection to transgenic mice; detection, however, was still by *ex vivo* autoradiography [123].

1.8.2. Magnetic resonance imaging (MRI)

The ^{19}F-amyloidophilic ligand FSB, (E,E)-1-^{19}F-2,5-bis(3-hydroxycarbonyl-4-hydroxy)styrylbenzene, was used as a probe for the ^{19}F MRI detection of Aβ plaques in APP transgenic mice [124]. FSB, and consequently, MRI technology, were implemented for a number of significant reasons. In contrast to PET technology, many popular PET isotopes (e.g. ^{11}C-labeled compounds) have short radioactive half-lives, while MRI probes are capable of long-term storage and usage. Additionally, background noise resulting from ^{19}F is essentially low because of the relative lack of endogenous ^{19}F, as compared with some carbon containing compounds which have a greater abundance in the body. In a second contrast to PET, MRI has a high spatial resolution, which is useful in imaging small structures, such as the hippocampus. Furthermore, though the popular PET ^{11}C Pittsburgh-B (PIB) compound has been successful clinically [125], its results are mixed in transgenic mice. For example, Klunk *et al* found low brain retention (> 1 binding site per 1000 molecules Aβ) of PIB using the PET modality in mice [126]; the results were, thus, unsuccessful. Meanwhile, Bacskai *et al* employed *in vivo* multiphoton microscopy, by taking

advantage of the intrinsic fluorescence of PIB, to show amyloid labeling in mice [127]. This discrepancy may be due to differences in experimental design, such as modality, transgenes, age, or strain. In fact, Bacskai imaged two different transgenic models, and found that labeling "was not specific to one model of the disease [127].

In reference to the FSB experiment [124], the radiolabel was administered by intravenous injection to APP mice (Tg2576), which were subsequently subjected to ^{1}H and ^{19}F MRI. The data were consistent with fluorescence enhancement of Aβ plaques by FSB. For example, before injection of FSB, the plaques were detected with low signal intensities on T_2- weighted ^{1}H MRI; no detectable signals were observed at all on T_1-weighted ^{1}H and ^{19}F MRI, however, post-injection of FSB, the amyloid plaques were enhanced on the T_1-weighted ^{1}H images. The ^{19}F signals were particularly strong in the hippocampus and entorhinal cortex, and these signals co-localized with Aβ distribution observed from ^{1}H signals. Similarly, ^{1}H and ^{19}F signals were detected in the cortex. The T_2- weighted images remained unchanged; the authors suggest that a shorter T_2 relaxation time by the amyloid plaques may be responsible for this phenomenon [124]. Nonetheless, the enhanced *in vivo* T_1-weighted images indicate the feasibility of FSB as a contrast agent for amyloid imaging, with ^{19}F and ^{1}H MRI technology. The caveat, of course, of bulky MRI ligands is their low ability to cross the BBB. However, the authors did observe increased T_1 ^{1}H signals, which

were enhanced in a time-dependant manner. Consequently, advantage of the proton time-dependant signal can be taken to increase the SNR, by simply adjusting the scan time, post administration of the radioligand.

In another attempt at using the MRI modality for plaque imaging, Wadhiri *et al* co-injected transgenic mice (both APP and APP/PS1 mice) with Gd-DTPA-Aβ1-40 and 15% mannitol [128]. The Gd-DTPA (gadolinium-diethyltriaminepentaacetic acid) was used as a paramagnetic contrast agent, and was complexed with Aβ1-40 to selectively bind Aβ *in vivo* (DTPA is a chelator); mannitol was employed to temporarily open the BBB. The site of injection was the common carotid artery, and the complex was introduced at a rate slow enough (0.25 mL/kg/s, 400μg peptide in 700μL volume PBS and mannitol) to avoid hypertensive opening of the BBB. In parallel experiments, Aβ1-40 was adsorbed onto the surface of monocrystalline iron oxide nanoparticles (MION), and co-injected with mannitol into transgenic mice; here, the MION was the contrast agent. Imaging commenced 6 hours post-injection to limit nonspecific vascular labeling, although vessels were still distinguished.

The authors observed a 100% success rate on *in vivo* T_2 and T_2* -weighted MR imaging of Gd-DTPA-Aβ1-40 in both sets of transgenic mice (APP and APP/PS1) [128]. The signal intensities, likewise, correlated with matched histological sections. Furthermore, intensity signals were not seen in wild type controls subjected to the same injection protocols, nor were they detected in non-

injected transgenic controls. Similarly, signals were neither detected in transgenic or wildtype mice injected with Gd-DTPA and mannitol (no Aβ1-40), nor were they detected in transgenic mice injected with Gd-DTPA-Aβ1-40 (no mannitol). Data were similar in the MION-Aβ1-40 experiments, except that the imaging was done *ex vivo*. These methods of amyloid detection by MRI are successful; however, our experimental compound designs are different because they freely cross the BBB. Thus, our scheme may be more practical in terms of limiting the perturbation to the animal's system.

Lastly, Vanhoutte *et al* took advantage of the iron overabundance in the amyloid plaques of APP[V717I] transgenic mice to non-invasively investigate *in vivo* imaging by T_2*-weighted MRI [129]. This approach, therefore, is unique in its kind because no external labeling was used, since endogenous iron provided the T_2* contrast. The authors observed dark spots indicative of the amyloid signal, in the bilateral thalamus and subiculum of the transgenic mice; these findings were confirmed on thioflavin-S staining. The hypointense signals were not observed in MR images of the age-matched wild type controls. Also, MR did not detect any plaques in the transgenic mice in the cortex or hippocampus, although very small plaques in these areas were found on histology. Since iron staining confirmed the presence of iron in the plaques in the thalamus, the absence of cortical plaques on MRI may suggest that these two areas contained different

types of plaques, which exhibit differences in iron loading, and perhaps even differences in plaque formation (or stages of formation) [129].

One advantageous aspect of this method is that the imaging can begin as soon as the experiment starts (i.e. after anesthesia) since one doesn't have to worry about external labels clearing the vascular and RES systems. Iron signals from the cerebrovascular system, however, must be considered, and such signals were not observed in the direct vicinity of the plaques. Additionally, the wild type controls did not show any decreased T_2* values, which would have indicated cerebrovascular iron. The imaging time for these experiments was just over an hour (68 min), which was long enough to obtain a T_2* signal on the 7T system. Since MR sensitivity to iron increases with field strength [130], this appears a feasible imaging paradigm. The authors, however, wished to improve imaging parameters (such as resolution, sensitivity, SNR, etc.), and so elected to perform *ex vivo* imaging with longer imaging times. As expected, the *ex vivo* images correlated with the *in vivo* signals. Therefore, it appears that the use of MRI to detect endogenous iron signals from amyloid plaques may be a viable method of Aβ detection in transgenic mice.

1.8.3.   Near-infrared fluorescence imaging (NIRF)

The oxazine derivative AOI987 was synthesized as a NIRF ligand to target Aβ plaques in APP23 transgenic mice [131].   The compound, a low molecular weight (<500 Da) ligand that freely crosses the BBB, showed intense fluorescence brain signaling upon intravenous administration into the AD mouse model. Furthermore, brain retention of the compound (observed by fluorescence), was longer in the transgenic mice, as compared with age-matched wild type littermates. There were no significant differences in signal intensities between 6 month old transgenic and control mice, however the 9 month old transgenic mice showed significantly stronger fluorescent brain signals at 4 hours post-administration of the ligand. Thus, NIRF demonstrated an increasing amyloid burden with age in the experimental model.

Ex vivo plaque detection by fluorescence microscopy confirmed the *in vivo* labeling and imaging results of the transgenic mice. Similarly, *ex vivo* signals were not obtained from the wild type mice. The imaging paradigm in this scheme appears feasible for *in vivo* detection; however, quantification of the plaques can be problematic. For example, light scatters in biological tissues in such a way that an increasing depth of the (fluorescent) signal results in decreased spatial resolution. Thus, quantification of the plaques is only achieved by

integration of the spatial signal intensity, and therefore, it is impossible to resolve

individual plaques "when imaging through the intact cranium and scalp [131]."

2. THE BLOOD BRAIN BARRIER

The blood brain barrier (BBB) is the homeostatic defense mechanism of the brain against pathogens and toxins. Complex and highly regulated, the BBB screens the biochemical, physicochemical and structural features of solutes at its periphery, thus affording barrier selectivity in the passage of desired molecules into the brain parenchyma. Early revelations of the BBB illustrated its biological character in the murine model, and provided insights into contemporary understandings of its physiology. Electron microscopic analyses of isolated cerebral cortices, after the intravenous injection of the enzymatic tracer horseradish peroxidase (HRP), exposed the presence of exogenous HRP in the vascular space and in endothelial cell pinocytotic vacuoles [132]. The pinocytotic vacuoles were not found to transport the enzyme, and furthermore, no peroxidase was found beyond the vasculature endothelium, which suggested a "barrier" between the blood and the brain.

2.1. BIOLOGY of the BBB

Cerebral capillaries are created by the process of angiogenesis, which is the development of blood vessels from those existing in previously formed complexes. Figure 1 (please see pg. 42) shows a depiction of the cerebral capillaries, while the features of the BBB are exhibited in Fig. 2 (please see pg.

34

43). During angiogenesis, endothelial cells (EC) traverse the extracellular matrix (ECM) and degrade the basement membrane to create a microvascular network [132, 133], thus subsequent proliferation of EC. Proliferation of endothelial cells is influenced by neural determinants that confer characteristic physiological properties upon the BBB, and consequently, cerebral EC are distinguished from the EC of the periphery. For instance, brain EC have fewer endocytotic vacuoles than peripheral EC, which limits the transcellular flux at the BBB. Additionally, endothelial cells of the brain are joined by occluded tight junctions, whose great electrical resistance imposes barriers to paracellular flux. The structural properties of cerebral EC, mentioned above, help to define the selectiveness at the BBB. Furthermore, cerebral EC have more mitochondria [133] than peripheral EC, which drives the increased metabolic workload necessary to maintain ionic gradients across the BBB.

The electron-dense layers of the basement membrane fuse EC and astrocytes, while dividing EC and pericytes from the surrounding extracellular space. Pericytes lie along the outer axes of cerebral capillaries and perform in contractility. This close association (and function) helps to monitor blood flow, and thus, the adhesion of pericytes with the microvasculature indirectly regulates EC activity and BBB transport. Pericytes also manage endothelial growth and development by inhibiting cell proliferation [134], and in a contrasted dual role, by contributing to angiogenesis [135].

Lastly, astrocytes envelop more than 99% of the basal capillary membrane [136], and they serve in the BBB induction of high paracellular electrical resistance. A gap of only 20 nm separates the astrocytes from the EC and the pericytes. Likewise, the significant interplay amongst the three cells contributes to the solute transportation. Namely, the molecular route into the brain (from the blood) is first accomplished by moving beyond the astrocytic processes, and then by moving through the immediate perivascular spaces, and on to the pericytes bordering the capillaries. Consequentially, transporters, receptors and enzymes located on the plasma membranes of astrocytes and pericytes govern the fates of solutes before they reach the EC [136, 137].

2.1.1. MOLECULAR PHYSIOLOGY of the BBB

The BBB bars solute entry into the brain (by the transcellular route) as a result of increased electrical resistances between endothelial cells at the tight junctions (TJ). The intact BBB exhibits estimated electrical resistances up to 8000 Ω/cm^2, whereas leaky endothelia demonstrate resistances between 100 and 200 Ω/cm^2 [138-141]. Key indispensable proteins, claudins 1-, 3-, and 5-, occludin and the junctional adhesion molecule (JAM), compose the tight junction [141-145]. The claudins form the seal of the TJ by homotypically binding to each other on adjacent EC cells. In an interesting review of the pathophysiology of tight junctions, Mitic *et al* provide convincing evidence for the role of claudins

in fibrilizing and forming the TJ seal [146]. However, the claudins are not the sole components of the fibrils, this role being shared with occludin. In addition, the occludin protein directs the BBB to decrease paracellular permeability by localizing into the intramembrane strands of the TJ [147]; the number of localized proteins parallels the impedance to solute flux [148]. Meanwhile, JAM regulates leukocyte transmigration at the BBB [144]. Of particular interest, leukocyte passage instigates BBB compromise [133]. As well, a host of other transmembrane [146] proteins lie in accessory to the integral proteins. According to Reichel *et al* [149], "the expression of complex tight junctions between the ECs is one of the most critical features because of their consequences on the function of the BBB: (i) nearly complete restriction of the paracellular pathway, (ii) enforcement of transendothelial passage and hence, control over the CNS penetration, (iii) association with expression of specific carrier systems for hydrophilic solutes essential for the brain (e.g. nutrients), and (iv) differential (i.e., polarized) expression of receptors, transporters, and enzymes at either the luminal or abluminal cell surface allowing the BBB to act as a truly dynamic interface between the body periphery (blood) and the central compartment (brain)".

2.2. BBB BREAKDOWN and MECHANISMS of DISEASE

Decomposition of the BBB occurs in response to initiators such as infection (e.g. bacterial, viral), inflammation, cerebrovascular disease, and neoplasia. Motivators of BBB breakdown augment permeability, and underlie a myriad of neuropathologies. In pneumonia, the pneumococcus bacterium joins the BBB via platelet-activating factor receptors [150]. The outcome of bacterial adhesion is an increased vesicular transport across the endothelial cells, thus permitting separation of the tight junctions, and creating an entry for inflammatory peptides. Likewise, infection of the brain space ensues. The consistency of the BBB is also influenced by the actions causing bacterial meningitis. The meningococcus bacterium enters the body through the nose, and thereafter infiltrates the endothelia (via the pili) of the cerebrum to cause infection of the CNS [151]. Viral invasions of the CNS pronounce less impairment to the BBB than do bacterial interferences, and therefore, the integrity of the BBB is upheld to a greater extent following viral attack [152]. Inflammatory stimuli such as pain induce the extravasation of lymphoid cells through the BBB [153], opening the barrier to cytokines and chemokines, and resulting in autoimmune inflammatory disorders like multiple sclerosis (MS) and CNS lupus. In addition, the BBB can be compromised in cerebrovascular disease, for example stroke, by

hypertension and ischemia. Ischemia then complicates the disease progression by activating cytokines and proteases [152].

As previously mentioned, degradation of the BBB occurs in states of pathology, such as hypertension, ischemia, and hydrocephalus or in cases of trauma. The various factors involved in BBB breakdown and homeostasis are compiled in Table 1. Degradation leads to leakiness, and the consequential unrestrained migration of malicious agents into the cerebrum. In addition to existing pathological conditions, and even in the intact BBB, crucial parameters must be regarded when ascertaining the capabilities of molecules to cross, especially for the intended purpose of drug design. The implication is that targeted, controlled drug delivery through the BBB, would promote a greater understanding at the molecular level of many unfathomable neurological disorders, as well as aid in their early diagnoses, and their therapeutic advancements.

2.3. DRUG TRANSPORT ACROSS the BARRIER and TARGETING MECHANISMS

The BBB is circumferential, being formed by polarized luminal (apical) and abluminal (basal) endothelial membranes (and other tissue [3] interfaces), which lie in series. Thus, solutes must pass a set of membranes to gain brain

entry, making the BBB dynamic in its regulation. Also, the barrier takes up essential nutrients, hormones and vitamins, while enzymatically degrading many peptides and neurotransmitters through a so-called "enzymatic BBB". Additionally, the energy-requiring toxin efflux mechanisms help to maintain cerebral vitality by removing injurious substances. Kinetic flux analyses reveal a unidirectional, concentration-dependant movement of the solutes [154]. Furthermore, the direction of flow is from the plasma to the brain, or vice versa, with these two parameters defining influx and efflux (see Fig. 3). Thus, net flux is the difference between the two unidirectional rates, and is greatly influenced by the nature of the BBB. Importantly, BBB flux is a determinant in drugs reaching therapeutic concentrations within the CNS [155].

Numerous transport mechanisms define the BBB. For example, small, lipophilic molecules most easily pass from the capillaries. Likewise, those molecules that are charge-bearing, large or hydrophilic require gated channels, ATP, proteins and/or receptors, to facilitate passage through the BBB. One exceptional regulatory aspect of the BBB is that it is not fully present throughout the brain. The circumventricular organs, which border the ventricles of the brain, do not possess a BBB. These organs are concerned with chemosensation, hormonal adjustment (from the autonomic nervous system), circadian rhythm, vomiting and the regulation of bodily fluids. The absence of a BBB at these checkpoint organs encourages the maintenance of a constant cerebral internal

atmosphere by monitoring the blood make-up and by activating feedback controls, as necessary.

Transport mechanisms at the BBB can be manipulated for cerebral drug targeting. Naturally, ideal drug candidates should be small, lipophilic (as measured by the octanol:water partition coefficient), hydrophobic, and compact (a parameter measured by the polar surface area). Physicochemical factors notwithstanding, though, the nature of the drug candidate within the biological system is paramount to the drug design. In the peripheral circulation, systemic enzymatic attack and plasma protein opsonization can lead to the metabolism of the drug before it reaches the brain. The factors influencing drug transport into the brain are given in Table 2. Moreover, the probability of cellular sequestration and the clearance rate of the drug in the bloodstream are additional issues to consider in drug targeting. An understanding of the clearance rate of the candidate drug in the brain is imperative, and as such, focus should be given to the concentration of the drug in the brain, with respect to the concentration of the drug in the blood, called the log BB. Finally, in drug design, it is extremely important to consider several parameters such as drug concentration, lipophilicity, and polar surface area. As such, efflux proteins and other obstacles at the BBB must be surmounted before the drug reaches the interior of the brain.
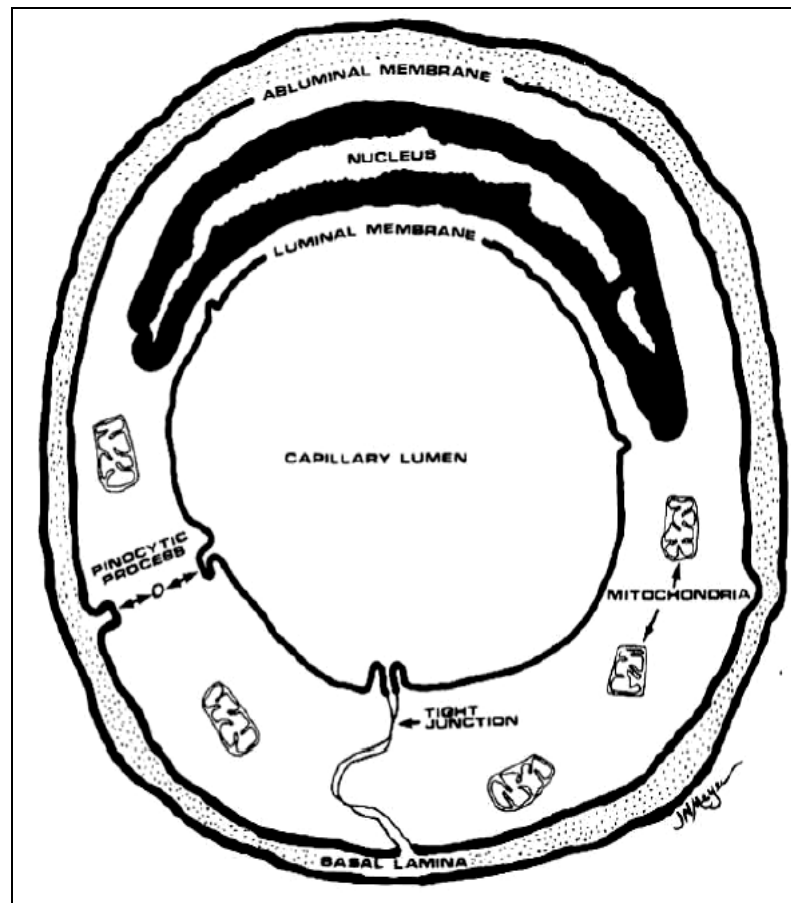
Fig. 1. Characteristic features of the BBB are represented in this schematic diagram of a cerebral capillary. Note the tight junctions and the scarcity of pinocytic vacuoles. Note also the presence of the mitochondria, which are denser in cerebral EC as compared to peripheral EC. This may be attributed to the extra metabolic workload required to maintain ionic gradients at the BBB. (Figure taken from: Burns E., Dobben G., Kruckeberg T., Gaetano P., Blood-brain barrier: Morphology, physiology, and effects of contrast media, Adv. Neurol., 30, 159-165, Carney A. ed., Raven Press NY, 1981.)
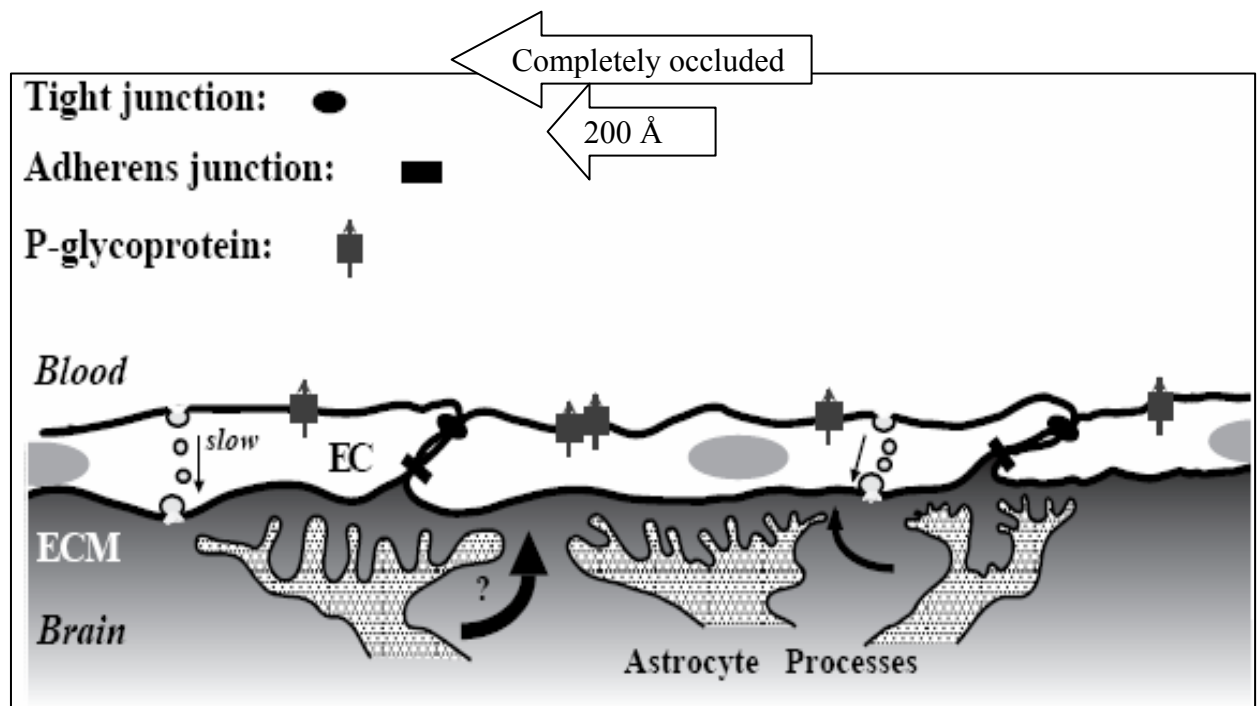
Fig. 2. Features of the BBB. The endothelial cells (EC) of the BBB are coupled by tight junctions (TJ) that are completely occluded and adherens junctions (200 Å). The increased electrical resistance at the TJ strains paracellular movement of substances into the brain. Proteins of the adherens junction work in accord with TJ proteins for cellular adherence. Astrocytic processes (glial cells) in the extracellular matrix (ECM) envelope the capillaries and influence transport across the EC. Questions once arose as to whether or not astrocytes actually participated in the BBB, however, it is now accepted that the 20 nm gap between adjacent astrocytes supports the fact that they do not. P-glycoproteins (P-gp) on the apical EC membrane efflux substances from the brain into the bloodstream. (Reprinted, with permission, from *Annual Review of Neuroscience,* Volume 22 © 1999 by Annual Reviews www.annualreviews.org)

Table 1. BBB degradation and homeostatic organs

Causes of BBB degradation	BBB homeostatic organs	Focus of homeostatic regulation
Hypertension	Pineal gland	Circadian rhythm
Abnormal development	Neurohypophysis	Posterior pituitary hormones
Microwaves	Area postrema	Vomiting reflex
Radiation	Subfornical organ	Bodily fluids
Infection	Lamina terminalis	Chemosensory
Trauma	Median eminance	Anterior pituitary hormones
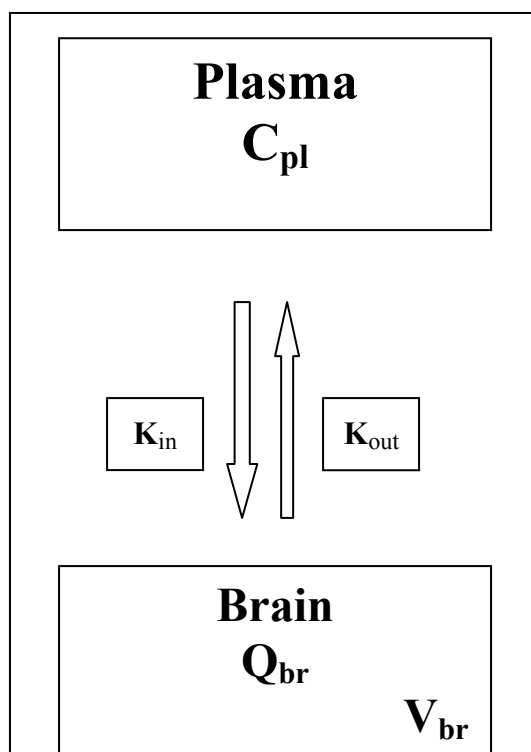
Fig. 3. Schematic representation of unidirectional, concentration-dependant solute flux. The transfer coefficient K quantitates the rates of influx (K_{in}) and efflux (K_{out}) at the BBB, which rely on solute concentrations in the blood plasma (C_{pl}), as well as in the brain. The concentration of the solute in the brain is represented as Q_{br}, which describes the quantity (Q) of the solute per gram weight of brain tissue. The concentration of solute in the brain is also determined by the brain volume of distribution (V_{br}); therefore, $C_{br} = Q_{br}/V_{br}$. Even though these specific quantitative variables are not explicitly stated in the text, the importance of BBB flux to drug delivery, is worthy of note. (Reprinted, with permission from, Q. Smith, A review of blood brain barrier transport techniques, From: Methods in Molecular Medicine: The Blood Brain Barrier: Biology and Research Protocols, Edited by S. Nag, Humana Press Inc., Totowa, NJ. 89 (2003) 193-205.)

Table 2. Considerations for drug transport into the brain

Factors at the BBB	Peripheral Factors
Concentration gradients of drug/polymer	Systemic enzymatic stability
Molecular weight (of drug)	Affinity for plasma proteins
Flexibility, conformation of drug/polymer	Cerebral blood flow
Amino acid composition	Metabolism by other tissues
Lipophilicity	Clearance rate of drug/polymer
Sequestration by other cells	Effects of existing pathological conditions
Affinity for efflux proteins (e.g. P-gp)	
Cellular enzymatic stability	
Existing pathological conditions	
Molecular charge (of drug/polymer)	
Affinity for receptors or carriers	

3. POLYMERIC NANOPARTICLES

Two basic paradigms in cerebral drug targeting are found for the molecular approach and the polymeric NP carrier approach. By the molecular approach, two further schemes can be probed. First, drugs can be targeted to the brain cells (based upon vital determinants such as lipophiliciity, hydrophobicity, size and polar surface area) and then activated once inside the target cell by specific enzymatic machinery. The disadvantage to this tactic, though, is the limited availability of such drugs and metabolic pathways for potential exploitation. Also, by the molecular approach, candidate drugs can be targeted to the BBB via receptor-mediation. However, receptor targeted moieties face additional challenges. In particular, many receptors are not specific to only one cell type. Thus, candidate drugs may have an affinity for cells other than their intended targets. The second major paradigm in cerebral drug targeting is by using particulate carriers. Examples of particulate carriers are liposomes, oil-in-water (O/W) emulsions, and polymeric nanoparticles.

Polymeric nanoparticles are advantageous in a number of ways. For one, they possess high drug-loading capacities, thereby increasing intracellular delivery of the drug. Secondly, the solid matrix of particulate carriers protects the incorporated drugs against degradation, thus increasing the chances of the drug reaching the brain. Furthermore, carriers can mediate the targeted delivery of drugs; this targeted delivery can be controlled. One additional benefit of

particulate carriers is that their surface properties can be manipulated in such a way as to evade recognition by the macrophages of the reticuloendothelial system (RES), hence improving the likelihood of nanoparticles reaching the brain. Kabanov and Batrakova [156] gave an interesting review of maximizing drug transport through the BBB by inhibiting efflux transporters by block copolymers, by using artificial hydrophobitization of peptides and proteins by fatty acids, and by using receptor-mediated drug encapsulated nanoparticles.

One potential of delivering drugs to the brain is the employment of nanoparticles. Nanoparticles are polymeric particles made of natural or artificial polymers ranging in size between 10 and 1000 nm (1 μm) [157]. Compared with other colloidal carriers, polymeric nanoparticles present a higher stability when in contact with biological fluids. Also, their polymeric nature permits the attainment of desired properties, such as controlled and sustained drug release. Different approaches in the fabrication of nanoparticles consisting of biodegradable polymers have been described, and likewise, methods for the preparation of surface-modified sterically stabilized particles [158-172] are reviewed in the literature.

Nanoparticles can be fabricated from preformed polymers or from a monomer during its polymerization, as in the case of alkylcyanoacrylates. As such, nanospheres *or* nanocapsules can be synthesized; their resultant structure depends upon the technology employed during polymerization. Nanospheres are

dense polymeric matrices into which the drug is dispersed. Nanocapsules, however, represent a liquid core surrounded by a polymeric shell. Most synthetic techniques involving the polymerization of monomers include the addition of the monomer into the dispersed phase of an emulsion, an inverse microemulsion or dissolved into a non-solvent of the polymer [158-172]. Starting from the preformed polymers, nanoparticles are formed by the precipitation of synthetic polymers, or by denaturation or gelification of natural macromolecules [157, 160-162, 164, 165, 167-170, 172]. Finally, two main approaches have been proposed for the preparation of nanoparticles by synthetic polymers. The theory of the first scheme follows the emulsification of a water-immiscible organic solution of the polymer, in a surfactant-containing aqueous phase, and followed by solvent evaporation. The second approach follows the precipitation of a polymer after the addition of a non-solvent of the polymer.

Thus far, the only successfully used nanoparticles for the *in vivo* administration of drugs targeted to the brain, is the rapidly biodegradable polybutylcyanoacrylate (PBCA) [173]. The mechanism of emulsion polymerization of polyalkylcyanoacrylates (PACA) is represented in Fig. 4. Kreuter *et al* have suggested that the passage of PBCA nanoparticles through the BBB probably occurs by phagocytosis or endocytosis by the endothelial cells [174]. Schroeder *et al* [175] replicated the work of Kreuter *et al* [174]. Schroeder *et al* further point to a model of diffusion of the NPs at the BBB [176]. Vauthier

et al refute endocytosis as the mechanism for EC uptake of PACA, and suggest NP adherence to the cell membrane with subsequent escape by the P-gp efflux proteins [177].

3.1. EMULSION POLYMERIZATION of POLYAKYLCYANOACRYLATES

The anionic polymerization of polyalklycyanoacrylate monomers into polymeric NPs follows the emulsion polymerization technique. By this method, the monomer is dispersed in aqueous solution as a uniform emulsion and stabilized by surfactants. The surfactants facilitate emulsification of the monomer into the aqueous phase by decreasing the surface tension at the monomer-water interface. Dispersion of the surfactant persists until the critical micellar concentration (CMC) is realized. The CMC is the concentration beyond which the surfactant no longer exists as a soluble dispersion, but rather as molecular aggregates called micelles [178]. Henceforth, equilibrium is maintained between the dispersed surfactant molecules and the micelles. Beyond the CMC, only micellar formation is possible.

Micelles contain both polar and non-polar ends. They aggregate with the polar heads lying outwards, allowing the nonpolar hydrocarbons to form the interior, where the monomer is solubilized. Upon addition of the monomer, and

with agitation, emulsification commences. Typically, water-soluble initiators are used in emulsions. The system contains monomer droplets in the aqueous phase, and the solubilized monomer in the interior of the micelle. With water-soluble initiators, chain growth starts at the surface of the micelle, it being hydrophilic. Once the monomer inside the micelle is expended, more droplets enter from the aqueous phase. Thus, polymerization proceeds inwards and continues until prohibited by free-radical termination. Many polymer chains grow within the system and eventually aggregate into fine particles. These particles are stabilized by the emulsifier layer of the micelle until the micelle bursts, releasing the particles. Nanoparticles are uniformly dispersed in the aqueous phase, and stabilized by the emulsion molecules, which originally formed the micelle [178].

3.2. NANOPARTICLES AND ALZHEIMER'S DISEASE

3.2.1. D-Penicillamine

The concentration of metal ions in the brain increases with age, the impact of which imparts lethal effects on the AD brain. Increases in the concentration of copper initiates oxidative stress, generating deadly hydroxyl radicals which disrupts DNA and modifies proteins and lipids [81]. It is known that amyloid plaques contain elevated levels of Cu ($\sim$ 400 μM) and Zn ($\sim$ 1 mM) compared to the healthy brain (70 μM Cu; 350 μM Zn) [179]. In an *in vitro* study of chelation

therapy for the possible treatment of AD, Cui *et al* conjugated the Cu (I) chelator D-penicillamine to NPs to reverse the metal-induced precipitation of the beta amyloid (Aβ) protein [179]. Nanoparticles were engineered from microemulsion precursors by melting the non-ionic emulsifying wax in the aqueous phase, before the addition of the surfactant Brij 78. The microemulsion was cooled with a constant stirring to obtain the NPs, to which sodium salts of 1,2-dioleoyl-*sn*-glycero-3phosphoethanolamine-N-[4-(p-maleimidophenyl)butyramide] (MPB-PE) or 1,2 dioleoyl-*sn*-glycero-3-phosphoethanolamine-N-[3-(2-pyridyldithio)-propionate] (PDP-PE) were incorporated. The sulfhydryl moiety of D-penicillamine was coupled to the MPB-PE or PDP-PE nanoparticles in water, and under nitrogen gas with proper pH adjustments. Conjugation was measured by gel permeation chromatography (GPC). The stabilities of GPC-purified D-penicillamine conjugated PDP-nanoparticles were studied at 4 and 25°C, and to salt as well as serum challenge, to determine the nature of the NPs in the biological environment. The Aβ 1-42 was induced to aggregate with $CuCl_2$, and samples were incubated with control (no chelator), EDTA (a metal chelator), D-penicillamine conjugated PDP-NPs, D-penicillamine, or PDP-NPs. The samples were centrifuged and the percent Aβ in the soluble fraction of the supernatant (% resolubilized) was calculated.

Nanoparticles (of MPB-PE or PDP-PE) conjugated with D-penicillamine were polymerized and fully characterized for aggregation, storage and pH

sensitivity. The D-penicillamine conjugated to both MPB-PE or PDP-PE by the thioether and sulfydryl groups, respectively. Stability studies were performed with reducing agents on PDP-NP to determine if the −SH moiety could be cleaved (since it is less stable than the thioether bond of MPB-PE). Coelution of the D-penicillamine with NPs on the GPC column verified conjugation, and NPs were stable under the tested conditions. It was found that the maximum amount of MPB-PE and PDP-PE that could be loaded onto NPs, while keeping the size < 100 nm was 10 % (w/w). At equimolar concentrations, the resolubilization of Aβ was 80 % with EDTA and 40 % with D-penicillamine, but at higher concentrations of D-penicillamine, resolubilization was just as effective. Importantly, though, the D-penicillamine conjugated to PDP-NPs did not resolubilize the peptide. However, after treating the NPs under basic conditions (and with increased temperature) to partially release the penicillamine, the plaques were solubilized by approximately 40 %.

Cui *et al* have shown that the D-penicillamine NPs resolubilized the plaques under reducing conditions <Cui, 2005 #209>. They conducted % release studies of the penicillamine, but in an *in vivo* study, they would also need to perform the time release studies. In the *in vivo* system, they postulated glutathione to be the reducing agent to release the D-penicillamine from the NPs. The authors based this on the fact that glutathione is a highly concentrated non-protein thiol under normal physiological conditions that can participate in

disulfide exchange. However, the authors did not explore the glutathione system, but they surmise the role of NPs in the *in vivo* investigation of AD through copper chelation [179].

3.2.2. Thioflavin-T

The hydrophilic, charged, fluorescent marker Thioflavin-T (ThT) has been previously described as a probe for the detection of Aβ in senile plaques [122]. Härtig *et al* delivered the encapsulated ThT NPs (of the butylcyanoacrylate polymer) into the murine brain by direct intrahippocampal injection, and followed the photoconversion of the ThT from the NPs in fixed tissues, post injection [180]. Core shell latex particles were synthesized by the emulsion polymerization of styrene in a water-ethanol mixture containing ThT. These particles were used in the seeded, aqueous polymerization of butylcyanoacrylate (BCA), which contained additional ThT in the polymerization media. The resulting core-shell NPs were administered to the mice by direct hippocampal stereotaxic injection. The brains were fixed three days post injection, and the NPs were localized by photoconversion of the ThT in a closed chamber enriched with oxygen.

Light microscopy localized photoconverted NPs in the dentate gyrus, and vacuoles were found in the cytoplasm near the aggregated latex nanoparticles. Transmission electron microscopy (TEM) verified the presence of NPs in

microglia and neurons. Additionally, high-powered TEM demonstrated that ThT was delivered from the NPs. As a result, the authors suggest that ThT core-filled latex particles can be used to probe the intracellular synthesis of Aβ, as well as its extracellular deposition [181]. They have not delivered these NPs to the brain through the systemic circulation; however, the chemical similarity of these NPs to butylcyanoacrylates, which have been shown to cross the BBB after intravenous administration [174], regards this promising approach as a potential Aβ detection method.
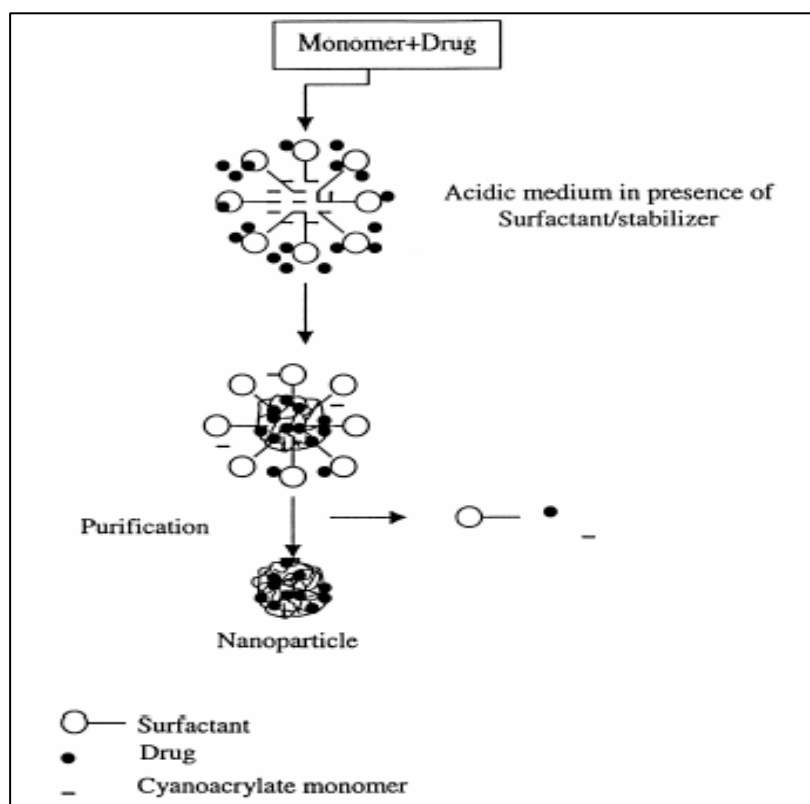
Fig. 4. Emulsion polymerization of alkylcyanoacrylates (Reprinted from J. Control. Rel. 70, K. S. Soppimath, A. R. Kulkarni, W. E. Rudziniski, T. M. Aminabhavi, Biodegradable polymeric nanoparticles as drug delivery devices, 1-20, © 2001, with permission from Elsevier).

LIST of SPECIFIC AIMS

1. **Crossing the Blood Brain Barrier**
   Hypothesis: Nanoparticles can be polymerized with the appropriate size, surface and surfactant characteristics, which render them suitable for passage across the blood brain barrier. Preliminary studies indicate that ^{125}ICQ has a residence time (in the brain) that is too short for sufficient brain imaging. Therefore, a drug carrier is required to improve the extravascuar retention of ^{125}ICQ. Butylcyanoacrylate nanoparticles (BCA NPs) were chosen as an appropriate drug carrier to increase the brain retention of ^{125}ICQ.

2. **Loading nanoparticles with amyloid affinity drugs**
   Hypothesis: Amyloid affinity drugs can be successfully radiolabelled, encapsulated within nanoparticles, and fully characterized *in vitro* and by *in vivo* biodistribution

3. **Labeling amyloid plaques with nanoparticles encapsulated with amyloid affinity drugs**
   Hypotheses: (1) Nanoparticles will act as drug carriers by delivering the desirable drugs to the brain tissue; (2) Amyloid proteins can be imaged using novel nanoparticles as drug carriers

4. **Labeling amyloid plaques with nanoparticles encapsulated with amyloid affinity drugs in the amyloid-bearing mice**
   Hypothesis: Amyloid plaques can be imaged with radiolabelled drugs that bind to them

RESULTS

4. CROSSING THE BLOOD BRAIN BARRIER

Hypothesis: Certain monomers polymerized to nanoparticles with the appropriate size, surface and surfactant characteristics will pass across the blood brain barrier

The purpose of this project was to develop novel imaging agents, and nanoparticles to transport these agents across the blood brain barrier in murine models of Alzheimer's disease, in order to radiolabel and microimage the amyloid-beta (Aβ) proteins responsible for the pathology. Some common radiolabels presently employed in *in vivo* Aβ microimaging include ^{11}C, ^{18}F, ^{123}I and ^{99m}Tc; common amyloid-binding dyes comprise derivatives of Thioflavins (T- and S-) and Congo red. Thus, the most important concern of the project was to synthesize *carriers* of amyloid-binding agents that have the appropriate characteristics of crossing the blood brain barrier. These carriers should have characteristics consistent with other agents that easily pass the BBB, thus they should be small, lipophilic, and neutral. To facilitate the small-animal imaging arm of the project, (i.e. good spatial and temporal resolution) the carriers should have a rapid clearance from the blood and the normal brain.

Nanoparticles were polymerized from n-butylcyanoacrylate monomers in acidic media (0.1N HCl), in the presence of surfactant (Tween 80, 1% v/v) and stabilizer (Dextran 70,000, 1%, w/v). The surfactant forms a micellar shell, into

which the drug is added during polymerization. The drug becomes encapsulated within the polymeric matrix, and after purification of the polymer, drug encapsulated nanoparticles ensue. Nanoparticles are advantageous because of their high loading capacities, which mean that more of the drug can be delivered to the target organ. Moreover, the matrix of the nanoparticles protects the incorporated drugs against degradation. They can also be designed to escape recognition by the reticuloendothelial system. Thus, drug delivery by nanoparticles can be both targeted and controlled. When the nanoparticles are designed with appropriate surfactants and suitable surface characteristics, they can cross the blood brain barrier.

4.1. BUTYLCYANOACRYLATE NANOPARTICLES

4.1.1. Experimental Methods and Procedures

4.1.1.1.Radioiodination of Clioquinol

CQ was radiolabelled with ^{125}I (2 mCi, Perkin Elmer) by the Chloramine-T (CT) method of radioiodination. All experiments were carried out under a radiochemistry hood, behind lead shielding; reagents were analytical grade, and purchased from Sigma Chemical Co. (St. Louis, MO). Briefly, the iodination of CQ (5-chloro-7-iodo-8-hydroxyquinoline, 100 μg) was carried out in a 16 x 100 mm reaction vessel, and catalyzed by HPO_4^- ion (30 μL, from 0.5M phosphate buffer, pH 7.4). CT (20 μg) was used as the oxidizing agent to release I_2 from

NaI. The reaction mixture was briefly vortexed (2 mins) before being stopped by the addition of metabisulfite (50 µg, added as a reducing agent). Purification of ^{125}I-CQ was performed by solvent extraction in dichloromethane (DCM) and H_2O. The organic layer (e.g. DCM) was evaporated under N_2 gas, and the ^{125}I-CQ was dissolved in dimethylsulfoxide (DMSO, 1mL). The ^{125}I-CQ was analyzed by thin layer radiochromatography (RTLC). The purity was > 95%.

4.1.1.2. Polymerization of n-Butylcyanoacrylate Nanoparticles

NPs were prepared by different polymerization techniques for *in vivo* biodistribution in order to find an appropriate candidate for *in vivo* imaging of amyloid beta plaques [182]. Briefly, the CQ was radioiodinated (please see section 10.1.1.1.) and incorporated within PBCA nanoparticles for the *in vivo* biodistribution in wild type Swiss webster mice (20-25 g). The NPs were polymerized as per the modified procedure of Kreuter *et al* [174]. Briefly, an acidic polymerization medium containing Dextran 70,000 and Tween-80 (polysorbate 80) were used (both at a concentration of 1% each in 0.1 N HCl) (Sigma, USA). ^{125}I-CQ (300 x 10^6 CPM) was added to the solution just prior to the addition of butylcyanoacrylate (BCA) monomer. Butylcyanoacrylate 1% (Sichelwerke, Hannover, Germany) was added under constant magnetic stirring at 400 rpm. After 3h of polymerization, the NP suspension was neutralized with 0.1

N NaOH to complete the polymerization. This solution was filtered with 0.2 μm filter and purified by ultracentrifugation (45K rpm, 1h). The pellet was washed and redispersed in water, which contained 1 % Tween-80. The PBCA nanoparticles were then overcoated with 1% Tween-80 by stirring for 30 min in phosphate buffer solution (PBS), just before *in vivo* administration. A 1 mg of the nanoparticle was administered by intravenous injection and the particle size was determined by a Zetasizer 3000 HS (Malvern, UK).

4.1.2. Preliminary Results

In preliminary experiments, the radiolabel $[^{125}I]$-iodo-deoxy uridine ($[^{125}I]dU$), was incorporated into cyanoacrylate nanoparticles. Two derivatives of the cyanoacrylate monomer were polymerized to yield a C_4 butyl- product (BCA) and a C_8 octyl- product (OCA). Physicochemical characterizations of the nanoparticles were performed, and the mean diameter of the prototype butylcyanoacrylate NPs was found at 45 nm (please see Fig. 5). Biodistribution was performed by *ex vivo* gamma (γ) counting of organs of interest, namely the brain, blood, liver and the spleen (please see Table 1 in Appendix 1). Briefly, animals were sacrificed at 2, 5, 15, 30, 60, 90, 120, 240 and 24 h post injection of the drugs (CQ-encapsulated NPs or non-encapsulated CQ); the organs of interest were extracted and analyzed by scintillation counting.
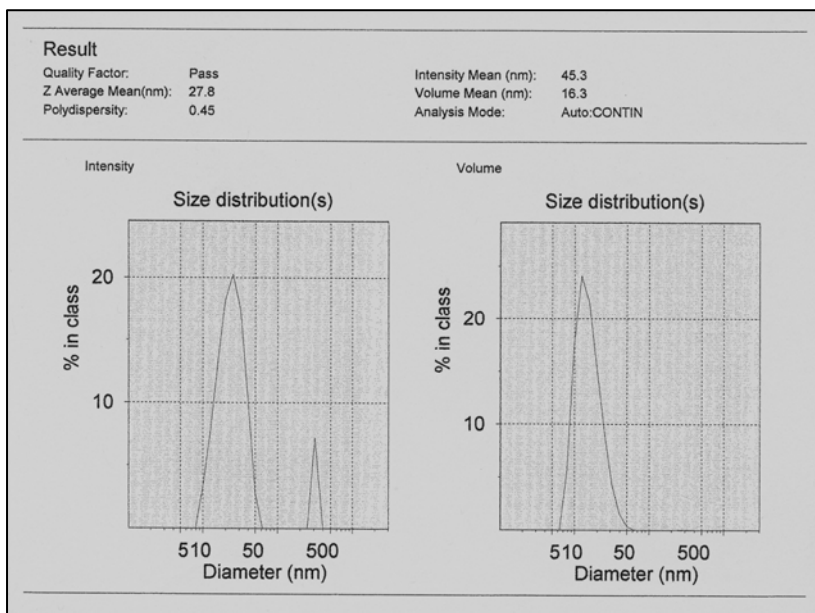
Fig. 5. Dynamic Light Scattering (DLS) data of n-Butyl-2-cyanoacrylate NPs showing the size distribution of the NPs in solution, mean diameter 45nm (3/20/03). Both graphs depict the size distribution of the NPs in solution, over the range of 5 nm to 500 nm. The graph on the left depicts size distribution when the fractional intensity of the NPS (in solution) was considered (the smaller peak at 500 nm may have been due to an impurity in the solution). The graph on the right depicts size distribution when the volume of the NPS (in solution) was considered.

4.1.3. DISCUSSION

The incorporation of the [125I]dU radiolabel into the nanoparticles permitted key interpretation of the activities of the radiolabelled complex in the

wild type murine system. First, the surfactant-coated (Tween-80) **nanoparticles cross the blood brain barrier**, and enhance the uptake of the radiolabel [^{125}I]dU (versus the brain uptake of [^{125}I]dU administered as a free drug). Secondly, NPs whose surfaces are not coated with surfactants do not easily cross the BBB. This is because surfactant surface coating increases the lipophilicity of the NPs. In addition, when the radiolabel is encapsulated within both cyanoacrylate derivatives (OCA and BCA NPs), the wild type mice have a higher brain uptake of the [^{125}I]dU encapsulated within the OCA NPs, versus the [[^{125}I]dU within the] BCA NPs; however, by personal experience, reproducibility of OCA was a problem. Moreover, [^{125}I]dU only provides a source of gamma emitting radioisotope. The [^{125}I]dU has no affinity for amyloid plaques, and therefore, the ligand has no functional relevance to Alzheimer's disease. Consequently, the choice of radioligand had to be concentrated towards a compound with more specificity for the amyloid-beta plaques. Furthermore, given the limited reproducibility of the octylcyanoacrylates, it was decided to expand the polymers/polymeric techniques with which to attempt to deliver drugs across the BBB. **Nontheless, the conclusion to Specific Aim 1 is that NPs can be successfully polymerized with the appropriate surface characteristics to cross the blood brain barrier. Fundamentally, NPs with the encapsulated**

radiolabel show an increased brain uptake when compared to the unencapsulated control.

4.2. MICROEMULSIONS

In a second technique, called oil-in-water-microemulsion, solid NPs were engineered (as per the modified method of Koziara *et. al.* [183]) from microemulsion templates using emulsifying wax or Brij 72 as the oil phase matrix material.

4.2.1. Experimental Methods and Procedures

Emulsifiying wax (2 mg, Spectrum Chemicals) (or 2 mg Brij 72, Reuger Chemicals) and water (1 mL) were added together and stirred while heating (60-65 °C). To this mixture, either Brij 78 (3mM, Reuger Chemicals) or Tween-80 (0.1 mL) was added as the surfactant. A variety of experiments with combinations of the surfactant and oil phase matrix material(s) were performed. Stirring continued, but the temperature was discontinued to allow spontaneous particle formation. The nanoparticles were isolated by microcentrifugation (13K RPM, 15 mins), and analyzed by Dynamic Light Scattering (DLS, Zetasizer 3000 HS, Malvern, UK). The various amyloid affinity dyes (e.g. Congo red, Thioflavin-S,

Thioflavin-T) were adsorbed onto the surfaces of the NPs, and the polydispersive

indices were determined (please see Appendix 2).

4.2.2. RESULTS
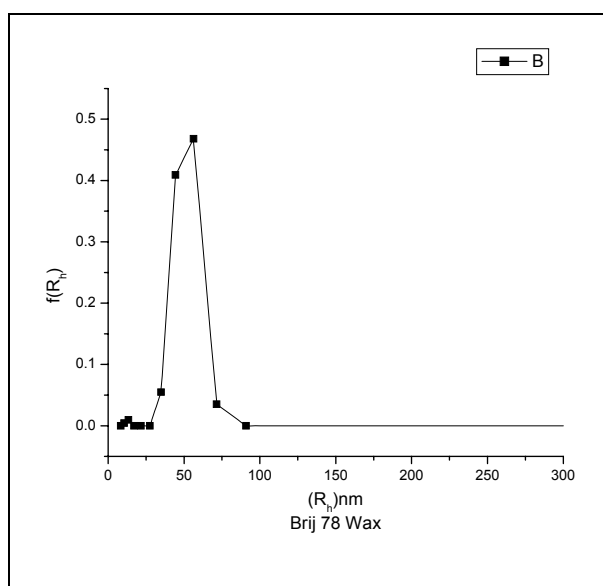
Fig. 6. Emulsifiying Wax nanoparticles (with Brij 78 surfactant, no dye), mean radius 50nm (6/13/03)

4.2.3. DISCUSSION

Adsorption of the dyes onto the nanoparticles did not significantly increase the mean radii of the particles. For example, the average radius (R_h) of unloaded Emulsifying wax/Brij 78 NPs is 50 nm. After *adsorbing* Congo red onto the surfaces of the nanoparticles (by stirring an aliquot of the dye in the reaction media) the average radius of the Brij 72/Tween-80 nanoparticles was 75 nm, and the average radius of the Emulsifying wax/Brij 78 nanoparticles was 70 nm (please see Appendix 2). However, isolation of the dye-associated nanoparticles by dialysis was futile, due to the affinity of the charged dyes (e.g. Congo red) with the dialysis bags. Furthermore, charged dyes do not easily pass the BBB, and consequently, no further studies were pursued using this approach.

4.2.4. **Chapter Four Appendices (1-6)**

Appendix 1. *In vivo* biodistribution of [^{125}I]dU in normal mice.

Table 1. *In vivo* biodistribution of [^{125}I]dU in normal mice. Biodistribution studies of wild type mice injected with the [^{125}I]dU (as a free drug), and injected with the [^{125}I]dU   encapsulated within octyl and butyl cyanoacrylate nanoparticles, the surfaces of which were coated with the surfactant Tween-80 (denoted by the terms butyl coated or octyl coated). Measurements were by *ex vivo* γ counts of organs of interests (in counts per minute (CPM)). The ID was 1,097,368 CPM [^{125}I]dU in 1.2 mg NPs. At 15, 60, and 120 minutes, there is increased brain uptake of the [^{125}I]dU encapsulated nanoparticles, as compared to the free [^{125}I]dU. More specifically, there is increased brain uptake of the [^{125}I]dU encapsulated octyl coated nanoparticles, as compared with the ([^{125}I]dU) butyl coated nanoparticles. (4/30/02-10/23/02)

Group	Time (min)	Blood/g ± SEM	Brain/g ± SEM	Spleen/g ± SEM	Liver/g ± SEM
[^{125}I]dU Control	15	2333 ± 214	143 ± 50	2070 ± 514	1237 ± 155
Butyl coated		8933 ± 304	228 ± 22	2174 ± 89	2297 ± 183
Octyl coated		4868 ± 312	312 ± 33	1996 ± 264	4319 ± 338

p = 0.05

Group	Time (min)	Blood/g ± SEM	Brain/g ± SEM	Spleen/g ± SEM	Liver/g ± SEM
[^{125}I]dU Control	60	2022 ± 467	65 ± 22	1298 ± 169	1026 ± 309
Butyl coated		3294 ± 60	212 ± 15	1597 ± 575	2898 ± 379
Octyl coated		2164 ± 68	310 ± 47	1237 ± 34	1020 ± 70

p = 0.05

Group	Time (min)	Blood/g ± SEM	Brain/g ± SEM	Spleen/g +/- SEM	Liver/g ± SEM
[^{125}I]dU Control	120	1105 ± 108	52 ± 5	1166 ± 562	930 ± 111
Butyl coated		1973 ± 33	107 ± 7	1281 ± 457	1499 ± 437
Octyl coated		860 ± 86	155 ± 14	653 ± 56	435 ± 45

p = 0.05

Brain Uptake of [^{125}I]dU at 60 minutes

Activity (CPM)

Brain/g

control
butyl coated
octyl coated

Brain Uptake of [^{125}I]dU at 15 minutes

Activity (CPM)

Brain/g

control
butyl coated
octyl coated
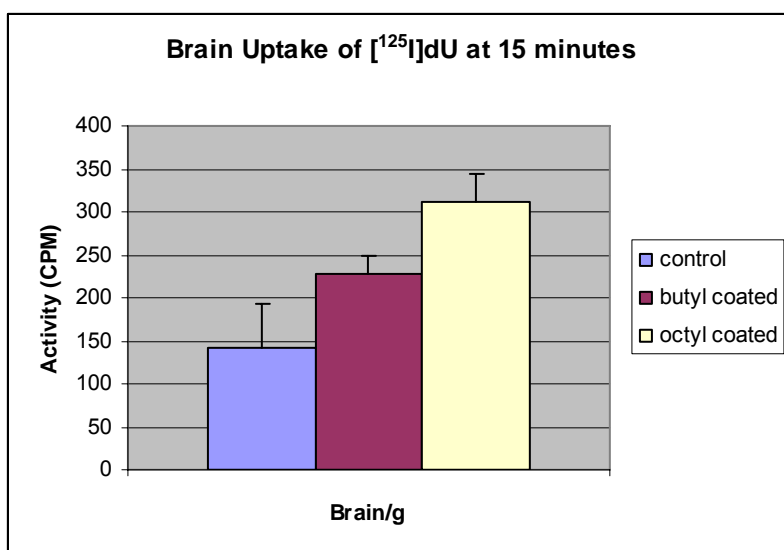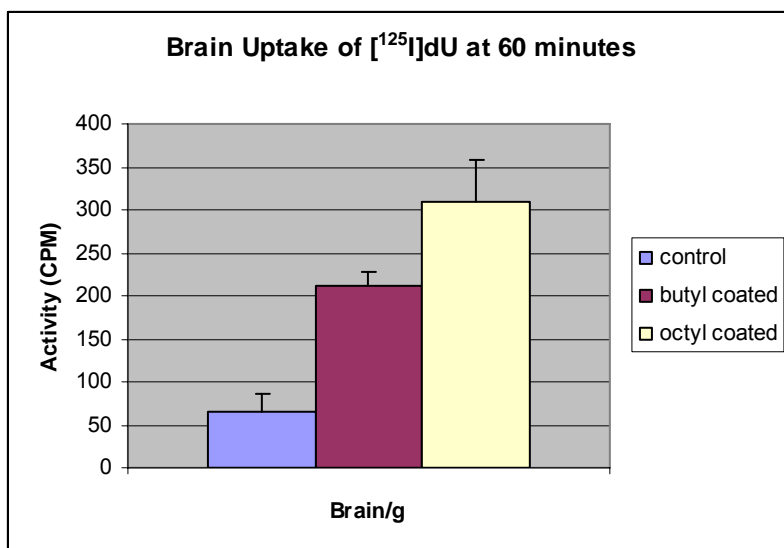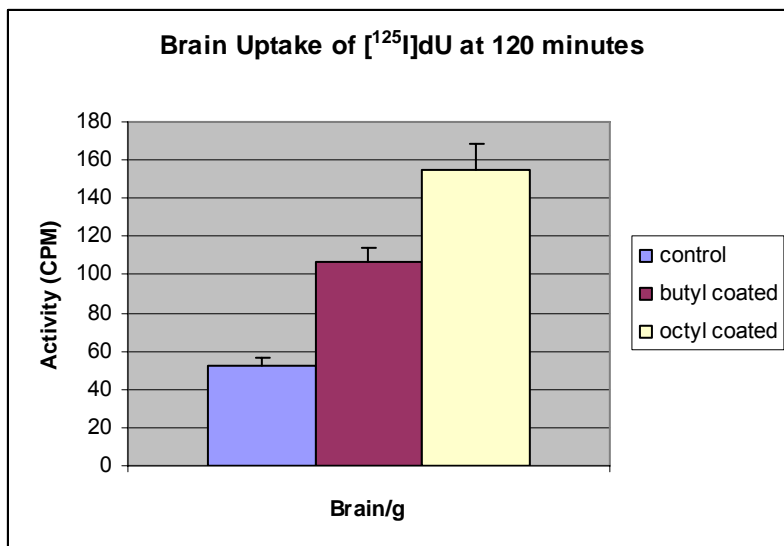
Figure 1. *In Vivo* brain uptake of [^{125}I]dU-n-octyl- (OCA) and n-butyl-cyanoacrylate (BCA) nanoparticles in wild type mice at 15, 60 and 120 min (mean ± SEM). This graphical data represents the values listed in Table 3 (please see pg. 63). Note higher brain uptake of both NP derivatives versus the free [^{125}I]dU (control) at each time interval. Octyl nanoparticles show enhanced brain uptake (of the [^{125}I]dU*) versus butyl nanoparticles, however OCA NPs are difficult to reproduce. (4/30/02-10/23/02).

Appendix 2. DLS of Microemulsions
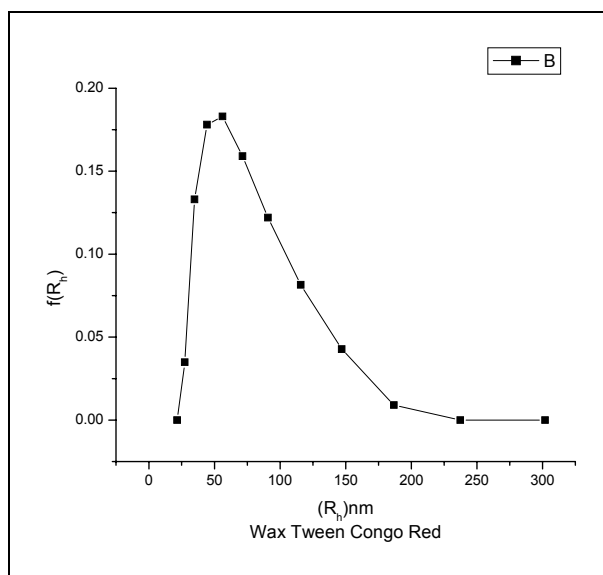
Figure 2. Emulsifying Wax nanoparticles (with Brij 78, tween-80 surfactants, loaded with congo red dye) mean radius 70nm (6/17/03)
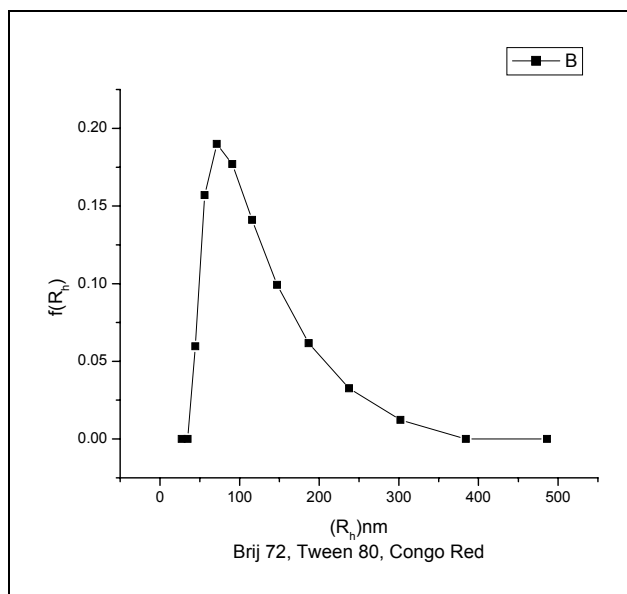
Figure 3. Brij 72 nanoparticles (with Tween-80 surfactant, congo red dye) mean radius 75nm (6/18/03)
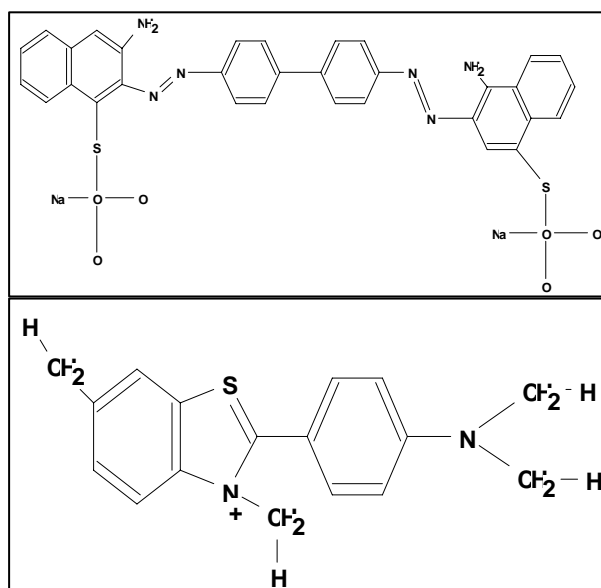
Figure 4. Structure of Congo red (top), MW = 696.7 and Thioflavin-T (bottom), MW = 318.9

Appendix 3. DLS data of n-Butylcyanoacrylates with Amyloid Affinity Dyes
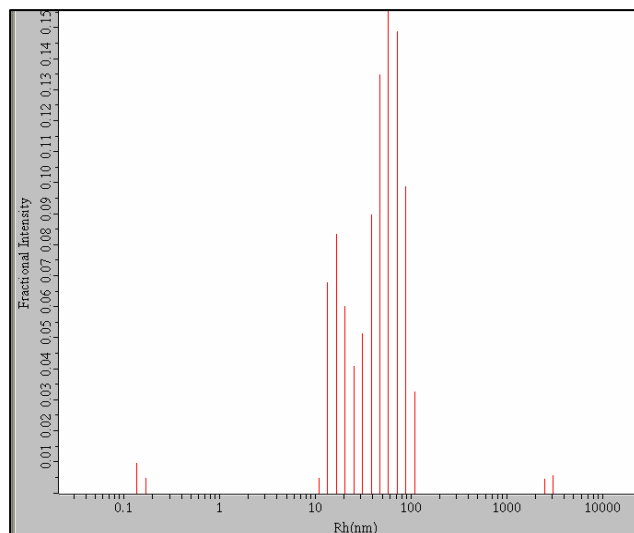
Figure 5. DLS data of CR NP; Rh = 36.7 ± 0.3 nm (1% Tween-80) (mean ± SEM);
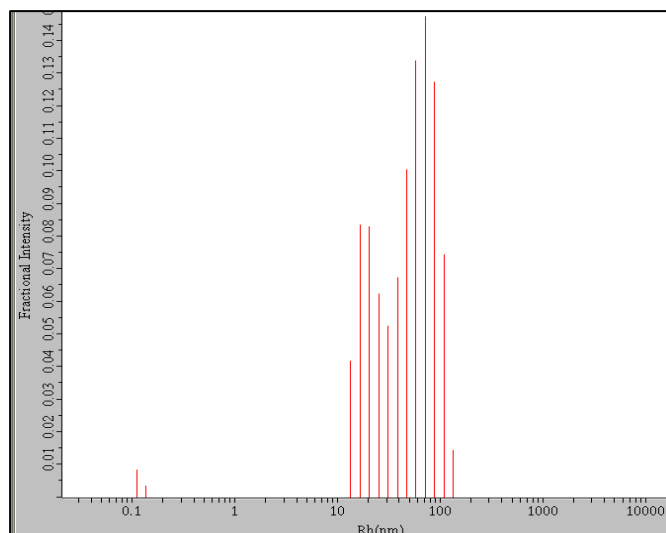
Figure 6. DLS data of ThT NP; Rh = 39.3 ± 0.3 nm (1% Tween-80) (mean ± SEM)
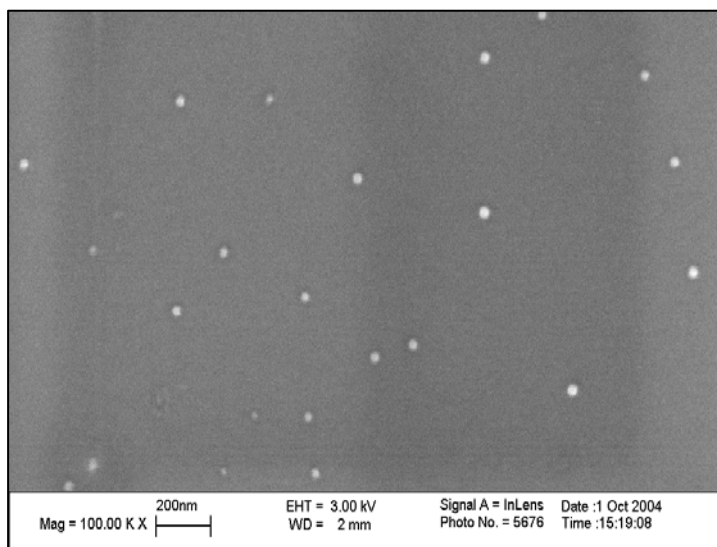
Figure 7. SEM, ThS NP
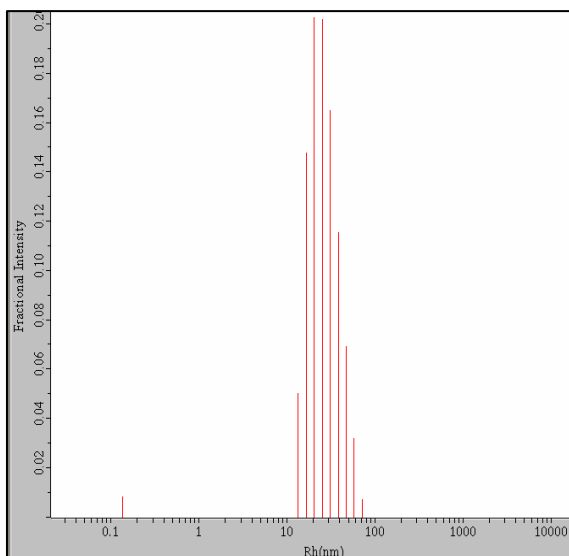
Figure 8. DLS data of ThS NP; Rh = 23.5 ± 0.1 nm (1% Tween-80) (mean ± SEM)
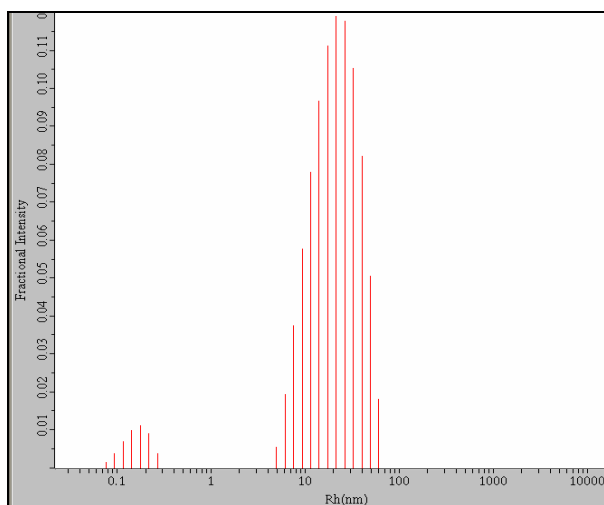
Figure 9. DLS data of 0.1% Congo red loaded nanoparticles coated with 2 % Tween-80; Rh = 19.4 ± 0.4 nm (mean ± SEM); (08/09/04)
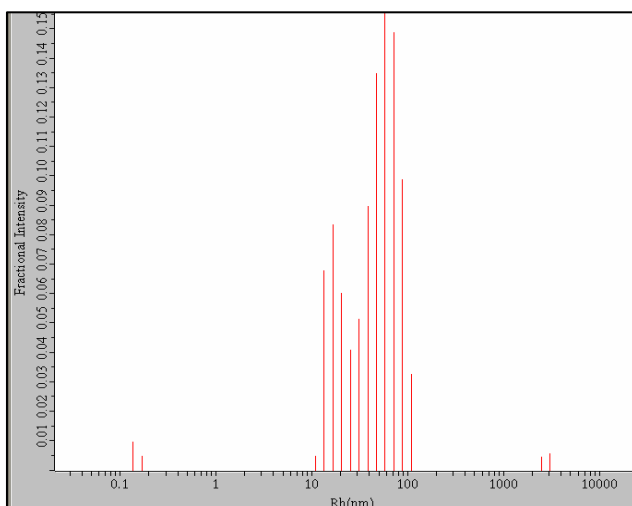
Figure 10. DLS data of 0.1% Congo red loaded nanoparticles coated with 1 % Tween-80; Rh = 36.7 ± 0.3 nm (mean ± SEM); (10/01/04)
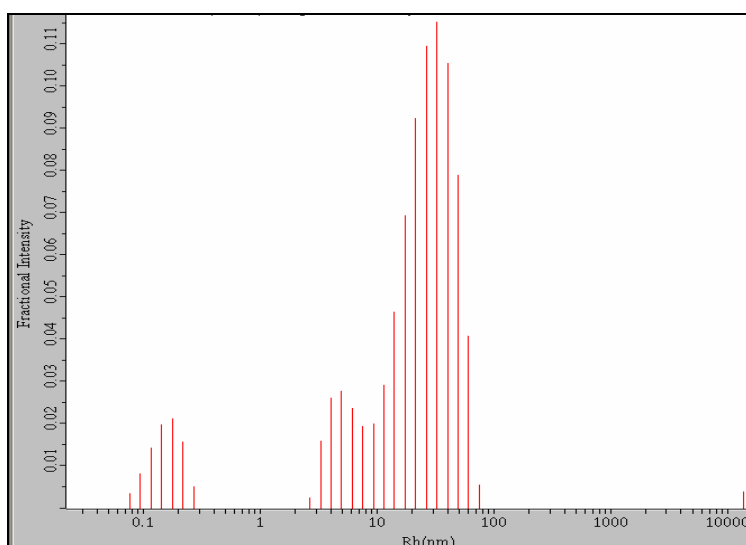
Figure 11. DLS data of 0.1% Thioflavin-T loaded nanoparticles over-coated with 2 % Tween-80; Rh = 19.1 ± 0.4 nm (mean ± SEM); (08/09/04)
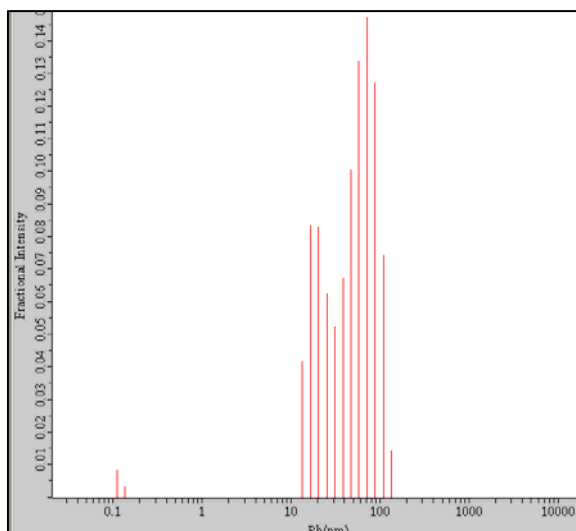
Figure 12. DLS data of 0.1% Thioflavin-T loaded nanoparticles over-coated with 1 % Tween-80; Rh = 39.3 ± 0.3 nm (mean ± SEM); (10/01/04)
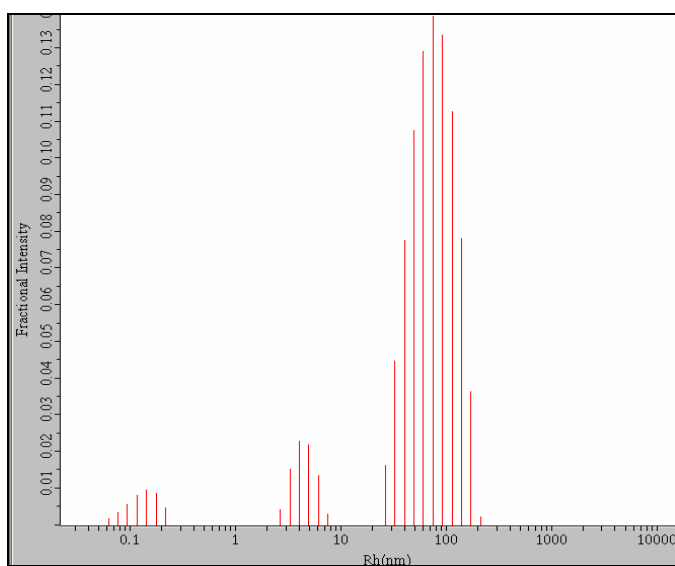
Figure 13. DLS data of 0.1% Thioflavin-S loaded nanoparticles over-coated with 2 % Tween-80; Rh = 50 ± 1.4 nm (mean ± SEM); (08/09/04)
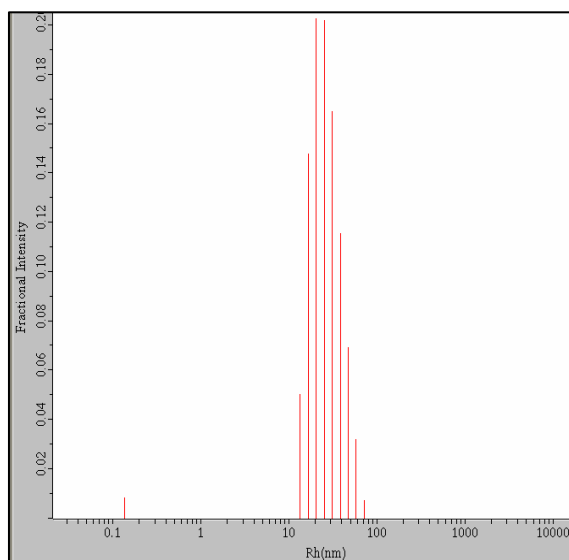
Figure 14. DLS data of 0.1% Thioflavin-S loaded nanoparticles over-coated with 1 % Tween-80; Rh = 23.5 ± 0.1 nm (mean ± SEM); (10/01/04)

Appendix 4. Surfactant Effects on n-Butylcyanoacrylates
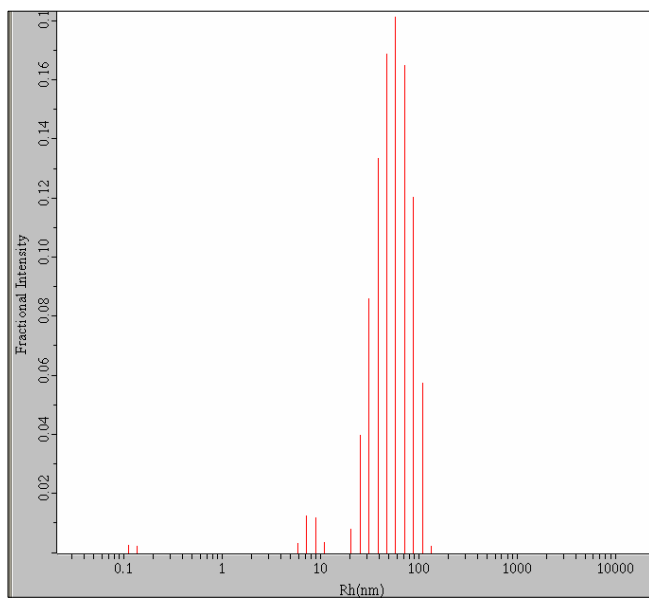
Figure 15. DLS data of BCA NPs polymerized in 1% Tween-80; Rh = 46.8 ± 0.3 nm (mean ± SEM) ; (02/04/05)
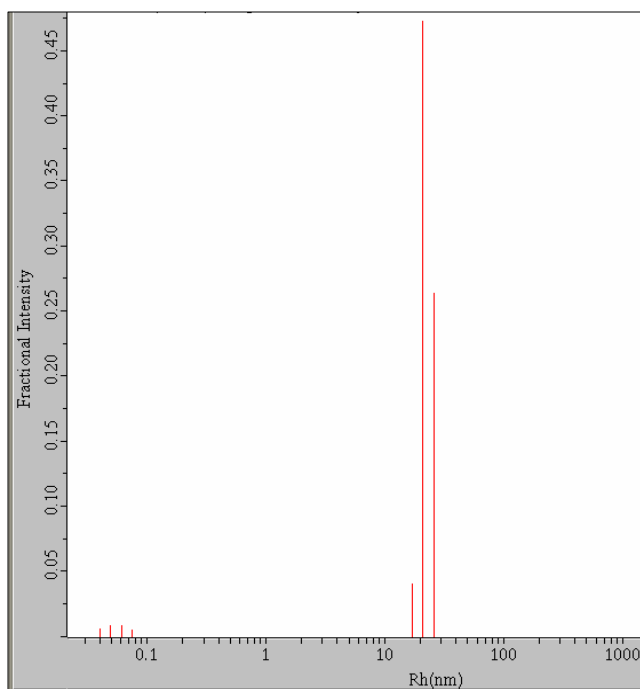
Figure 16. DLS data of BCA NPs polymerized in 2 % Tween-80; Rh = 20.5 nm ± 1.4 (mean ± SEM); (02/04/05)
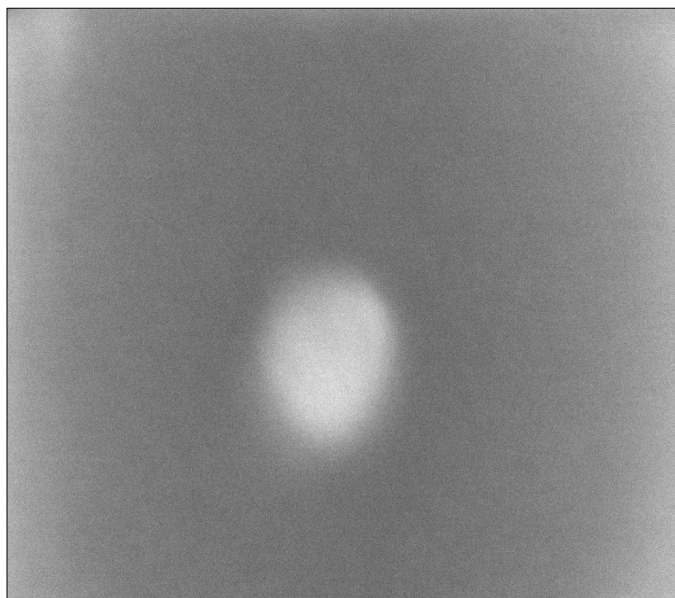
Figure 17. SEM of individual BCA NP (polymerization performed in 1% Tween-80)
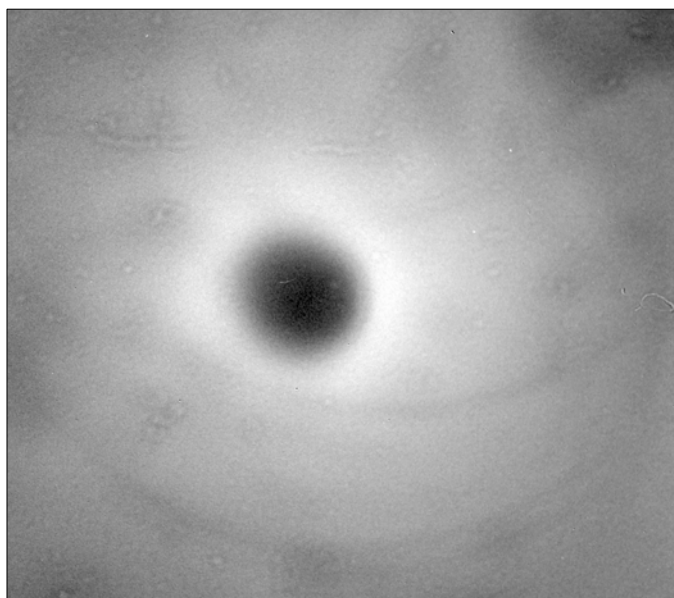
Figure 18. TEM of individual BCA NP (polymerization performed in 1 % Tween-80)
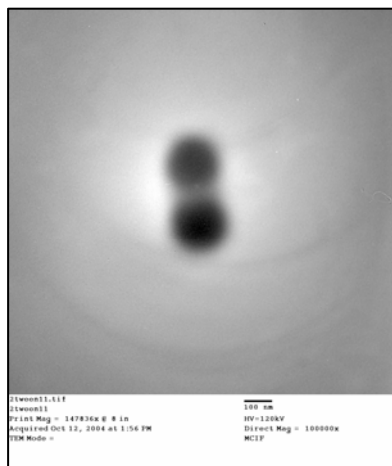
Figure 19. TEM of two BCA NPs (polymerization performed in 2% Tween-80)

Appendix 5. Effect of Acid Concentration on n-Butylcyanoacrylates
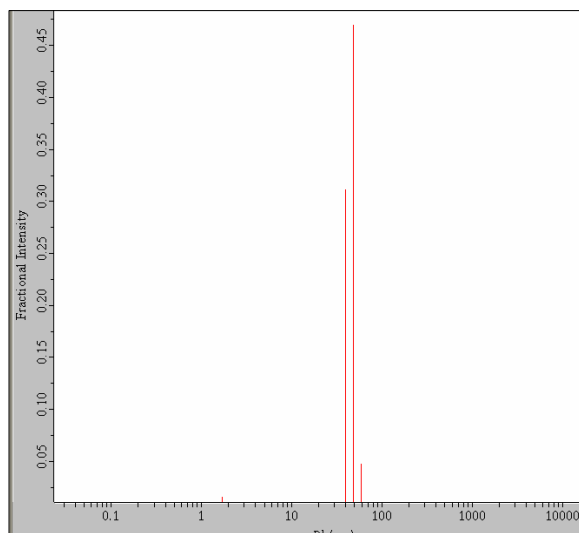
Figure 20. DLS data of NPs polymerized at pH 3; Rh = 58 nm (1% Tween-80, surfactant)
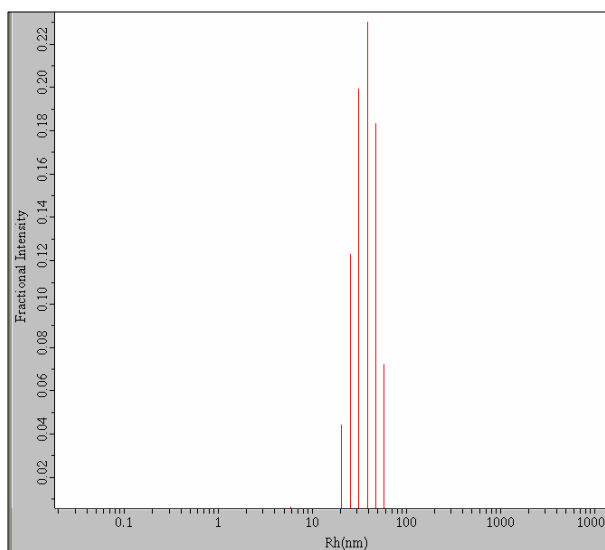
Figure 21. DLS data of NPs polymerized at pH 2; Rh = 41 nm (1 % Tween-80, surfactant)
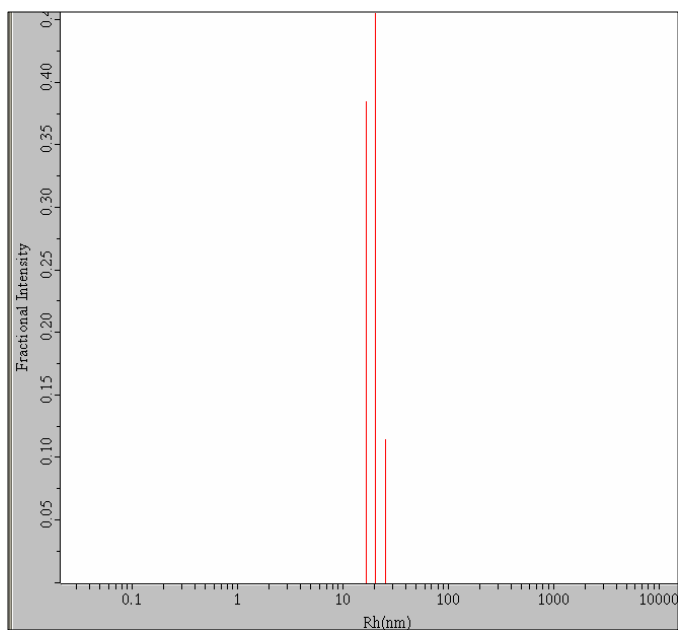
Figure 22. DLS data of NPs polymerized at pH 1; Rh = 20 nm (1 % Tween-80, surfactant)

Appendix 6. Clearance of ^{125}I-CQ-BCA-NPS and ^{125}I-CQ in Blood and Brain
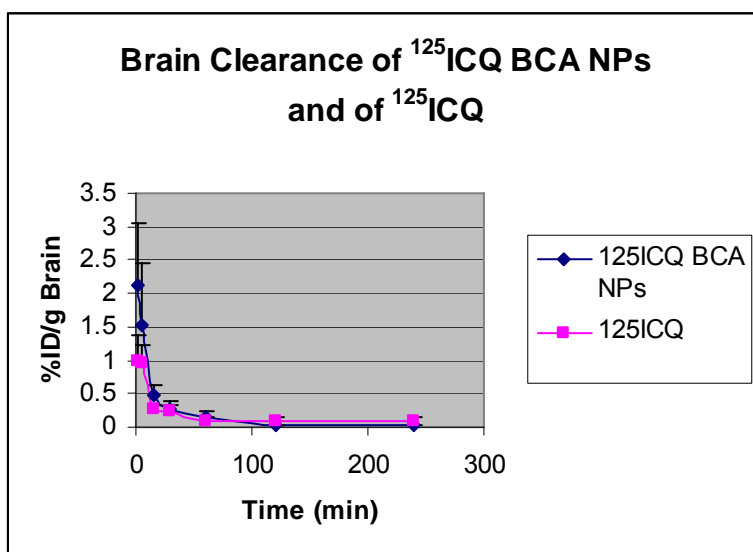
Figure 23. Brain clearance of ^{125}I-CQ-BCA-NPs and ^{125}I-CQ; IV administration; NPs formulated in 1 % Tween-80 with 1 % Dextran 70,000 stabilizer; ^{125}I-CQ diluted in 1X PBS
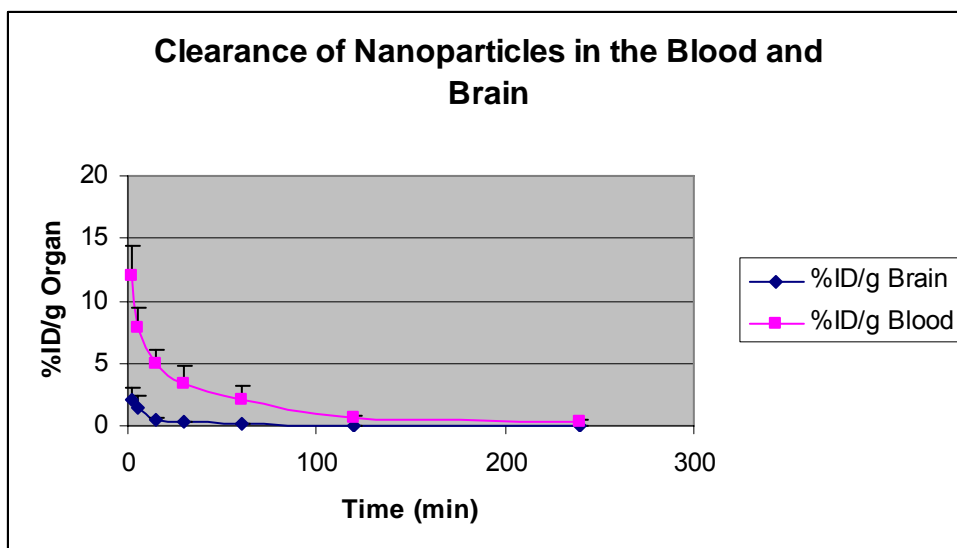
Figure 24. *In vivo* clearance of ^{125}ICQ BCA NPs in the blood and brain

5. LOADING NANOPARTICLES WITH THE AMYLOID AFFINITY DRUGS

Hypothesis: Amyloid affinity drugs can be successfully radiolabelled and encapsulated within nanoparticles. This carrier complex can be fully characterized by in vitro methods, and by in vivo biodistribution

Amyloid beta plaques are hypermetallated since the concentration of metals in the brain increases with age. Specifically, Aβ plaques are hypermetallated with Cu^{2+}, Fe^{3+} and Zn^{2+} metal ions. In particular, however, the Cu^{2+} and Fe^{3+} ions are redox active. Thus, when the Aβ metalloprotein presents Cu^{2+} in the presence of O_2 and endogenous reducing agents such as vitamin C or cholesterol, redox cycling occurs and produces hydrogen peroxide (H_2O_2). The H_2O_2 oxidizes the reduced metal ions (e.g. from Fe^{2+} to Fe^{3+}), and subsequently, reacts (with O_2) to form deadly hydroxyl (OH^-) radicals. These radicals function to damage DNA, oxidize lipids and proteins, and aggregate proteins, including the Aβ protein. This phenomenon, which is called oxidative stress, is also seen in other neurodegenerative disorders. For example, the defective superoxide dismutase protein of Lou Geherig's disease also leads to oxidative stress, as do the alpha synuclein protein of Parkinson's disease and the α-crystallin protein, the latter implicated in cataracts.

To elucidate zinc's role in AD pathology, Ashley Bush of Harvard University has shown that Zinc precipitates Aβ at physiological pH [57, 64]. And,

Lee has shown that when the zinc receptor is knocked out in experimental mice, and those mice are crossed with AD transgenic mice, their progeny have a significantly reduced cerebral deposition of the Aβ protein [74]. But, zinc plays a dual role, because it both precipitates the protein and suppresses the production of hydrogen peroxide [72]. However, Opazo has shown that the plaques are not loaded with enough zinc to sufficiently abolish the oxidative effects of the peroxide [73]. Furthermore, at low pH, zinc is displaced by copper, which largely mediates the production of H_2O_2 [73]. **The hypothesis of this project is that the metal ion binding sites on amyloid beta aggregates provide a target for the development of new diagnostic and therapeutic agents.** *The hypothesis was tested with a prototype chelator of copper, zinc and iron metal ions, called Clioquinol, or CQ.*

Clioquinol is a USP approved antibiotic that is hydrophobic and freely crosses the blood brain barrier. It binds copper, zinc and iron metal ions, and it inhibits the production of H_2O_2. Such actions prevent the manufacture of the deadly hydroxyl radicals which are responsible for the aggregation of the Aβ metalloprotein. In the 1970s, Clioquinol was withdrawn as an oral antibiotic in humans because it was associated with a neurological disorder called subacute myelo-optic neuropathy (SMON), and was speculated to be initiated by vitamin B_{12} deficiency; the chelator has since been proven as a safe therapeutic option with B_{12} supplements.

5.1.1. EXPERIMENTAL METHODS AND PROCEDURES

5.1.1.1.Radioiodination of CQ

To quantitatively study the effects of CQ, the drug was radiolabelled with ^{125}I (2 mCi, Perkin Elmer) by the Chloramine- T (CT) method of radioiodination (please see section 10.1.1.1.).

5.1.1.2.*In Vitro* Labeling Of Amyloid Plaques

In vitro assays were performed by incubating human post-mortem (1 mg) cortical frontal AD and control brain tissue (15 min incubation time, 800 µL buffer solution of 0.1 % FBS in 1X PBS) in the presence of ^{125}I-CQ (7 x 10^5 CPM in 100 µL PBS). Brain homogenates were centrifuged (13K RPM, 15 mins) and the percent binding was calculated (please see Fig. 7).

5.1.2. RESULTS

5.1.2.1.*In Vitro* Binding Of ^{125}I-CQ To Brain Tissue
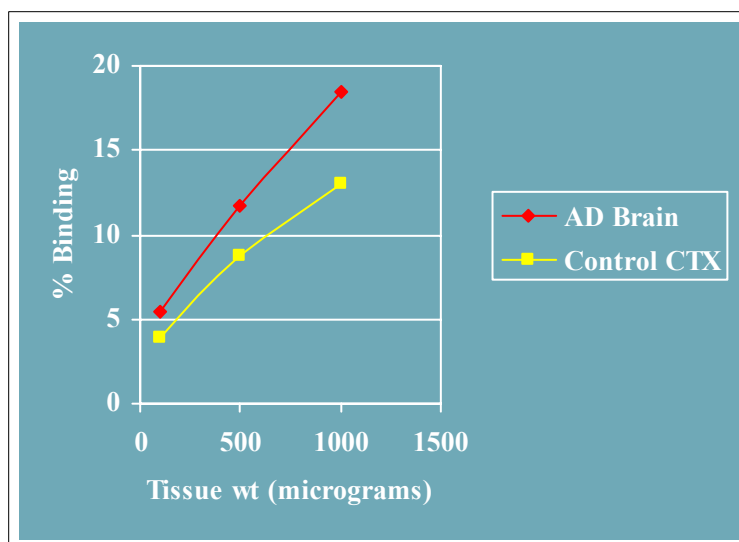
Fig. 7. *In vitro* binding of ^{125}I-CQ to Brain Homogenates

5.1.2.2.PHYSICOCHEMICAL DATA
5.1.2.2.1. DLS Data Of n-Butylcyanoacrylates (Zetasizer 3000HS instrument, Malvern, UK)
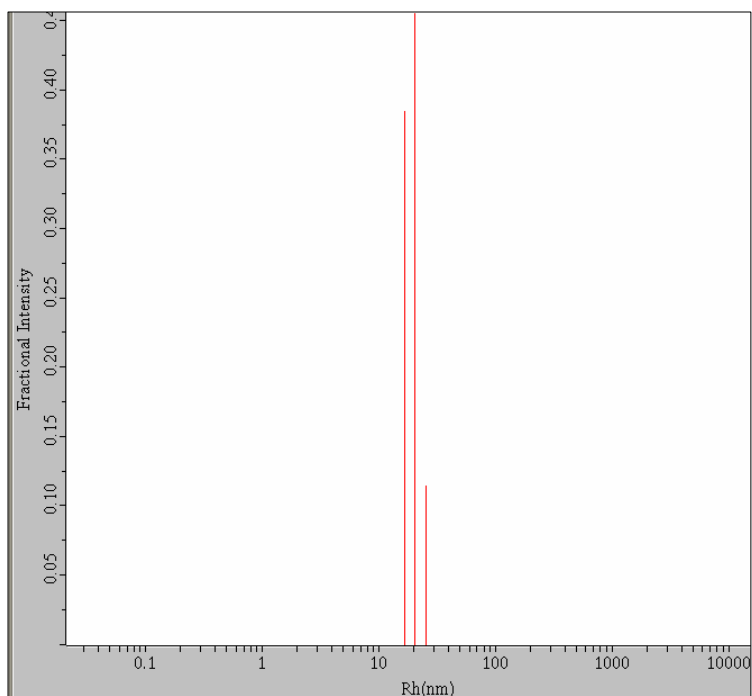
Fig. 8. DLS data of unloaded BCA NP; pH 1; Rh = 20 nm (1 % Tween-80)

Table 3. Summary of surfactant effects on the Rh of NPs loaded with amyloid affinity dyes

Dye	Surfactant concentration	Radius (nm)
0.1 % Congo red	2%	19.4
0.1 % Congo red	1%	36.7
0.1 % Thioflavin-T	2%	19.1
0.1 % Thioflavin-T	1%	39.3
0.1 % Thioflavin-S	2%	50
0.1 % Thioflavin-S	1%	23.5

Table 4. Summary of surfactant effect on unloaded nanoparticles

Date	Surfactant Concentration	Radius (nm)
10/1/04	1 %	39.6
2/4/05	1 %	46.8
2/4/05	1 %	30
8/9/04	2 %	19
10/21/04	2 %	15
2/4/05	2 %	20.5
10/1/05	2 %	23.2

Table 5. Effect of acid concentration on average radius of NPs (polymerized with 1% Tween-80)

pH	Rh (nm)
3	58
2	41
1	20

5.1.2.2.2. *In Vivo* Biodistribution of ^{125}I-CQ BCA NPs

Table 6. *In Vivo* Biodistribution of ^{125}I-CQ-BCA-NPs by IV Administration in wild type mice (n = 105) (NP polymerized in the presence of 1 % Dextran 70,000 and 1 % Tween-80; table represents organ uptakes in %ID/g ± SD)

Time (min)	Brain	Blood	Spleen	Liver	Brain:Blood Ratio
2	2.3 ± 0.9	12 ± 2.5	1.6 ± 0.4	15 ± 2.1	0.2 ± 0.1
5	1.5 ± 0.9	7.9 ± 1.6	1.8 ± 0.5	11.4 ± 1.5	0.2 ± 0.1
15	0.5 ± 0.2	4.9 ± 1.2	1.4 ± 0.5	8.1 ± 2.1	0.1 ± 0.1
30	0.3 ± 0.1	3.4 ± 1.5	0.9 ± 0.7	6.6 ± 2.4	0.1 ± 0.0
60	0.2 ± 0.1	2.1 ± 1.1	0.5 ± 0.3	3.9 ± 1.6	0.1 ± 0.0
120	0.03 ± 0.0	0.7 ± 0.2	0.2 ± 0.03	2.3 ± 0.4	0.1 ± 0.0
240	0.02 ± 0.0	0.4 ± 0.0	0.1 ± 0.1	1.4 ± 0.1	0.01 ± 0.0

$p = 0.05$

Table 7. *In Vivo* Biodistribution of ^{125}I-CQ by IV Administration in wild type mice (n = 105) (table represents organ uptakes in %ID/g ± SD)

Time (min)	Brain	Blood	Spleen	Liver	Brain:Blood Ratio
2	1 ± 0.4	9.2 ± 2.8	2.6 ± 0.1	12.5 ± 0.8	0.1 ± 0.1
5	1 ± 0.3	5.7 ± 1.3	N/A	15.5 ± 5.6	0.2 ± 0.01
15	0.3 ± 0.1	2.9 ± 0.7	1.2 ± 0.1	3.8 ± 0.7	0.1 ± 0.1
30	0.3 ± 0.1	2.3 ± 0.4	1.3 ± 1	5.2 ± 2.2	0.1 ± 0.1
60	0.1 ± 0.1	1.3 ± 0.7	0.5 ± 0.3	3.6 ± 2.3	0.3 ± 0.5
120	0.03 ± 0.03	0.1 ± 0.1	0.6 ± 0.4	1.3 ± 0.5	0.2 ± 0.1
240	0.04 ± 0.02	0.6 ± 0.2	0.4 ± 0.3	0.9 ± 0.2	0.1 ± 0.1

$p = 0.05$

5.1.2.2.3. NP Stabilizer Effect

In this experiment, PEGylated nanoparticles were polymerized as per the the modified method of Kreuter [174]. PEG was used as the stabilizer instead of Dextran 70,000. Briefly, 1% w/v BCA monomer was magnetically stirred in the presence of 25 mL 0.1N HCl, 1% PEG and 1% Tween-80 for 3 hours. Neutralization, filtration and centrifugation of the PEGylated NPs was the same as the procedure for the NPs polymerized with Dextran stabilizer. Although we were able to corroborate literature findings of decreased RES uptake of PEGylated NPs, we did not find that PEGylation increased brain uptake (please see Appendix 7). Figure 39 shows the effect of PEGylated NPs on the RES system. Namely, the organs of the RES (e.g. spleen, liver) have a reduced uptake

of the PEGylated NPs (please see Appendix 7), versus the NPs polymerized with

Dextran-70,000 (please see Appendix 7).

5.1.2.2.4. Effect of Route of Administration on NP Brain Uptake
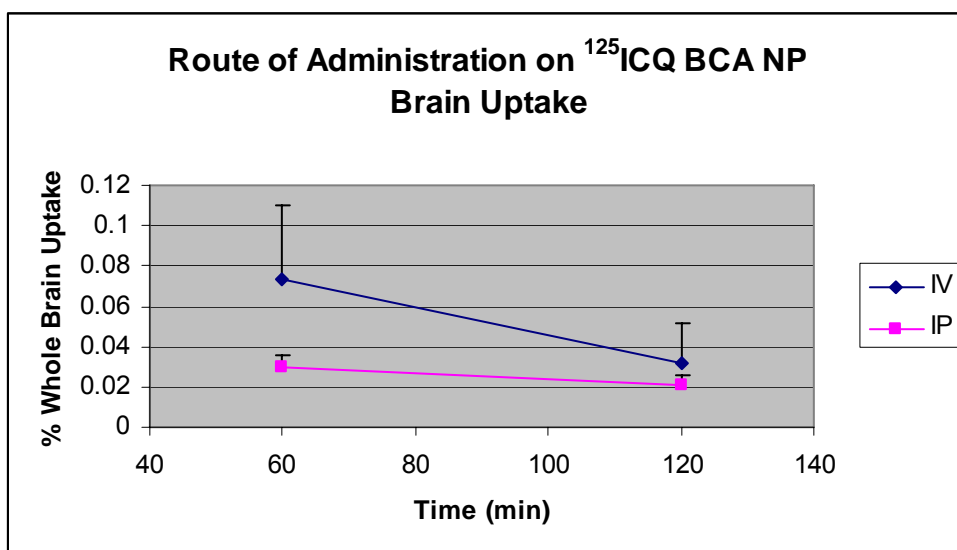
Fig. 9. IV administration enhances brain uptake

5.1.2.3.DISCUSSION
5.1.2.3.1. *In Vitro* Binding

The experimental results provided evidence of preferential binding by ^{125}I-CQ to the AD brain tissue, as compared to cortical control brain tissue. **Thus, it**

was shown that an amyloid-affinity drug could be successfully radiolabelled; the radioligand discriminated between AD brain tissue and control brain tissue.

5.1.2.3.2. Encapsulation of BCA NPs With Amyloid Dyes

The CQ was successfully radiolabelled, and ^{125}I-CQ was an effective discriminant between AD and control brain tissue. Prior to encapsulating the ^{125}I-CQ into the butylcyanoacrylate nanoparticles, the *in vitro* integrity of the BCA drug carrier system had to be proven in the presence of a more common scheme (e.g. Congo red, Thioflavin-T, Thioflavin-S). Thus, the physicochemical characteristics of BCA NPs were assessed by various techniques, which included using the amyloid dyes as well as varying surfactants, stabilizers, and acid concentrations. *In vivo* biodistribution of BCA NPs in wild type Swiss Webster mice was performed using the encapsulated ^{125}I-CQ and the free ^{125}I-CQ as control (please see Tables 6 and 7).

Polymerization and isolation of unloaded NPs yielded a mean radius (Rh) of 20 nm (Fig. 8), with a narrow size distribution range. The size distribution range of the CR NPs was slightly broader than the range of NPs; however, the mean radius of the CR NPs was only 36.7 nm (Table 3). Therefore, the drug encapsulation (0.1 % loaded) did not appreciably change the sizes of the

nanoparticles. The same was true of the NPs which were loaded with Thioflavin-T; the mean radius of the ThT NPs was 39.3 NPs (Table 3). More significantly, however, the mean radius of the Thioflavin-S nanoparticles (ThS NPs) was 23.5 nm (Table 3).

5.1.2.3.3. Effects of Surfactant and Acid Concentrations

While the encapsulation of the dyes (added at a concentration of 0.1% v/v during polymerization) showed no appreciable effect on the sizes of the nanoparticles, it was found that changes in the concentrations of the surfactant (Tween-80) and acid media (HCl) significantly affected NP size. For example, NPs polymerized at higher $[H^+]$ (lower pH), and higher surfactant concentrations (2 % vs. 1 % v/v), yielded smaller sized particles (please see Tables 4 and 5). With ultimate intentions of crossing the blood brain barrier *in vivo*, the smaller sized particles are most desirable.

Similar effects (of smaller sized particles at increased surfactant concentrations) were seen when the nanoparticles were loaded with the amyloid-affinity dyes. For example, CR NPs polymerized in 2 % Tween-80 yielded particles with an average Rh of 19.4 nm (Table 3), while CR NPs polymerized in 1 % Tween-80 had an average Rh of 36.7 nm (Table 3). Likewise, ThT NPs that were surface-coated in 2 % Tween-80 had average radius of 19.1 nm (Table 3),

while ThT NPs surface-coated with 1 % Tween-80 had an average radius of 39.3 nm (Table 3). However, the ThS encapsulated nanoparticles did not follow this trend. For example, ThS NPs polymerized in 2 % Tween-80 yielded particles in the size range of 50 ± 1.4 nm (Table 3), while ThS NPs polymerized in 1 % Tween-80 yielded particles in the size range of 23.5 ± 0.1 nm (Table 3). When the nanoparticles were introduced *in vivo,* the surfactant effect on NP size did not show significant differences in brain uptake (biodistribution was performed using ^{125}I-CQ-BCA NPs; analyses was performed by *ex vivo* scintillation counting of organs of interest, e.g. brain, blood, spleen, liver, kidneys).

5.1.2.3.4. *In Vivo* Biodistribution

In vivo biodistribution experiments showed that the free ^{125}I-CQ had a rapid brain uptake, as well as rapid blood clearance in normal mice. Furthermore, ^{125}I-CQ cleared the brain quickly; the % ID/g for the brain at 2 min was 0.99 ± 0.40 %, and at 4 hours, it was 0.04 ± 0.02 %. When the ^{125}I-CQ was encapsulated within the BCA NPs, the brain/g uptake was enhanced. At two minutes, the wild type mice exhibited 2.31 ± 0.89 % uptake of the ^{125}I-CQ BCA NPs in the brain. Brain and blood clearances of the ^{125}I-CQ BCA NPs was rapid; the % ID/g (brain) at 4 hours was 0.02 % (please see Appendix 6). Finally, **the data showed that ^{125}I-CQ BCA NPs have an increased brain uptake versus ^{125}I-CQ.**

5.1.2.3.5.   Effect of Steric Stabilizer

Dextran 70,000 (1% w/v) was found as the stabilizer which most enhanced whole brain uptake of ^{125}I-CQ-BCA-NPs surface coated with Tween-80 (1 % w/v) surfactant (please see Appendix 7). Furthermore, it has been proposed [168] that the hydrophilic polyethylene glycol (PEG) stabilizer decreases the chances of NP attachment with the plasma opsonin proteins. Opsonins normally deliver foreign solutes to the liver and spleen; in this context, the opsonin-NP association decreases NP uptake by the reticuloendothelial system (RES), which provides the NPs with a longer circulation time. Thus, binding of the NPs with the plasma opsonins should theoretically improve NP brain uptake, as compared with the uptake of non-PEGylated nanoparticles.

When the polymerization stabilizer was changed to the hydrophilic polyethylene glycol (PEG, MW 3,350 g/mol), the PEG-NPs were sterically stabilized against the opsonin plasma proteins, which normally deliver foreigners to the liver and the spleen. The objective was to provide the PEG-NPs with an increased chance of reaching the brain. Fig. 26 (Appendix 7) shows a graph of the *in vivo* RES biodistribution (liver and spleen) of PEGylated nanoparticles at two, thirty and sixty minutes. Both RES organs (liver and spleen) clearly show decreased uptake of PEG-NPs versus NPs. **Therefore, NPs can be designed to escape recognition by the Reticuloendothelial system.** However, we were not

able to correlate decreased RES uptake with an increased brain uptake. For example, the % brain uptake (whole organ) with Dextran 70,000, which was the standard stabilizer in our NP polymerizations, was 0.839 % at 2 min, compared to 0.659 % (whole organ brain uptake) with PEG. At 60 min, the % brain uptake with Dextran was 0.102 %, compared to 0.028 % with PEG (please see the Figure 25 in Appendix 7).

5.1.2.3.6.   Route of Administration

Intravenous administration (i.v.) of ^{125}I-CQ-BCA-NPs, as compared with administration by the intraperitoneal (i.p.) route improves the whole brain uptake of the encapsulated ligand. The NPs were injected into BALB/c mice and the mice were sacrificed at late time points (e.g. 40 mins to 140 mins) to account for the longer circulation time by the I.P. route. Upon sacrifice, the mouse brains were extracted and measured for radioactive ^{125}I by gamma counting. Figure 9 shows that the highest brain uptake of the ^{125}I was at 60 minutes post-I.V. injection.

5.1.2.3.7. Chapter Five Appendix (7)

Appendix 7. Effect of PEGylation on Brain Uptake and on the RES
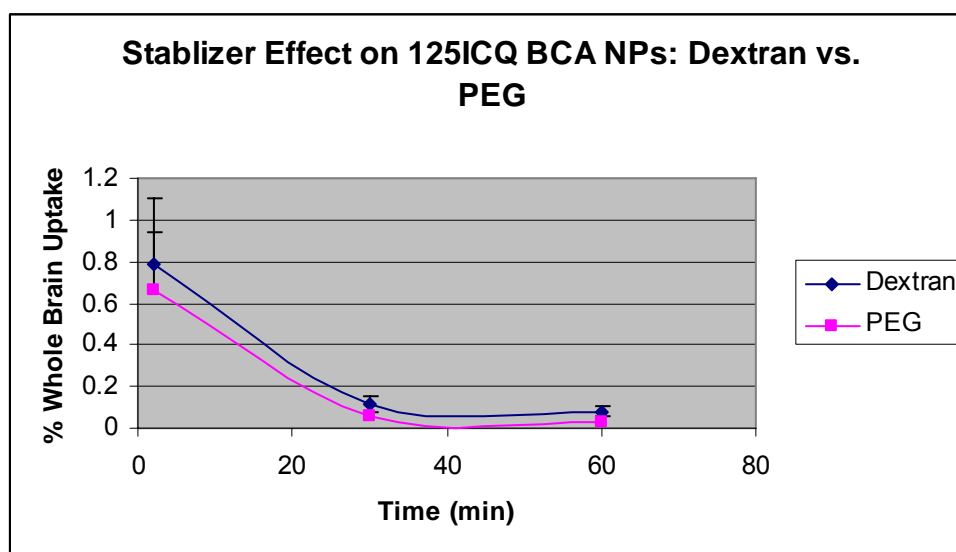
Figure 25. PEGylation does not improve brain uptake; IV administration of ^{125}I-CQ-BCA-NPs; NPs formulated in 1 % Tween-80 (Dextran 70,000 concentration was 1 % w/v, PEG concentration was 2 % w/v).
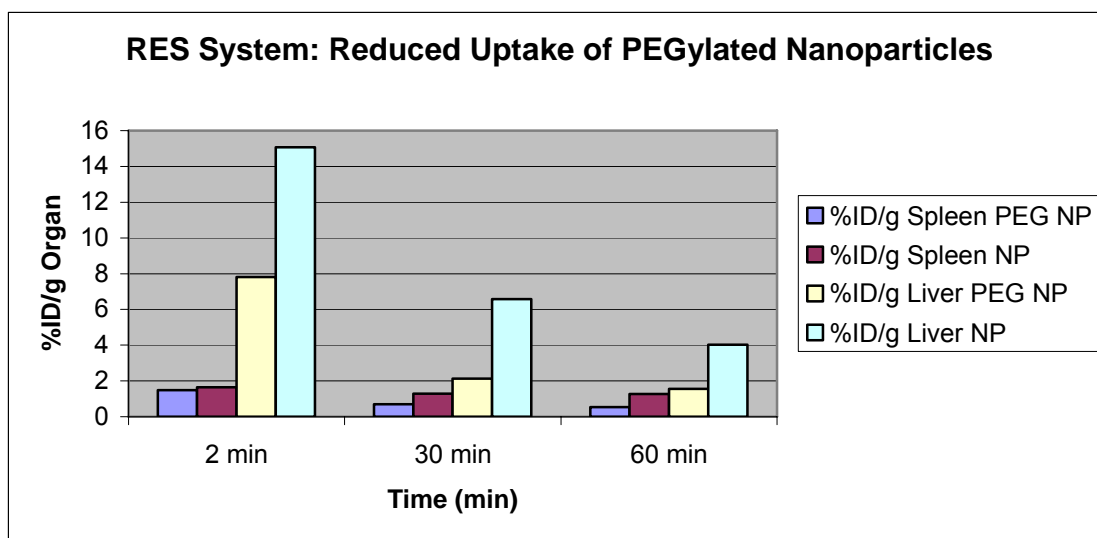
Figure 26. PEGylated nanoparticles decrease RES uptake. Note the greatest change in RES uptake by the liver, which is the organ system that exhibits the most significant uptake of nanoparticles.

6. LABELING AMYLOID PLAQUES WITH NANOPARTICLES ENCAPSULATED WITH AMYLOID AFFINITY DRUGS

Hypotheses: (1) Nanoparticles will act as drug carriers by delivering the desirable drugs to the brain tissue. (2) Amyloid proteins can be imaged using novel nanoparticles as drug carriers.

6.1. Experimental Methods and Procedures

Paraffin-fixed histologic slides of post-mortem human AD frontal cortical brain tissue and age-matched cortical control brain tissue were obtained from Charles White, M.D. (Alzheimer's Disease Core, UT Southwestern Medical Center). Histologic slides (not fixed in paraffin) of control mouse brain slices, and triple transgenic (mutant by the APP/PS1/Tau genes) mouse brain slices obtained from Malu Tansey, Ph.D. All slides were incubated in the presence of ^{125}I-CQ, before being exposed to autoradiographic film for Storage Phosphor Imaging. Briefly, the slides (at 25 °C) were deparafinized in two quick changes of xylene, 100 % ethanol, 95 % ethanol, and distilled water. The mouse brain slides (not fixed in paraffin) were incubated at room temperature in 4 % paraformaldehyde (PFA) prior to incubation in the reaction media (incubation media). The slides were then incubated, for 30 minutes, in incubation media which contained either ^{125}I-CQ or ^{125}I-CQ BCA NPs (2.0×10^6 CPM ^{125}I-CQ in 0.5mL solution of 0.1 % FBS in PBS). After incubation, the slides were washed

for 5 minutes each with 0.1 % FBS (x3), then with a solution containing 1% Tween-80 in PBS (x2). The slides were allowed to air dry before exposure to the Storage Phosphor Imaging screen for 7-10 min. Analyses were performed by *in vitro* autoradiography on a PerkinElmer Cyclone® Storage Phosphor Imaging System (autoradiography system) using OptiQuant quantitative data analysis software (Please see Figure 30 in Appendix 8).

6.2. Results

125ICQ BCA NP labelling
Human post mortem brain tissue

control

AD

2x10⁶ CPM 125ICQ BCA NP in 0.1% FBS in PBS; 1hr incubation, 7 min film exposure
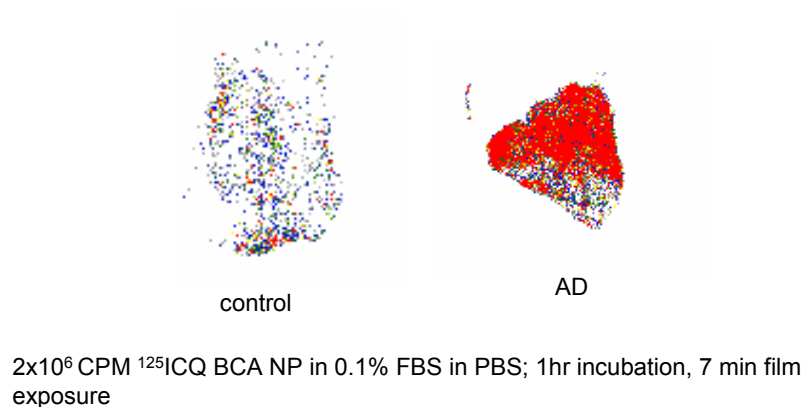
Fig. 10. *In vitro* labeling of post-mortem human AD and control frontal cortex by ^{125}I-CQ BCA NPs (2-18-05). The AD cortex is preferentially labeled by ^{125}I-CQ BCA NPs, as compared to the control cortex.

6.3. DISCUSSION
6.3.1. *In Vitro* Imaging of Human Brain Tissue Sections

These studies showed an increased brain uptake of the ^{125}I-CQ by the AD cortex, as compared to the control brain cortex. Likewise, parallel experiments were conducted with the ^{125}I-CQ-BCA NPs. Results show preferential labeling of the AD cortex by the ^{125}I-CQ-BCA NPs, as compared with the control cortex

(please see Appendix 8).   **Thus, BCA NPs are targeted drug carrier systems. Furthermore, *in vitro* imaging of post-mortem AD brain tissue by ^{125}I-CQ-BCA NPS provides valid data to show that this system may represent a feasible mechanism for *in vivo* detection of the Aβ peptide.**

6.3.2. *In Vitro* Imaging of Triple Transgenic Mouse Brain Sections

In vitro autoradiography provides support for *in vivo* brain imaging and uptake analysis studies of the ^{125}I-CQ-BCA NPs in AD transgenic mice, and in mice where the Aβ peptide aggregates were artificially delivered by stereotaxic implantation.   The data showed greater labeling efficiency by the ^{125}I-CQ (encapsulated within BCA-NPs) of the triple transgenic brain slices, compared to the control brain slices (Please see Figure 29 in Appendix 8).   Therefore, it was hypothesized that the *in vivo* imaging (autoradiography or small-animal PET or SPECT with ^{124}I- or ^{123}I- radioisotopes) would show similar results of preferential labeling of the AD^{+} tissue by the ^{125}I-CQ-BCA NPs.

6.3.3. Chapter Six Appendices (8-12)

Appendix 8. *In Vitro* Autoradiography of ^{125}ICQ BCA NP with Human Post Mortem Brain Tissue and AD Transgenic Brain Tissue

Human post mortem brain slices incubated in ^{125}ICQ BCA NPs

AD

control

Human AD and control brain slices were incubated in 2x10^6 CPM ^{125}ICQ
BCA NPs. The AD brain shows greater activity than the control brain.

Figure 27. *In-vitro* labeling of post-mortem human and control AD frontal cortex by ^{125}I-CQ BCA NPs. The color scale goes from blue to red, indicating a level of radioactivity from low to high . Therefore, the color red represents the highest uptake of ^{125}I-CQ BCA NPs. Thus, in this experiment, the Aβ plaques of the AD tissue have been preferentially labeled by the amyloid-binding radioligand ^{125}I-CQ (7-14-04).

Human post mortem brain slices incubated in ^{125}ICQ BCA NPs

control   AD

Human AD and control brain slices were incubated in 2x10^6 CPM ^{125}ICQ
BCA NPs. The AD brain shows greater activity than the control brain.

Figure 28. *In vitro* labeling of post-mortem human AD and control frontal cortex
by ^{125}I-CQ-BCA NPs. This experiment was performed under the same
experimental conditions as the experiment represented in Fig. 43. Experimental
conditions were controlled to ensure that the CPM delivered to all tissues was the
same. Results show that the Aβ plaques of the AD tissue were preferentially
labeled by ^{125}I-CQ-BCA NPS (8-20-04).

In vitro imaging of triple transgenic (3XTg) AD mice with
^{125}ICQ BCA NPs
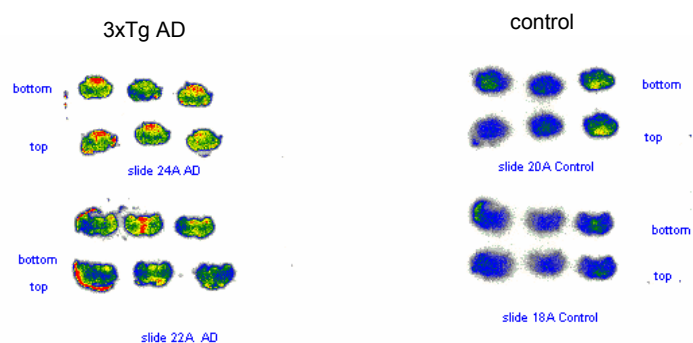
Protocol: RT brain slices are incubated for 1hr with 1.6X10^6 ^{125}ICQ BCA NPs in 0.1%FBS in PBS. Slices are washed for 5 min each in (3x 0.1% FBS in PBS, 2x PBS in 1% Tween-80. Air dried slides are exposed to Phosphor film for 30 min, and developed using the Optiquant Imaging Software

Figure 29. This image depicts the *in vitro* autoradiography results of triple transgenic (APP/PS1/Tau) and control mouse brain slides incubated in the presence of ^{125}ICQ BCA NPs. The transgenic brain slices were preferentially labeled by the ^{125}ICQ BCA NPs, as compared to the control brain slices.

Figure 30. PerkinElmer Cyclone Storage Phosphor Imaging System. In storage phosphor imaging, or autoradiography, a radioactive sample is placed atop a phosphor screen in order to locate and measure the amount of radioactivity in the sample. The screen is composed of phosphor crystals that absorb the energy of the radioactivity in the sample. The crystals store this energy as a direct representation of the original location of the radioactivity in the sample. Therefore, the intensity of light-energy on the storage screen is proportional to the amount of radioactivity in the sample. The screen is then positioned around a circular drum, which is placed within the Cyclone instrument. A linear reader within the Cyclone's apparatus scans the phosphor screen and determines the distribution of the activity in the sample and its location and intensity.

Appendix 9. Y Maze Data
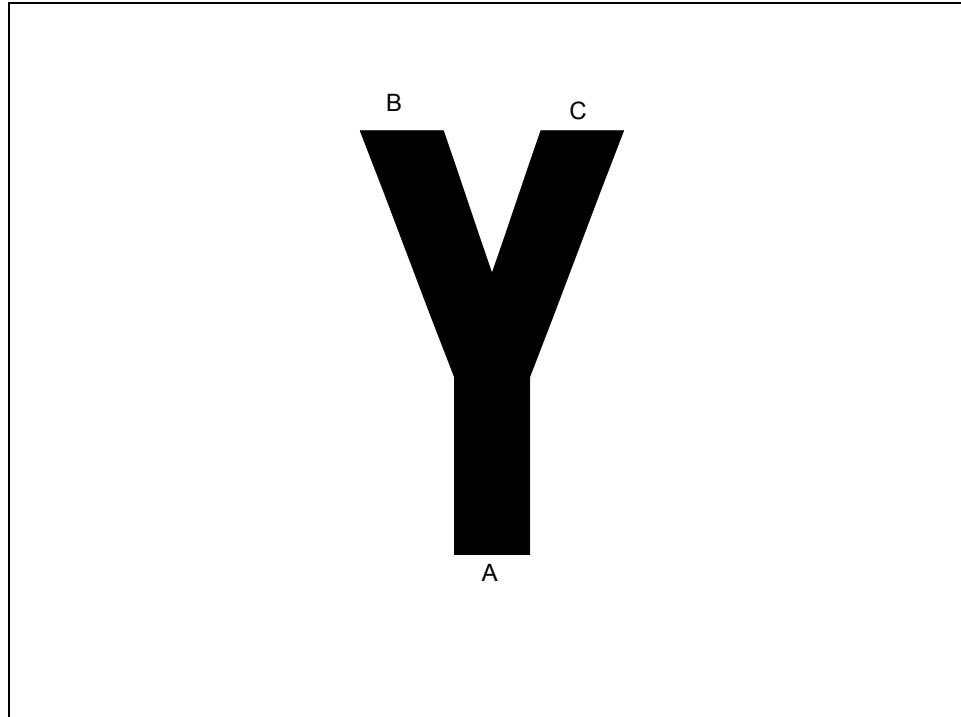
Figure 31. Schematic of Y-maze

Table 2. Y-maze testing data of AD transgenic mice. The Y-maze is a cognitive behavioral test of working spatial (short-term) memory. Please note that the 5 m.o. AD mice score in the testing range of the 18 m.o. control mice (please see next table).

Age in months	Date of Birth	Animal Number	Strain	Date of Y-Maze Test	% Score on Test (Working Spatial Memory)	Testing Range
4 mo.	4/26/05	E56-13-24-10	B6/129 (C57BI6J;129S6/SvEv)	8/18/05	50	
4 mo.	4/26/05	E56-13-24-7	B6/129 (C57BI6J;129S6/SvEv)	8/18/05	66.7	
(Mean ± SD)					58.4	
5 mo.	11/29/04	E64-1-10-15	B6/129 (C57BI6J;129S6/SvEv)	4/29/05	53.9	
5 mo.	11/16/04	E64-1-79	B6/129 (C57BI6J;129S6/SvEv)	4/29/05	56.5	
5 mo.	12/7/04	E56-13-5-2	B6/129 (C57BI6J;129S6/SvEv)	5/4/05	60	
5 mo.	12/7/04	E56-13-5-3	B6/129 (C57BI6J;129S6/SvEv)	5/4/05	61.5	
(Mean +/- SD)					58 ± 3.5	54.5-61.4
6 mo.	10/13/04	E64-1-44	B6/129 (C57BI6J;129S6/SvEv)	4/29/05	61.1	
7 mo.	10/1/04	E64-1-1-4	B6/129 (C57BI6J;129S6/SvEv)	5/4/05	53.3	
7 mo.	1/4/05	E56-13-24	B6/129 (C57BI6J;129S6/SvEv)	8/18/05	43.3	
7 mo.	1/4/05	E56-13-23	B6/129 (C57BI6J;129S6/SvEv)	8/18/05	57.6	
(Mean ± SD)					53.8 ± 7.7	46.2-61.5
9 mo.	1/4/05	E56-13-24	B6/129 (C57BI6J;129S6/SvEv)	9/27/05	48.7	
9 mo.	1/4/05	E56-13-23	B6/129 (C57BI6J;129S6/SvEv)	10/21/05	69.2	
10 mo.	12/7/04	E56-13-5-2	B6/129 (C57BI6J;129S6/SvEv)	9/26/04	64	
10 mo.	12/7/04	E56-13-5-3	B6/129 (C57BI6J;129S6/SvEv)	9/26/04	0	
(Mean ± SD)					32	
11 mo.	6/15/04	APS 556-13	B6C3F1/J	5/4/05	48	
12 mo.	4/7/04	APS 64-7	B6C3F1/J	4/29/05	37.5	
12 mo.	10/1/04	E64-1-1-4	B6/129 (C57BI6J;129S6/SvEv)	9/27/05	66.7	
(Mean ± SD)					52.1	
13 mo.	3/26/04	D56-3	B6C3F1/J	5/4/05	52.4	
18 mo.	3/26/04	D56-3	B6C3F1/J	9/28/05	48.5	

Table 3. Y-maze testing data of AD Control mice

Age in months	N	Strain	Date of Y-Maze Test	% Score on Test (Working Spatial Memory) (Mean ± SD)	Testing Range
2 mo.	8	Swiss Webster	8/27/04	67.7 ± 7.1	60.6-74.8
8 mo.	10	B6C3F1/J	10/22/05	58.2 ± 10.2	48-68.4
9 mo.	10	C57BL/6	10/21/05	59.7 ± 9.7	50-69.4
6 mo.	5	Swiss Webster	5/17/05	54.4 ± 14.2	40.2-68.6
18 mo.	8	Swiss Webster	8/13/04	57.7 ± 8	49.7-65.7

Table 4. Y maze testing data of AD Triple Transgenic mice

Age in months	N	Strain	Date of Y-Maze Test	% Score on Test (Working Spatial Memory) (Mean ± SD)	Testing Range
12	1	3xTg	02/27/06	50	

Table 5. Y maze testing data of AD Triple Transgenic Control mice

Age in months	N	Strain	Date of Y-Maze Test	% Score on Test (Working Spatial Memory) (Mean ± SD)	Testing Range
12	1	B6C3F1/J	02/27/06	51.7	

Table 6. Y maze testing data of Aβ$_{42}$ (1ug) Injected Mice 3 Days Post Operation

Age in months	Date of Birth	Strain	Date of Y-Maze Test	% Score on Test (Working Spatial Memory) (Mean ± SD)	Testing Range
2 mo.	6/10/05	BALB/c	8/11/05	60	
2 mo.	6/10/05	BALB/c	8/11/05	60	
3 mo.	6/1/05	BALB/c	8/29/05	65.4	
		BALB/c		61.8 ± 3.1	58.7-64.9
2 mo. (n=10)	10/4/05	BALB/c	12/8/05	59.3 ± 5.7	53.6-64.9

Table 7. Y maze testing data of Aβ$_{42}$ (5ug) Injected Mice 3 Days Post Operation

Age in months	Date of Birth	Strain	Date of Y-Maze Test	% Score on Test (Working Spatial Memory) (Mean ± SD)	Testing Range
2 mo. (n=9)	02/06	Swiss Webster	04/03/06	61.5 ± 7	54.5-68.4

Table 8. Y maze testing data of Aβ$_{42}$ (5μg) Injected Mice 7 Days Post Operation

Age in months	Date of Birth	Strain	Date of Y-Maze Test	% Score on Test (Working Spatial Memory) (Mean ± SD)	Testing Range
2 mo. (n=9)	02/06	Swiss Webster	04/07/06	63.4 ± 9.3	54.1-72.7

Table 9. Y maze testing data of Aβ$_{42}$ (1μg) Injected Mice 7 Days Post Operation

Age in months	Date of Birth	Strain	Date of Y-Maze Test	% Score on Test (Working Spatial Memory) (Mean ± SD)	Testing Range
2 mo.	6/10/05	BALB/c	8/15/05	46.2	
2 mo.	6/10/05	BALB/c	8/15/05	78.8	
3 mo.	6/1/05	BALB/c	8/29/05	54.3	
		BALB/c		59.74 ± 17	42.8-76.7
2 mo. (n=8)	10/4/05	BALB/c	12/12/05	35.9 ± 19.7	16.1-55.6

Table 10. Y maze testing data of Aβ₄₂ Control Mice 3 Days Post Operation

Age in months	Date of Birth	Strain	Date of Y-Maze Test	% Score on Test (Working Spatial Memory) (Mean ± SD)	Testing Range
2 mo.	6/10/05	BALB/c	8/11/05	44.7	
3 mo.	6/1/05	BALB/c	8/29/05	59.1	

Table 11. Y maze testing data of Aβ₄₂ Control Mice 7 Days Post Operation

Age in months	Date of Birth	Strain	Date of Y-Maze Test	% Score on Test (Working Spatial Memory) (Mean ± SD)	Testing Range
2 mo.	6/10/05	BALB/c	8/15/05	56.5	
3 mo.	6/1/05	BALB/c	8/29/05	73.3	

Appendix 10. Experiments in mice injected with the aggregated $A\beta_{42}$ peptide. DLU/mm^2 values of *in vivo* imaging data (student T test analyses included)

TABLE 12. $A\beta_{42}$ Injection 08/17/05 in DLU/mm^2 (mean $\pm$ SD)

Time (min)	AB B	AB A	Control
12	$1.13 \times 10^6 \pm 5.13 \times 10^4$	$1.40 \times 10^6 \pm 1.42 \times 10^5$	$1.23 \times 10^6 \pm 1.48 \times 10^5$
30	$9.64 \times 10^5 \pm 3.02 \times 10^4$	$1.36 \times 10^6 \pm 5.90 \times 10^4$	$1.10 \times 10^6 \pm 1.05 \times 10^5$
60	$3.62 \times 10^5 \pm 2.93 \times 10^4$	$4.56 \times 10^5 \pm 5.66 \times 10^4$	$4.64 \times 10^5 \pm 6.50 \times 10^4$
120	$2.47 \times 10^5 \pm 7.15 \times 10^3$	$3.35 \times 10^5 \pm 5.56 \times 10^4$	$3.64 \times 10^5 \pm 7.58 \times 10^4$

$p=0.05$; 3.3 mg BCA NP; 7×10^6 CPM ^{125}ICQ

12 min-

Question: Is there a significant difference in the uptake between AB A and control

t test   0.0475024   t distribution   0.9627838

Answer: At 12 minutes, AB A has a significantly higher uptake of NPs than does the control

Question: At 12 minutes, is there a significant difference between AB B and control?

t test   0.1308874   t distribution   0.8984601

Answer: At 12 minutes, there is no significant difference between AB B and control

30 min-

Question: At 30 min, is there a significant difference between AB A and control?

t test   0.0007987   t distribution   0.9993784

Answer: At 30 min, the AB A has a significantly higher uptake of NPs than control

Question: At 30 min, is there a significant difference between AB B and control?

t test   0.0218626   t distribution   0.983093

Answer: At 30 min, the control has a significantly higher uptake of NPs than does AB B

60 min-

Question: At 60 min, is there a significant difference between AB A and control?

t test   0.6985652   t distribution   0.4898699

There is no significant difference between AB A and control at 60 minutes

Question: At 60 min, is there a significant difference between AB B and Control?

t test   8163E-06   t distribution   0.9999936

Answer: At 60 min, the control has a significantly higher uptake than the AB B and Control

2 hours-

Question: At 2 hrs, is there a significant difference between AB A and Control?

t test   0.0019614   t distribution   0.9984701

Answer: At 2hrs, is there a significantly higher uptake of NPs than does AB A

Question: At 2 hrs, is there a significant difference between AB B and Control?

t test   0.0036411   t distribution   0.9971742
Answer: At 2 hrs, AB B is significantly greater than control

Table 13. Abeta injection 09/02/05

Time	AB 42	Control
12	$1.56 \text{ x}10^6 \pm 5.12 \text{ x}10^5$	$1.17 \text{ x}10^6 \pm 1.96 \text{ x}10^5$
30	$1.95 \text{ x}10^7 \pm 2.89 \text{ x}10^5$	$1.71 \text{ x}10^6 \pm 2.34 \text{ x}10^5$
70	$1.89 \text{ x}10^6 \pm 3.01 \text{ x}10^5$	$1.96 \text{ x}10^6 \pm 2.57 \text{ x}10^5$
90	$2.11 \text{ x}10^6 \pm 3.62 \text{ x}10^4$	$1.93 \text{ x}10^6 \pm 1.82 \text{ x}10^5$
120	$6.58 \text{ x}10^5 \pm 2.84 \text{ x}10^5$	$3.63 \text{ x}10^5 \pm 9.43 \text{ x}10^4$

$p = 0.05$

Table 13 Analysis:

12 mins-

Question: At 12 minutes, is there a significant difference in the uptake of the AB 42 and control mice (NPs)?
t test   0.0666915   t dist   0.9479256
Answer: At 12 minutes, the AB 42 has a significantly higher uptake than does the control brain

30 mins-

Question: At 30 minutes, is there a significant difference between AB 42 and control?
t test   0.0126339   t dist   0.9899983
Answer: At 30 minutes, the AB 42 has a significantly higher uptake than the control

70 mins-

Question: At 70 minutes, is there a significant difference in the uptake of the AB 42 and control mice (NPs)?
t test   0.6690556   t dist   0.5161256
Answer: At 70 minutes, there is no significant difference in the uptake of AB 42 and control mice (NPs)

90 mins-

Question: At 90 minutes, is there a significant difference in the uptake of the AB 42 cand control mice (NPs)?

t test 0.2682726 t dist 0.7934538

Answer: At 90 minutes, there is no significant difference in the uptake between AB 42 and control mice (NPs)

120 mins-

Question: Is there a difference in the ex vivo brains of AB 42 and control (NPs)?

t test 0.0533087 t dist 0.9587931

Answer: The ex vivo AB 42 brain has a significantly higher uptake than does the control (NPs)

TABLE 14. AB Injection 04/11/06 in DLU/mm^2 (mean ± SD)

Time (min)	AB	Control
10	$1.62 \times 10^5 \pm 2.08 \times 10^4$	$1.69 \times 10^5 \pm 9.34 \times 10^3$
30	$1.75 \times 10^5 \pm 2.06 \times 10^4$	$1.44 \times 10^5 \pm 1.88 \times 10^4$
60	$1.84 \times 10^5 \pm 2.23 \times 10^4$	$1.88 \times 10^5 \pm 2.14 \times 10^4$
90	$1.25 \times 10^5 \pm 2.34 \times 10^4$	$9.30 \times 10^4 \pm 1.38 \times 10^4$

 p = 0.05

Table 14 Analysis:

10 min- No significant difference

30 min-

t test 0.007075 t distribution 0.994448

sig? yes

Answer The experimental is significantly great than control

60 min-

t test 0.695077

sig? no

Answer   There is no significant difference between the two

90 min-

t test   0.002106   t distribution   0.998344

sig?   yes

Answer: The AB mice is significantly greater than the control mouse

Table 15. AB injection 04/17/06 in DLU/mm^2 (mean ± SD)

Time (mins)	AB 1	AB 2	AB 3	Control
7	1.63 x10^5 ± 2.56 x10^4	1.71 x10^5 ± 2.25 x10^4	1.58 x10^5 ±2.08 x10^4	1.58 x10^5 ± 1.32 x10^4
40	1.58 x10^5 ± 1.99 x10^4	1.63 x10^5 ± 2.77 x10^4	1.49 x10^5 ±2.20 x10^4	1.23 x10^5 ± 1.34 x10^4
60	1.25 x10^5 ± 2.24 x10^4	Animal moved	1.42 x10^5 ± 2.48 x10^4	1.10 x10^5 ± 9.82 x10^3
90	1.70 x10^5 ± 2.34 x10^4	1.89 x10^5 ± 3.34 x10^4	1.60 x10^5 ±2.69 x10^4	1.36 x10^5 ± 1.57 x10^4

p=0.05; 1 mg BCA NP; 1.38 x 10^6 CPM ^{125}ICQ

Table 15 Analysis:

40 min-

AB1 versus control:

t test   0.001397   t distribution   0.998905

AB1 is significantly greater than control

AB2 versus control:

t test   0.002471   t distribution   0.998061

AB2 is significantly greater than control

AB3 versus control

t test   0.014833   t distribution   0.988375

AB3 is significantly greater than control

60 min-

AB1 versus control

t test   0.140069   t distribution   0.891386

no significant difference

AB3 versus control

t test   0. 011267   t distribution   0.991212

AB3 significantly great than control

90 min-

AB1 versus control

t test   0.004296   t distribution   0.996633

AB 1 is significantly greater than control

AB2 versus control

t test   0.004965   t distribution   0.99612

AB 2 is significantly greater than control

AB3 versus control

t test   0.077447   t distribution   0.939544

94% chance that AB3 is greater than control significantly

Table 16. AB injection 04/27/06 in DLU/mm^2

Time (mins)	AB A	AB B	Control
5	7.19 x10^5 ± 1.25 x10^5	6.03 x10^5 ± 6.10 x10^4	6.07 x10^5 ± 7.47 x10^4
30	4.78 x10^5 ± 8.50 x10^4	Animal died	4.12 x10^5 ± 4.26 x10^4
60	3.68 x10^5 ± 7.12 x10^4		3.25 x10^5 ± 3.45 x10^4
90	7.56 x10^5 ±1.50 x10^5		5.26 x10^5 ± 5.34 x10^4

p=0.05; 3.55x10^6 CPM ^{125}ICQ in 1 mg NPs

Table 16 Analysis:

5 mins-

Question: AB A versus control
t test   0.040853   t dist   0.967952
Sig?   yes
Answer: AB A is significantly greater than control

30 mins-

t test   0.058659   t dist   0.954053
sig?   yes
Answer: AB A is significantly greater than control

60 mins-

t test   0.160407   t dist   0.875026
sig?   no
Answer: There is no significant difference between the two

90 mins-

t test	0.00586	t dist	0.99544
sig?	yes		

Answer: The experimental is significantly greater

Appendix 11. *In Vivo* Autoradiography and Histology of Aβ$_{42}$ mice

Intracranial injection of 1μg AB$_{42}$
Intravenous injection of 3 mg ^{125}ICQ BCA NP

(A)

(B)
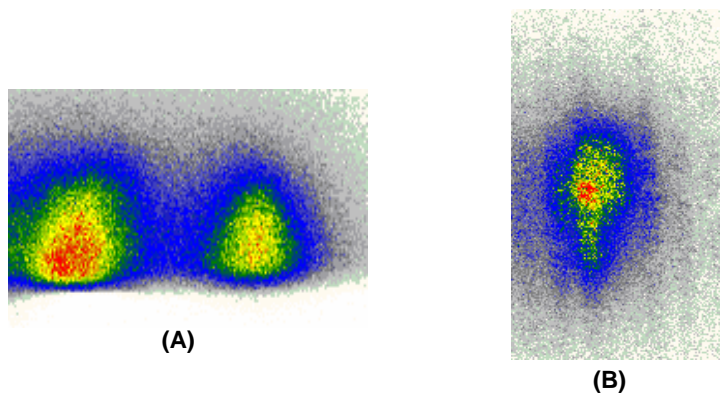
(A) At 30 mins PI, the AB$_{42}$ brain (left) had a significantly higher uptake of ^{125}I CQ BCA NPs (7×10^6 CPM ^{125}ICQ in 3.3 mg NPs) than did the control brain (right).

(B) The AB$_{42}$ brain was imaged *ex vivo* 2 hours post injection, and was found to have an area of localized activity.

Fig. 32. ^{125}ICQ BCA NP administration to mice intracranially injected with 1μg of the aggregated Aβ$_{42}$ peptide

Intracranial injection of 1µg AB$_{42}$
Intravenous injection of 3 mg ^{125}ICQ BCA NP

(A)   (B)
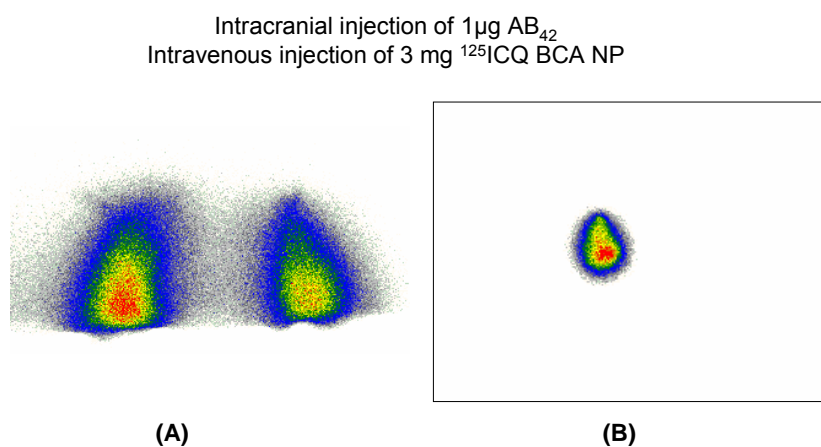
(A) At 30 mins PI, the AB$_{42}$ brain (left) had a significantly higher uptake of ^{125}I CQ BCA NPs (7.5×10^6 CPM ^{125}ICQ in 3 mg NPs) than did the control brain (right).

(B) The AB$_{42}$ brain was imaged *ex vivo* 2 hours post injection, and was found to have an area of localized activity.

Fig. 33. ^{125}ICQ BCA NPs administered to mice intracranially injected with 1µg of the aggregated Aβ$_{42}$ peptide.

Aβ$_{42}$ injected mice (5 μg)
90 mins post administration of ^{125}I CQ BCA NPs

Aβ$_{42}$ Aβ$_{42}$ Aβ$_{42}$ Control
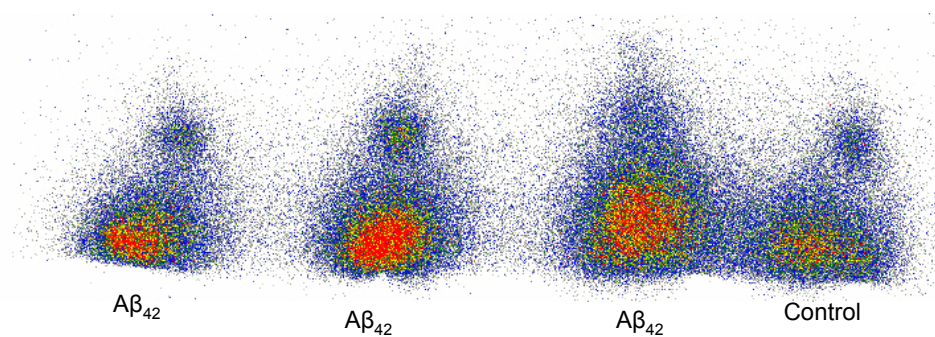
Fig. 34. ^{125}ICQ BCA NPs administered to mice intracranially injected with 5 μg aggregated amyloid peptide. At 18 days post injection of the peptide, the experimental mice showed a significantly greater brain uptake of the nanoparticles, as compared to the control mouse.

Aβ$_{42}$ (5µg) mouse and saline control:

90 minutes post injection of ^{125}ICQ BCA NPs

control   Aβ$_{42}$
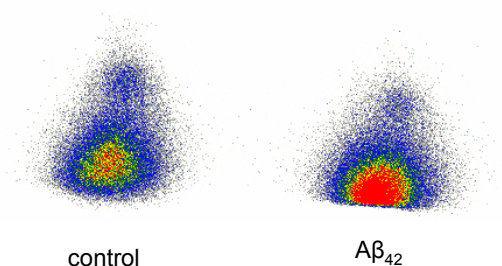
At 90 minutes post injection of nanoparticles, the Aβ$_{42}$ mouse has a
significantly greater brain uptake, as well as the longest retention of the NPs

Fig. 35. ^{125}ICQ BCA NPs administered to mice intracranially injected with 5 µg aggregated amyloid peptide. At 29 days post injection of the peptide, the experimental mouse showed a significantly greater brain uptake of the nanoparticles, as compared to the control mouse.

Birefringence of Congo red
Aβ$_{42}$ mouse 12 days post surgery

Experimental

Control
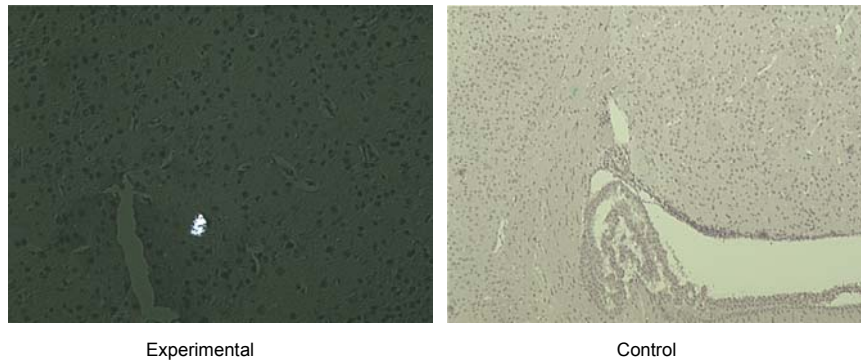
Mouse aged 3 months; 12 days post injection of Aβ$_{42}$ 4/11/06

Fig. 36. Histological stains of brain slices extracted from a 3 mo. Aβ$_{42}$ mouse, 12 days post injection of the aggregated peptide. The image on the left represents a positive Congo red stain; the birefringence of Congo red indicates the presence of the aggregated amyloid peptide (as shown). The image on the right represents a negative Congo red stain of a control mouse brain slice (control mouse injected with saline).

Cortical aggregates in Aβ$_{42}$ mouse
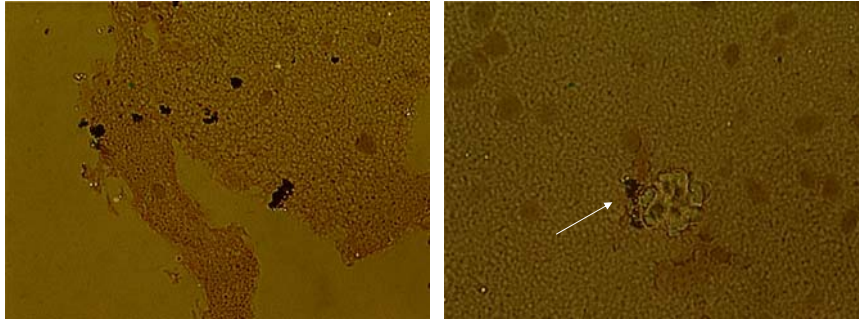
5 µm slice; frontal cortex; mouse aged 4 mo; 4/11/06

Fig. 37. Congo red stain of aggregated amyloid plaques in a 4 mo. Aβ$_{42}$ mouse.

Hippocampal aggregates in Aβ$_{42}$ mouse
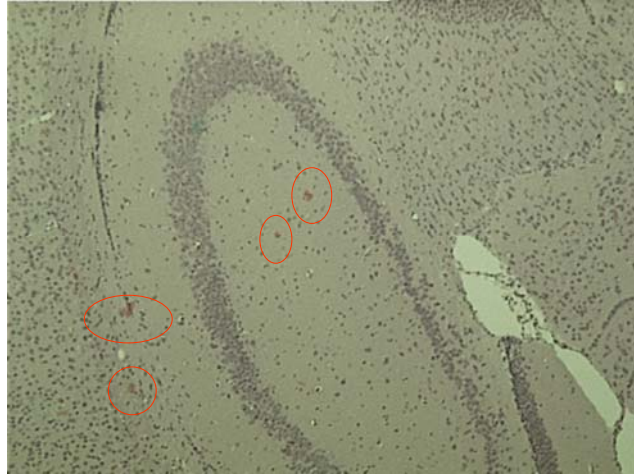
5 μm slice; hippocampus; mouse aged 4 mo; 4/11/06

Fig. 38. Congo red stain of aggregated amyloid plaques in a 4 mo. Aβ$_{42}$ mouse.

Aβ$_{42}$ saline control negative for amyloid plaques
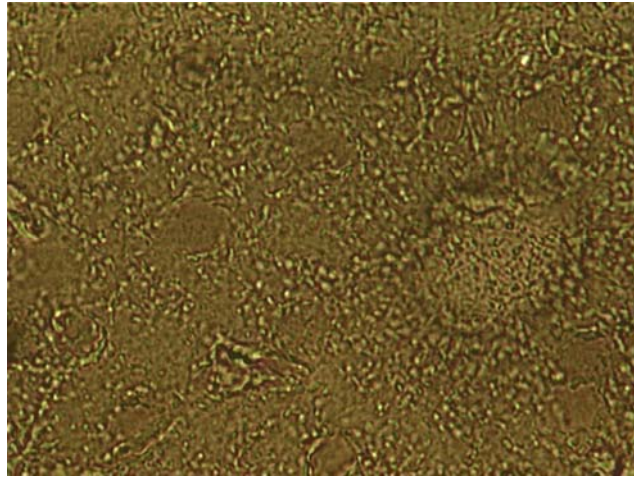
5 µm slice, Congo red staining

Fig. 39. Congo red stain negative for the presence of amyloid in an Aβ$_{42}$ saline control mouse.

Birefringence of Congo red
Aβ$_{42}$ mouse 29 days post surgery

Experimental
Polarized light

Control
Bright light
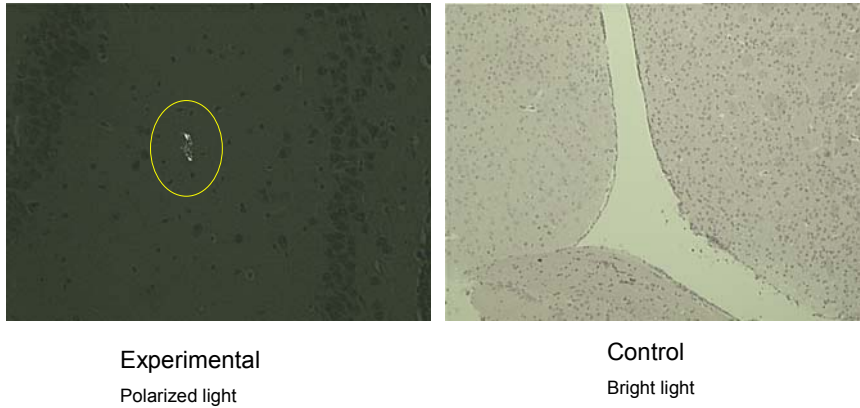
5µm slice   4/28/06

Fig. 40. Birefringence of Congo red in an Aβ$_{42}$ mouse 29 days post surgery

Appendix 12. EXPERIMENTS in TRANSGENIC MICE. DLU/MM^2 VALUES of *IN VIVO* IMAGING DATA (STUDENT T TEST ANALYSES INCLUDED)

Table 17. ^{125}ICQ BCA NPs administered to in-house Transgenic Mice (12 month old), and control mice (9 month old) (mean ± stdev in DLU/mm^2); (n=4)

Time (min)	9 month Control B	9 month Control A	12 month TgB (in-house)	12 month TgA (in-house)
10	1.35 x10^5 ±1.29x10^4	1.29 x10^5± 2.31 x10^4	2.01 x10^5± 3.48 x10^4	1.60 x10^5± 2.47 x10^4
30	1.47 x10^5± 1.15x10^4	1.78 x10^5 ± 2.81 x10^4	2.13 x10^5± 3.03 x10^4	1.19 x10^5± 9.77 x10^3
60	1.32 x10^5± 1.23 x10^4	1.58 x10^5± 2.75 x10^4	2.17 x10^5± 5.06 x10^4	1.58 x10^5 ± 1.98 x10^4
90	1.33 x10^5± 2.34 x10^4	1.35 x10^5± 2.91 x10^4	1.84 x10^5 ± 3.69 x10^4	1.43 x10^5± 2.67 x10^4

p = 0.05; ID = 780,514 CPM ^{125}ICQ in 1 mg BCA NP (in 500 µL PBS)

TABLE 18. 8 month AD transgenic with 9 month Control with ^{125}ICQ BCA NPs 12/02/05 in DLU/mm^2 (mean ± SD)

Time (mins)	9 mo Control	8 mo Russell Transgenic
10	1.27 x10^5 ± 1.66 x10^4	1.18 x10^5 ± 1.92 x10^4
30	7.70 x10^4 ± 1.05 x10^4	9.46 x10^4 ± 1.28 x10^4
60	8.24 x10^4 ± 9.70 x10^3	8.42 x10^4 ± 6.94 x10^3
90	1.08 x10^5 ± 1.34 x10^4	8.75 x10^4 ± 7.27 x10^3

p=0.05; 1 mg BCA NP; 403,557 CPM ^{125}ICQ

Table 18 Analysis:

10 min-

Question: At 10 min, is there a significant difference in the uptake of NPs by the 8 mo Russ and the 9 mo Control?

t test   0.40596516   t distribution   0.69425068

sig diff ?   no

Answer: At 10 min, there is no significant difference in the uptake of the NPs by the 8 mo Russ and the 9 mo Control

30 min-

Question: At 30 min, is there a significant difference in the uptake of NPs by the 8 mo Russ and the 9 mo Control?

t test   0.0224059   t distribution   0.98252545

sig diff ?   yes

Answer: At 30 min, the 8 mo Russell has a significantly higher uptake of the NPs than does the 9 mo Control

60 min-

Question: At 60 min, is there a significant difference in the uptake of NPs by the 8 mo Russ and the 9 mo Control?

t test   0.69199243   t distribution   0.50025858

sig diff ?   no

Answer: At 60 min, there is no significant difference in the uptake of the NPs by the 8 mo Russell and the 9 mo Control

90 min-

Question: At 90 min, is there a significant difference in the uptake of NPs by the 8 mo Russell and the 9 mo Control?

t test   0.01041232   t distribution   0.99189712

sig diff ?   yes

At 90 min, the 9 mo Control has a significantly higher uptake of the NPs than does the 8 mo Russell

Table 19. 8 mo. Transgenic and 8 mo. Control in DLU/mm^2

Time	Russell Transgenic	Control
5	$9.86 \times 10^6 \pm 4.08 \times 10^6$	$8.37 \times 10^6 \pm 2.07 \times 10^6$
30	$2.58 \times 10^5 \pm 2.46 \times 10^4$	$1.99 \times 10^5 \pm 1.06 \times 10^4$
60	$9.27 \times 10^6 \pm 2.16 \times 10^6$	$7.32 \times 10^6 \pm 2.63 \times 10^6$
90	$1.01 \times 10^7 \pm 6.80 \times 10^6$	$3.94 \times 10^6 \pm 5.05 \times 10^5$

p= 0.05; 7,536,369 CPM ^{125}ICQ in 1mg BCA NPs

Table 19 Analysis:

5 mins-

t test   0.352528733   t dist   0.729346191
no significant difference

30 mins-

t test   1.33038 E-05   t dist   0.99998956
transgenic mouse is significantly greater than the control

60 mins-

t test   0.075400869   t dist   0.940609459

90 mins-

t test-   0.037711599   t dist   0.970537738
transgenic is significantly greater

TABLE 20. 7 and 8 mo AD transgenic with 9 mo Control CQ 12/14/05 in DLU/mm^2 (mean $\pm$ SD)

Time (mins)	9 mo control B	9 mo Control A	7 mo Jackson B	7 mo Jackson A	8 mo Russell
10	2.05 x10^5 $\pm$ 3.15x10^4	1.64 x10^5 $\pm$1.75x 10^4	2.26 x10^5 $\pm$ 4.22 x10^5	1.63 x10^5 $\pm$ 1.78 x10^4	1.99 x10^5 $\pm$ 2.80 x10^4
30	1.71 x10^5 $\pm$ 2.42 x10^4	1.76 x10^5 $\pm$3.49 x10^4	1.63 x10^5 $\pm$ 2.44 x10^4	1.40 x10^5 $\pm$ 1.71 x10^4	1.91 x10^5 $\pm$ 3.36 x10^4
60	1.13 x10^5 $\pm$ 1.75 x10^4	1.06 x10^5 $\pm$ 1.57 x10^4	7.04 x10^4 $\pm$ 1.14 x10^4	7.94 x10^4 $\pm$ 6.98 x10^3	8.86 x10^4 $\pm$ 1.27 x10^4
90	2.29 x10^5 $\pm$ 2.65 x10^4	1.98 x10^5 $\pm$ 2.22 x10^4	2.54 x10^5 $\pm$ 5.31 x10^4	2.06 x10^5 $\pm$ 1.81 x10^4	2.17 x10^5 $\pm$ 3.17 x10^4

p=0.05; 1 mg BCA NPs; 795,338 CPM ^{125}ICQ

Table 20 Analysis:

10 min-

Question: At 10 min, is there a significant difference in the uptake of 125ICQ by the 8 mo Russell and the Control A?

t test   0.00464205   t distribution   0.996353579

sig diff ?   yes

Answer: At 10 min, the 8 mo Russell has a significantly higher uptake of 125ICQ than does the Control A

Question: At 10 min, is there a significant difference in the uptake of 125ICQ by the 8 mo Russell and the Control B?

t test   0.701601537   t distribution   0.493007543

sig diff ?   no

Answer: At 10 min, there is no significant difference in the uptake of 125ICQ by the 8 mo Russell and the Control B

Question: At 10 min, is there a significant difference in the uptake of 125ICQ by the 7 mo Jackson A and the Control A?

t test   0.958495295   t distribution   0.356727149

sig diff ?   no

Answer: At 10 min, there is no significant difference in the uptake of 125ICQ by the 7 mo Jackson A and the Control A

Question: At 10 min, is there a significant difference in the uptake of 125ICQ by the 7 mo Jackson A and the Control B?

t test   0.013440408   t distribution   0.989497301

sig diff ?   yes

Answer: At 10 min, the Control B has a significantly higher uptake of 125ICQ than does the 7 mo Jackson A

Question: At 10 min, is there a significant difference in the uptake of 125ICQ by the 7 mo Jackson B and Control A?

t test   0.001166795   t distribution   0.999084409

sig diff ?   yes

Answer: At 10 min, the 7 mo Jackson B has a significantly higher uptake of 125ICQ than does the Control A

Question: At 10 min, is there a significant difference in the uptake of 125ICQ by the 7 mo Jackson B and the Control B?

t test   0.261465592   t distribution   0.797289549

sig diff ?   no

Answer: At 10 min, there is not significant difference in the uptake of 125ICQ by the 7 mo Jackson B and the Control B

30 min-

Question: Is there a significant difference in the uptake of 125ICQ between the 8 mo Russell and the 9 mo control A, at 30 min?

t test   0.364734229   t distribution   0.720400858

sig diff ?   no

Answer: At 30 in, there is no significant difference in the uptake of 125ICQ by the 8 mo Russell and the 9 mo Control A

Question: Is there a significant difference in the uptake of 125ICQ between the 8 mo Russell and the 9 mo Control B, at 30 min?

t test   0.195794786   t distribution   0.847584195

sig diff ? no

Answer: At 30 min, there is no significant difference in the uptake of 125ICQ bye the 8 mo Russell and the 9 mo Control B

Question: Is there a significant difference in the uptake of 125ICQ between the 7 mo Jackson A and the 9 mo Control A, at 30 min?

t test   0.025684431   t distribution   0.979871558

sig diff ?   yes

Answer: At 30 min, the 9 mo Control A has a significantly higher uptake of the 125ICQ than does the 7 mo Jackson A

Question: Is there significant difference in the uptake o 125ICQ between the 7 mo Jackson A and the 9 mo Control B, at 30 min?

t test   0.014853372   t distribution   0.988374697

sig diff ?   yes

Answer: At 30 min, the 9 mo Control B has a significantly higher uptake of the 125ICQ than does the 7 mo Jackson A

Question: Is there a significant difference in the uptake of 125ICQ between the 7 mo Jackson B and the 9 mo Control A, at 30 min?

t test   0.411476341   t distribution   0.686542435

sig diff ? no

Answer: At 30 min, there is no significant difference in the uptake of 125ICQ between the 7 mo Jackson B and the 9 mo Control A

Question: Is there a significant difference in the uptake of 125ICQ between the 7 mo Jackson B and the 9 mo Control B, at 30 min?

t test   0.499180623   t distribution   0.62540441

sig diff ?   no

Answer: At 30 min, there is no significant difference in the uptake of 125ICQ between the 7 mo Jackson B and the 9 mo Control B

60 min-

Question: At 60 min, is there a significant difference in the uptake of 125ICQ by the 8 mo Russell and the 9 mo Control A?

t test   0.10831098   t distribution   0.91589145

sig diff ? no

Answer: At 60 min, there is no significant difference in he uptake of 125ICQ by the 8 mo Russell and the 9 mo Control A

Question: At 60 min, is there a significant difference in the uptake of 125ICQ by the 8 mo Russell and the 9 mo control B?

t test   0.019152095   t distribution   0.985034536

sig diff ? yes

Answer: At 60 min, the 9 mo Control B has a significantly higher uptake of the 125ICQ than does the 8 mo Russell

Question: At 60 min, is there a significant difference in the uptake of 125ICQ by the 7 mo Jackson A and the 9 mo Control A?

t test   0.035011102   t distribution   0.972928704

sig diff ?   yes

Answer: At 60 min, the 9 mo Control A has a significantly higher uptake than the 7 mo Jackson A

Question: At 60 min, is there a significant difference in the uptake of 125ICQ by the 7 mo Jackson A and the 9 mo Control B?

t test   0.003974093   t distribution   0.996907303

sig diff ?   yes

Answer: At 60 min, the 9 mo Control B has a significantly higher uptake of the 125ICQ than does the 7 mo Jackson A

Question: At 60 min, is there a significant difference in the uptake of 125ICQ by the 7 mo Jackson B and the 9 mo Control A?

t test   0.010760449   t distribution   0.99174821

sig diff ?   yes

Answer: At 60 min, the 9 mo Control A has a significantly higher uptake of the 125ICQ than does the 7 mo Jackson B

Question: At 60 min, is there a significant difference in the uptake of 125ICQ by the 7 mo Jackson B and the 9 mo Control B?

t test   0.001064489   t distribution   0.999173882

sig diff ?   yes

Answer: At 60 min, the 9 mo Control B has a significantly higher uptake of 125ICQ than does the 7 mo Jackson B

90 min-

Question: At 90 min, is there a significant difference in the uptake of 125ICQ by the 8 mo Russell and the 9 mo Control A?

t test   0.305661716   t distribution   0.767664657

sig diff ? no

Answer: At 90 min, there is no significant difference in he uptake of 125ICQ by the 8 mo Russell and the 9 mo Control A

Question: At 90 min, is there a significant difference in the uptake of 125ICQ by the 8 mo Russell and the 9 mo control B?

t test   0.516809557   t distribution   0.619269001

sig diff ? no

Answer: At 90 min, there is no significant difference in the uptake of the 125ICQ by the 8 mo Russ an the 9 mo Control B

Question: At 90 min, is there a significant difference in the uptake of 125ICQ by the 7 mo Jackson A and the 9 mo Control A?

t test   0.522409661   t distribution   0.615538817

sig diff ? no

Answer: At 90 min, the there is no significant difference in the uptake of 125ICQ by the 7 mo Jackson A and the 9 mo Control A

Question: At 90 min, is there a significant difference in the uptake of 125ICQ by the 7 mo Jackson A and the 9 mo Control B?

t test   0.151028509   t distribution   0.88369206

sig diff ? no

Answer: At 90 min, there is no significant difference in the uptake of the 125ICQ by the 7 mo Jackson A ad the 9 mo Control B

Question: At 90 min, is there a significant difference in the uptake of 125ICQ by the 7 mo Jackson B and the 9 mo Control A?

t test   0.034247684   t distribution   0.973353608

sig diff ?   yes

Answer: At 90 min, the 7 mo Jackson B has a significantly higher uptake of the 125ICQ, than does the 9 mo Control A

Question: At 90 min, is there a significant difference in the uptake of 125ICQ by the 7 mo Jackson B and the 9 mo Control B?

t test   0.316349509   t distribution   0.758241841

sig diff ?   no

Answer: At 90 min, there is no significant difference in the uptake of 125ICQ by the 7 mo Jackson B and the 9 mo Control B

TABLE 21. 12 mo AD transgenic with 9 mo control CQ and NPs 12/9/05 in DLU/mm^2 (mean ± SD)

Time (mins)	12 mo Russ CQ	12 mo Russ NP (B)	12 mo Russ NP(A)	9mo Control CQ	9 mo control NP
14	$7.14 \times 10^4 \pm$ 5.55×10^3	$1.69 \times 10^5 \pm$ 4.74×10^4	$2.02 \times 10^5 \pm$ 3.26×10^4	$1.67 \times 10^5 \pm$ 2.68×10^4	$2.04 \times 10^5 \pm$ 5.12×10^4
30	$7.62 \times 10^4 \pm$ 1.01×10^4	$6.88 \times 10^3 \pm$ 6.46×10^3	$1.30 \times 10^5 \pm$ 3.40×10^4	$1.11 \times 10^5 \pm$ 1.69×10^4	$1.24 \times 10^5 \pm$ 3.64×10^4
60	$6.99 \times 10^4 \pm$ 1.90×10^4	$1.07 \times 10^5 \pm$ 3.32×10^4	$1.22 \times 10^5 \pm$ 3.16×10^4	$9.18 \times 10^4 \pm$ 1.42×10^4	$1.30 \times 10^5 \pm$ 3.32×10^4
90	$4.86 \times 10^4 \pm$ 2.57×10^3	$1.28 \times 10^5 \pm$ 4.70×10^4	$9.30 \times 10^4 \pm$ 2.54×10^4	$6.38 \times 10^4 \pm$ 7.60×10^3	$1.03 \times 10^5 \pm$ 2.59×10^4

p=0.05; ID ^{125}ICQ = 805,998 CPM; ID ^{125}ICQ BCA NP = 757,998 CPM

Table 21 Analysis:

14 min-

Question: At 14 min, is there a difference in the control brains between the uptake of the NPs and the CQ?

t test   0.107475638   t distribution (95%)   0.916187667

sig diff ?   no

Answer At 14 min, there is no significance in the control brains between the uptake of the NPs and the CQ

Question: At 14 min, is there a difference in the uptake of the NPs by transgenic brain (A) and the control brain?

t test   0.943128235   t distribution (95%)   0.362813607

sig diff ?   no

Answer: At 14 min, there is no significant difference in the transgenic brain (A) and the control brain upon take of the NPs

Question: At 14 min, is there a difference in the uptake of the NPs by the transgenic brain (B) and the control brain?

t test 0.21807651   t distribution (95%)   0.83103392

sig diff ?   no

Answer: At 14 min, there is no significant difference in the uptake of the NPs by the transgenic brain (B) and the control brain.

Question: At 14 min, is there a significant difference in the uptake of the NPs by the two transgenic brains?

t test   0.185624701   t distribution (95%)   0.856117648

sig diff ?   no

Answer: At 14 min, there is no significant difference between the uptake of the NPs by the two transgenic brains

Question: At 14 min is there a difference in the uptake of radioactivity by the transgenic and the transgenic brain with CQ

t test 2.72384E-05   t distribution (95%)   0.999978803

sig diff ?   yes

Answer: At 14 min, the transgenic mouse (A) has a significantly grater uptake of NPs, compared to CQ

Question: At 14 min is there a difference in the uptake of radioactivity by the transgenic brain (B) and the transgenic brain (B) and the transgenic brain with CQ?

t test 0.003653247   t distribution (95%)   0.997164833

sig diff ? yes

Answer: At 14 min, the transgenic mouse (B) has a significantly greater uptake of NPs, compared to CQ

30 min-

Question: At 30 min, is there a difference in the control brains between the uptake of the NPs and the CQ?

t test   0.439101356   t distribution (95%)   0.669088761

sig diff ?   no

Answer: At 30 min, there is no difference in the control brains between the uptake of the NPs and the CQ

Question: At 30 min, is there a difference in the uptake of the NPs by transgenic brain (A) and the control brain?

t test   0.758254853   t distribution (95%)   0.464234593

sig diff ? no

Answer: At 30 min, there is no difference in the uptake of the NPs by the transgenic brain (A) and the control brain

Question: At 30 min, is there a difference in the uptake of the NPs by the transgenic brain (B) and the control brain?

t test   0.007404558   t distribution (95%)   0.994237706

sig diff ?   yes

Answer: At 30 min, the control brain has significantly more uptake of the NPs than does the transgenic brain.

Question: At 30 min, is there a significant difference in the uptake of the NPs by the two transgenic brains?

t test   0.006931156   t distribution (95%)   0.994620987

sig diff ?   yes

Answer: At 30 min, the transgenic brain (A) has a significantly greater uptake of NPs than does the transgenic brain (B)

Question: At 30 min is there a difference in the uptake of radioactivity by the transgenic brain (A) and the transgenic brain with CQ

t test   0.010775575   t distribution (95%)   0.991579575

sig diff ?   yes

Answer: At 30 min, the transgenic brain (A) has a significantly greater uptake of radioactivity than does the transgenic brain with CQ

Question: At 30 min is there a difference in the uptake of radioactivity by the transgenic brain (B) and the transgenic brain with CQ?

t test   0.193966373   t distribution (95%)   0.849737721

sig diff ? no

Answer: At 30 min, there is no difference in the uptake of radioactivity by the transgenic brain (B) and the transgenic brain with CQ.

60 min-

Question: At 60 min, is there a difference in the control brains between the uptake of the NPs and the CQ?

t test   0.024175689   t distribution (95%)   0.981145461

sig diff ?   yes

Answer: At 60 min, the control brain has a significantly greater uptake of the NPs than does the control brain with CQ

Question: At 60 min, is there a difference in the uptake of the NPs by transgenic brain (A) and the control brain?

t test   0.640484951   t distribution (95%)   0.532201195

sig diff ? no

Answer: AT 60 min, there is no difference in the uptake of the NPs by the transgenic (A) and the control brain.

Question: At 60 min, is there a difference in the uptake of the NPs by the transgenic brain (B) and the control brain?

t test   0.273232703   t distribution (95%)   0.790234234

sig diff ?   no

Answer: At 60 min, there is no difference in the uptake of the NPs by the transgenic brain (B) and the control brain.

Question: At 60 min, is there a significant difference in the uptake of the NPs by the two transgenic brains?

t test   0.451474058   t distribution (95%)   0.659698834

sig diff ? no

Answer: At 60 min, there is no significant difference in the uptake of the NPs by the two transgenic brain

Question: At 60 min is there a difference in the uptake of radioactivity by the transgenic brain (A) and the transgenic brain with CQ?

t test   0.001619501   t distribution (95%)   0.998729168

sig diff ? yes

Answer: At 60 min, the transgenic brain (A) has significantly greater uptake of radioactivity than does the transgenic brain with CQ.

Question: At 60 min is there a difference in the uptake of radioactivity by the transgenic brain (B) and the transgenic brain with CQ?

t test   0.06502608   t distribution (95%)   0.949319951

sig diff ? yes

Answer: At 60 min, there is a significant difference in the uptake of radioactivity by the transgenic brain (B) and the transgenic brain with CQ.

90 min-

Question: At 90 min, is there a difference in the control brains between the uptake of the NPs and the CQ?

t test   0.00081709   t distribution (95%)   0.999362687

sig diff ?   yes

Answer: At 90 min, the control brain has a significantly greater uptake of the NPs than does the control brain with CQ

Question: At 90 min, is there a difference in the uptake of the NPs by transgenic brain (A) and the control brain?

t test   0.388751394   t distribution (95%)   0.702285961

sig diff ?   no

Answer: At 90 min, there is no difference in the uptake of the NPs by the transgenic brain (A) and the control brain.

Question: At 90 min, is there a difference in the uptake of the NPs by the transgenic brain (B) and the control brain?

t test   0.21011321   t distribution (95%)   0.836231594

sig diff ?   no

Answer: At 90 min, there is no difference in the uptake of the NPs by the transgenic brain (B) and the control brain

Question: At 90 min, is there a significant difference in the uptake of the NPs by the two transgenic brains?

t test   0.0870588864   t distribution (95%)   0.931776283

sig diff ?   no

Answer: At 90 min, there is no significant difference in the uptake of the NPs by the two transgenic brains

Question: At 90 min, is there a difference in the uptake of radioactivity by the transgenic brain and the transgenic brain with CQ?

t test   0.000757125   t distribution (95%)   0.999405879

sig diff ?   yes

Answer: At 90 min, the transgenic brain (A) has a significantly greater uptake of radioactivity than does the transgenic brain with CQ.

Question: At 90 min is there a difference in the uptake of radioactivity by the transgenic brain (B) and the transgenic brain with CQ?

t test   0.001971836   t distribution (95%)   0.998454525

sig diff ?   yes

Answer: At 90 min, there is a significant difference in the uptake of radioactivity by the transgenic brain (B) and the transgenic brain with CQ

TABLE 22. 12 mo AD transgenic and 10 mo Control ^{124}I PET 45 min *ex vivo* 12/22/05 in DLU/mm^2 (mean ± SD)

Time (mins)	10 mo Control	12 mo Russell Tg
45	$4.31 \times 10^5 \pm 6.59 \times 10^4$	$1.65 \times 10^6 \pm 2.91 \times 10^5$
90	$2.72 \times 10^5 \pm 3.03 \times 10^4$	$1.40 \times 10^6 \pm 5.61 \times 10^5$

p=0.05; ID = 346 µCi ^{124}ICQ (transgenic) and 260 µCi ^{124I}CQ (control)

Table 22 Analysis

45 min-

Question: At 45 min exposure, is there a significant difference in the uptake of 124ICQ 2h ex vivo brains by the control and transgenic mice?

t test   0.000613346   t distribution (95%, 2 tail)   0.999520699

sig diff ?   yes

Answer: At 45 min exposure, the 12 mo transgenic brain has a significantly higher uptake of 124I CQ than doe the control brain

90 min-

Question: At 90 min exposure, is there a significant difference in the uptake of 124ICQ 2h ex vivo brains of the control and transgenic mice?

t test   0.00437324   t distribution 0.996606072

sig diff ? yes

Answer: At 90 min exposure, the 12 mo transgenic brain has a significantly higher uptake of 124I CQ than does the control brain.

TABLE 23. 7 mo Jackson CQ and NPs 12/09/05 in DLU/mm^2 (mean ± SD)

Time (mins)	7 mo Jackson (NP)	7 mo Jackson (CQ)
15	$1.25 \times 10^5 \pm 2.90 \times 10^4$	$9.76 \times 10^4 \pm 2.45 \times 10^4$
30	$1.48 \times 10^5 \pm 3.42 \times 10^4$	$1.11 \times 10^5 \pm 2.21 \times 10^4$
60	$1.26 \times 10^5 \pm 2.70 \times 10^4$	$5.67 \times 10^4 \pm 6.12 \times 10^3$
90	$1.18 \times 10^5 \pm 3.41 \times 10^3$	$7.20 \times 10^4 \pm 9.42 \times 10^3$

p=0.05; ID ^{125}ICQ = 805,998 CPM; ID ^{125}ICQ BCA NP = 757,998 CPM

Table 23 Analysis:

Question: Is there a significant difference between the Jackson Labs transgenic mice upon delivery of the NPs and the CQ?

15 min-

t test   0.094328055   t distribution   0.0926544874

sig diff ?   no

Answer: At 15 min, there is no significant difference between he uptakes of the CQ and the NPs by the Jackson transgenic mice

30 min-

t test   0.047357371   t distribution   0.963160847

sig diff ? yes

Answer: At 30 min, the Jackson mice have a significantly greater uptake of the NPs, compared to the CQ

60 min-

t test   0.001119144   t distribution   0.999131466

sig diff ?   yes

Answer: At 60 min, the Jackson mice have a significantly greater uptake of the NPs, compared to the CQ

90 min-

t test   0.047561221   t distribution   0.963002403

sig diff ?   yes

Answer: At 90 min, the Jackson mice have a significantly greater uptake of the NPs, compared to the CQ

TABLE 24. 8 mo Jackson with NPs 04/27/06

Time (min)	Jackson Labs Transgenic	Control A	Control B
10	$4.51 \times 10^5 \pm 6.18 \times 10^4$	$3.05 \times 10^5 \pm 2.10 \times 10^4$	$4.04 \times 10^5 \pm 4.70 \times 10^4$

p=0.05; 1 mg NP; 3.55×10^6 CPM ^{125}ICQ

Table 24 Analysis:

Jackson vs ContA

t test   6.0412E-06   t distribution   0.99999527

sig diff   yes

ans   Jackson is significantly greater than ContA

Jackson vs ContB

t test   0.06405325   t distribution   0.94959694

sig diff   yes

ans   Jackson is significantly greater than ContB

Table 25. Triple transgenic mice 02/10/06 in DLU/mm^2

Time (min)	Transgenic	Control
5	$4.60 \times 10^6 \pm 1.22 \times 10^6$	$4.94 \times 10^6 \pm 1.61 \times 10^6$
30	$1.77 \times 10^5 \pm 1.33 \times 10^4$	$1.53 \times 10^5 \pm 8.26 \times 10^3$
60	$6.28 \times 10^6 \pm 1.68 \times 10^6$	$3.92 \times 10^6 \pm 1.49 \times 10^6$
90	$4.85 \times 10^6 \pm 1.00 \times 10^5$	$3.94 \times 10^6 \pm 5.05 \times 10^5$

$P = 0.05$

Table 25 Analysis:

30 mins-

t test   0.00328   t dist   0.997448
answer   transgenic is significantly greater than control

60 mins-

t test   0.025397   t dist   0.980193
answer   tg is significantly greater than control

90 mins-

t test   0.063432   t dist   0.95056
answer   tg is significantly greater than control

7. Labeling Amyloid Plaques with Nanoparticles Encapsulated with Amyloid Affinity Drugs in Amyloid-Bearing Mice

Hypothesis: Amyloid plaques can be imaged in association with drugs that bind to them

To transition from the *in vitro* imaging results into an *in vivo* paradigm, two experiments were designed to verify the Aβ plaque labeling efficiency of the ^{125}I-CQ-BCA NPs. In the first design, wild type BALB/c mice were injected by direct stereotaxis with the aggregated Aβ$_{42}$ peptide, prior to nanoparticle administration and *in vivo* autoradiography. In the second design, nanoparticles were administered to AD transgenic mice prior to *in vivo* autoradiography. The experimental designs are explained below.

7.1. Experimental Methods and Procedures

7.1.1. Aggregation of the Aβ$_{42}$ Peptide

Amyloid protein (Aβ 1-42) (0.5 mg) was purchased from Bachem California (Torrance, CA), and dissolved in 1.15 mL PBS (pH 7.4) to a final concentration of 435 μg/mL (100μM) by magnetically stirring the solution (in a closed vessel) at 1200 RPM for 7 days at room temperature [184]. After 7 days, the aggregated peptide was visibly cloudy. The aggregated Aβ$_{42}$ was stored in 100 μL aliquots at -20 °C until use.

7.1.2. Intrahippocampal Sterotaxic Injection of Aggregated Aβ$_{42}$

Wild type BALB/c mice (8 week males, 20-25 g, Charles River Laboratories) were injected by direct stereotaxis with the aggregated Aβ$_{42}$ peptide at a concentration of 1μg/1μL, and at a constant flow rate of 60 sec. Please see Fig. 11. for a schematic of the stereotaxic instrument. The mice received unilateral injections of either saline or the Aβ peptide; the injection location corresponded to the mouse brain hippocampus structure CA1, at coordinates -1.5, -1.0, and -1.8, relative to Bregma [185, 186]. The animals were allowed to recover for 7-8 days, after which time the cognitive tests for behavior (Y-maze) were performed.
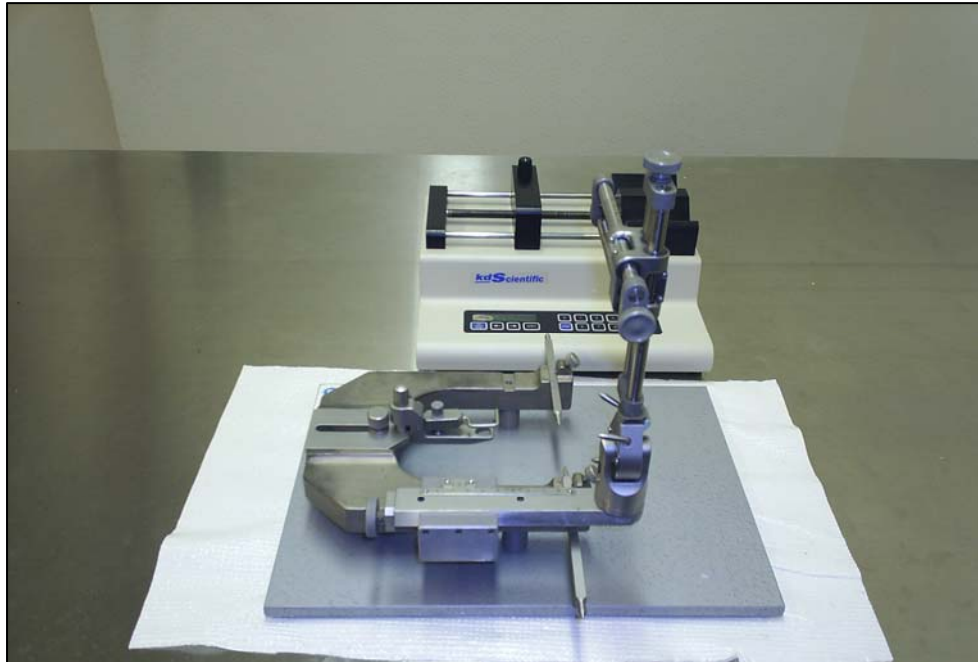
Fig. 11. Stereotaxic instrument for direct intracerebral injection of aggregated
amyloid peptide.

7.1.3. Y-Maze Testing of Cognitive Behavioral Skills

Short term memory, also called working spatial memory, was assessed in

the AD mouse models by statistically recording the animal's behavior in a Y

maze [187]. The Y maze was used to assess the spatial learning in the $A\beta_{42}$ mice

prior to the injection of the aggregated peptide (as a baseline assessment), and at 3

and 7 days post hippocampal injection of the peptide. Cognitive behavioral skills

were determined on-going in the AD transgenic mice and age-matched controls.

The Aβ_{42} mice were 8 weeks old, and the AD transgenic age range was 5 months to 21 months.

The Y maze was constructed of black painted plywood. The length of each arm was 40 cm, and the height was 13 cm. The arms were placed at equal angles to form the Y (Please see Figure 31 in Appendix 9 for a schematic diagram of the Y maze). The mice were consistently placed at the end of arm A; the spontaneous activities of each mouse was individually visually recorded during 8 min timed sessions, where an alternation trial was defined as consecutive entry into each of the arms. For example, ABC, CBA, BCA (etc.) were defined as alternation trials, whereas CCB, BBA, AAC (etc.) was not considered as an alternation trial. Arm entry was defined when both hind feet crossed the boundary of an arm. Entry at any time into the triangle defining the intersection of the 3 arms was not considered for statistical calculation of the results. Likewise, the initial entry into arm A was not considered for statistical calculation of the results. Thus, the number of maximum entries was the total number of arm entries minus two. The alternation percentage was calculated by dividing the total number of alternation trials by the difference of the maximum arm entries minus two (e.g.: (alternations/total entries – 2) x 100 %).

7.1.4. AD Transgenic Mice

Mice with a double mutation (APP/PS1) for Alzheimer's disease were purchased form Jackson Laboratories USA, (strain name B6C3-Tg(APPswe,PSEN1dE9)85Dbo/J)). This particular mouse model corresponds to a form of early onset disease, and expresses a mutant human presenilin 1 (DeltaE9) and a chimeric mouse/human amyloid precursor protein (APP$_{Swe}$).   The expression of both transgenes was directed by the mouse prion protein promoter. The APPswePS1 strain was developed on a B6C3HF2 background by coinjecting the pronuclei with two mouse prion promotor controlled expression plasmids containing cDNAs encoding human presenilin 1 and a chimeric amyloid beta (A4) precursor protein genes.   Insertion of the transgenes occurred at a single locus. The amyloid beta precursor protein was altered by taking mouse coding sequence and "humanizing" the A-beta domain by replacing three amino acids that differ between the two species with the human residues. This allows the mice to secrete a human A-beta peptide. The chimeric amyloid beta (A4) precursor protein was then further modified to encode the Sweedish mutations K595N/M596L in order to elevate the amount ot A-beta produced from the transgene by favoring processing through the beta-secretase pathway. The human presenilin 1 harbors the DeltaE9 mutation.

In addition to the comercially purchased mice, AD transgenic mice were also obtained from collaborations with UTSW investigators. Double transgenic

mice (same mutant strain and background as the commercial mice) were obtained

from David Russell, Ph.D., and AD transgenic mice mutant for the APP/PS1/Tau

transgenes, were obtained from Malu Tansey, Ph.D.

7.1.5. Nanoparticle Administration to AD Mouse Models

The ^{125}I-CQ-BCA NPs (1 – 3 mg) were administered to AD mouse models

by lateral tail vein injection. The $A\beta_{42}$ mice received the ^{125}I-CQ-BCA NPs at 8

days post-injection of the peptide, and the AD transgenic mice received on-going

NP administrations.

7.1.6. Perkin Elmer Cyclone Storage Phosphor Imaging For *In Vivo* and *Ex Vivo* Brain Imaging

Several experiments were performed in order to image the uptake of the

radiolabel (^{125}ICQ) in mice with and without aggregated amyloid deposits. For

example, ^{125}ICQ BCA NPs, ^{125}ICQ, and ^{124}ICQ were administered via intravenous

injection to 2 different sources of APP/PS1 double transgenic mice (mice bred in-

house with the collaboration of David Russell, Ph.D., and commercial mice

purchased from Jackson Laboratories). These chemicals were also administered

to mice mutant for the transgenes APP/PS1/Tau (in collaboration with Malu

Tansey, Ph.D.). In addition, the drugs were administered to C57BL/6 wildtype

aged-control mice, as well to the in-house mouse model of the injected aggregated amyloid peptide ($A\beta_{42}$).

Each mouse was anesthetized with 100-150 μL Ketamine HCl throughout the duration (5-90 minutes) of the imaging experiment; it was important that the mice remained sedated and completely still because any movement will ultimately impair the quality of the final image. Post-injection of the radiolabel, the mouse was placed on the phosphor screen with a lead sheet between the film and the animal's body, in such a way that the only exposed body part was the head. In this way, background radiation from the body was eliminated, and the activity source projected onto the film was from the animal's head region only.

Two important imaging parameters are necessary to satisfy a successful imaging experiment. Namely, the mice must be exposed to the phosphor film in the dark, and the film must be developed in the dark. This is because white light completely erases the image that is formed on the screen. Consequently, during the interval between subsequent time points, the film must be exposed to white light to erase the previous image. The Optiquant imaging software of the Cyclone system gives semi-quantitative readouts in Dynamic Light Units (DLU). When regions of interest are drawn in the brain space, one can obtain information in semi-quantitative units per volume space (DLU/mm^2). If the mouse is imaged over time, this information can be used to assess relative uptake/washout rates.

7.2. RESULTS and DISCUSSION

7.2.1. Experiments in Mice Injected with the Aggregated Amyloid-

Beta 42 (Aβ$_{42}$) Peptide

1. Administration of ^{125}ICQ BCA NP. 08/17/05; n=3

In this experiment, the information from the Y-maze was not entirely helpful, since two of the 3 mice showed improved scores (Please see Appendix 9 for Tables of Y maze values). An improvement in the testing score may indicate that the mice somewhat learned the maze. It should be mentioned that at day 3, the control mouse was observed with strange behavior, as if it were sick. For instance, it was observed that the mouse remained in the triangle (formed at the intersection of the three arms) for the majority of the eight minutes, and when it was in an arm, the movement was mostly concentric. This behavior was not observed in the two experimental mice, nor was it seen in this mouse at day 7. Therefore, the increased score in the control mouse may be explained by an improvement in its health. While this does not explain the increased score in the experimental mouse, it should be noted that the other experimental mouse did indeed show a decline in the cognitive skills through the maze.

At 8 days post-injection, the ^{125}I CQ BCA NPs was administered by tail vein injection. The injected dose was approximately 7 x 10^6 CPM ^{125}I CQ in 3.3

mg BCA NPs (injection volume = 500 µL PBS). During this experiment, the second $A\beta_{42}$ mouse received 2 injections of NPs because of technical difficulties encountered with the first injection. Consequently, the *in vivo* image of this mouse showed a concentrated uptake of the ^{125}I CQ BCA NPs in the tail region, and hence, little uptake in the brain. However, the injections of the control mouse, and the other mouse injected with the amyloid peptide, were successful. Comparing these two mice, the $A\beta_{42}$ mouse showed a significantly higher uptake at 12 minutes PI of the ^{125}I CQ BCA NPs, (DLU/mm^2 = 1.40 x 10^6 ± 1.42 x 10^5 versus 1.23 x 10^6 ± 1.48 x 10^5), than did the control mouse. The same trend was true at 30 minutes PI, where the uptake of the $A\beta_{42}$ (in DLU/mm^2) was approximately 1.36 x 10^6 ± 5.90 x 10^5 versus 1.10 x 10^6 ± 1.05 x 10^5. Unfortunately, the control mouse died after the 30 minute time point, and *in vivo* imaging did not resume. However, the experimental mouse was imaged *ex vivo* at 2 hours PI, and found to have an area of localized brain activity. Please see Appendix 10 for a table of DLU values.

The mice were sacrificed by cardiac perfusion through the left ventricle with 37°C heparinized saline. The brains were extracted and stored in paraformaldehyde, before being embedded in a wax solution and cut at a 5µm slice thickness. The slices were stained with the amyloid-affinity histological dye Congo red for verification of the presence of amyloid.

2. Administration of ^{125}ICQ BCA NP. 09/02/05; n = 2

At 3 days post-surgery, the Y maze behavioral scores for the experimental and control mice were 0.65 and 0.59, respectively. At 7 days, the scores were 0.54 and 0.73. In this experiment of cognitive behavior, the ability of the experimental mouse to proceed through the maze declined, while that of the control mouse improved. The hypothesis is that an improved testing score indicates learned behavior. Therefore, this experiment suggested that the Aβ_{42} mouse did not have the ability to "learn" the maze, with increased age, while the control mouse had that ability. If we look at this scenario another way, the data suggests that the Aβ_{42} mouse had indeed "forgotten" its way through the maze. Thus, we have shown a decline in memory with the experimental mouse (Appendix 9).

In vivo imaging commenced after 7 days; the injection dose was 7.54 x 10^6 CPM ^{125}I CQ in approximately 3 mg BCA NPS; the injection volume was 500 µL PBS. At 12 minutes PI, the Aβ_{42} mouse had a significantly higher uptake (DLU/mm^2 = 1.56 x 10^6 ± 5.12 x 10^5 versus 1.17 x 10^6 ± 1.96 x 10^5) of the ^{125}I CQ BCA NPS than did the control mouse. Likewise, at 30 minutes PI, the experimental brain showed a significantly higher uptake (DLU/mm^2 = 1.95 x 10^6 ± 2.89 x 10^5 versus 1.71 x 10^6 ± 2.34 x 10^5) than the control. At 70 and 90 minutes, there was no significant difference in the brain uptakes of the two mice.

At 2 hours PI, the *ex vivo* brain of the $A\beta_{42}$ mouse showed a significantly higher uptake ($DLU/mm^2 = 6.58$ x $10^5 \pm 2.84$ x 10^5 versus 3.63 x $10^5 \pm 9.43$ x 10^4) of the nanoparticles, than did the control brain. Furthermore, the *ex vivo* image showed localized activity in the experimental brain. Please see Appendix 10 for a table of DLU values.

3. Administration of ^{125}I CQ BCA NPs (1mg) 12 days post-injection of 5µg $A\beta_{42}$. 04-11-06; n = 5

At three days PI, the Y maze experimental mice scored 0.61 ± 0.07, and they scored 0.63 ± 0.09 at seven days PI. Thus, there was no significant change in the behavior of the experimental mice in this experiment. Twelve days post injection of the peptide, the mice were administered ^{125}I CQ BCA NPs (1.38x10^6 CPM ^{125}ICQ in 1 mg NPs), by intravenous injection, for *in vivo* Storage Phosphor imaging. One experimental and one control mouse died before imaging began.

This experiment was divided into two sets (n = 2 each set). During the first set, there was no significant difference between the two mice at 10 minutes PI. At 30 minutes PI, the brain uptake of the experimental mouse ($DLU/mm^2 = 1.75$ x $10^5 \pm 2.06$ x 10^4) was significantly greater than that of the control mouse (1.44 x $10^5 \pm 1.88$ x 10^4). At 60 minutes PI, there was no significant difference between the two mice, however at 90 minutes PI, the experimental mouse had a significantly higher brain uptake of the ^{125}ICQ (1.25 x $10^5 \pm 2.34$ x 10^4) than the

control mouse ($9.30 \times 10^4 \pm 1.38 \times 10^4$), suggesting that the retention of the

nanoparticles was longer in the experimental mouse. The results were repeatable

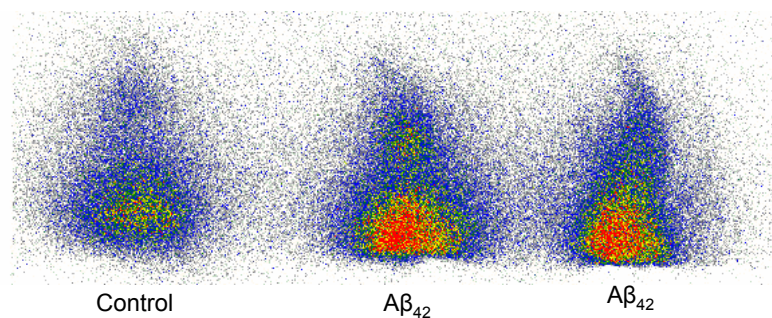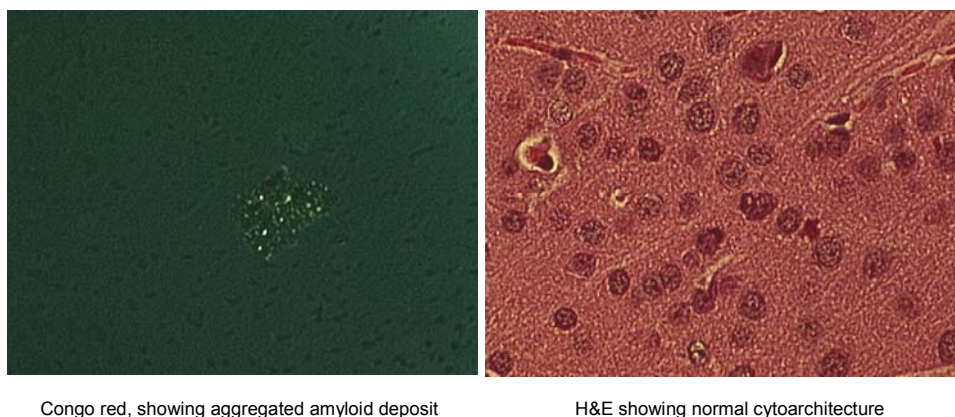in the second set of mice. Please see Appendix 10 for a table of DLU values.

Fig. 12. ^{125}ICQ BCA NPs administered to mice intracranially injected with 5 μg aggregated Aβ$_{42}$ peptide. The experimental mice had a significantly greater brain uptake of the tracer than did the control mouse, which was injected with saline.

Histological stains of Aβ$_{42}$ mouse

Congo red, showing aggregated amyloid deposit   H&E showing normal cytoarchitecture

5 µm slice; frontal cortex; 12 days post injection of 5µg Aβ$_{42}$; mouse aged 5 mo; 4/11/06

Fig. 13. Histological stains of brain slices extracted from a 5 mo. Aβ$_{42}$ mouse, 12 days post injection of the aggregated peptide. The image on the left represents a positive Congo red stain; the birefringence of Congo red indicates the presence of the aggregated amyloid peptide (as shown). The image on the right shows an H&E stain of the Aβ$_{42}$ mouse; this stain indicates the normal cytoarchitecture. Both slices are 5µm thickness, and represent the frontal cortex.

4. Administration of ^{125}I CQ BCA NPs (1mg) 18 days post-injection of 5µg Aβ$_{42}$. 04-17-06; n = 4

Eighteen days post injection of the peptide, the mice were administered ^{125}I CQ BCA NPs (1.381x10^6 CPM ^{125}ICQ in1 mg NPs), by intravenous injection, for *in vivo* Storage Phosphor imaging. At 7 minutes PI, there was no significant difference in the brain uptakes of the nanoparticles by the experimental mice (n=3) and the control mouse (n=1). At 40 minutes PI, all three experimental mice had

significantly greater (p = 0.05) brain uptakes of the ^{125}ICQ BCA NPs, versus the control mouse. At 60 minutes PI, one experimental mouse moved, and was not considered in the statistics; one experimental mouse had a significantly greater brain uptake (1.42 x 10^5 ± 2.48 x 10^4) than the control (1.10 x 10^5 ± 9.82 x 10^3). The other mouse had a higher brain uptake (1.25 x 10^5 ± 2.24 x 10^4) than the control, although the difference was not significant. At 90 minutes PI, all three experimental mice had greater brain uptakes of the ^{125}ICQ BCA NPs, versus the control mouse; two of the experimental mice had significantly greater uptakes at p = 0.05, and the other experimental mouse had significance at p = 0.04 (please see table of values, in DLU/mm^2). Please see Appendix 10 for a table of DLU values.

5. Administration of ^{125}I CQ BCA NPs (1mg) 29 days post injection of 5 ug Aβ$_{42.}$ 04-28-06; n = 3

Twenty nine days post injection of the peptide, the mice were administered ^{125}I CQ BCA NPs (3.55x10^6 CPM ^{125}ICQ in 1 mg NPs), by intravenous injection, for *in vivo* Storage Phosphor imaging. At five minutes post injection, the brain uptake of one Aβ$_{42}$ mouse (DLU/mm^2 = 7.20 x 10^5 ± 1.25 x 10^5, p=0.05) was significantly greater than that of the control (6.07 x 10^5 ± 7.47 x 10^4), while there was no significant difference between the other experimental mouse (6.03 x 10^5 ± 6.10 x 10^4) and the same control. By 30 minutes PI, one

experimental mouse had died. The experiment, therefore, continued with the remaining experimental mouse and the control. At 30 minutes PI, the brain uptake of the experimental mouse ($4.78 \times 10^5 \pm 8.50 \times 10^4$, p=0.05) was significantly greater than that of the control ($4.12 \times 10^5 \pm 4.26 \times 10^4$); there was no significant difference between the two at 60 minutes post injection. At 90 minutes PI, the brain uptake of the experimental mouse ($7.56 \times 10^5 \pm 1.50 \times 10^5$) was significantly greater than that of the control ($5.26 \times 10^5 \pm 5.34 \times 10^4$), suggesting that the nanoparticles had begun to wash from the control brain by 60 minutes. Thus, the brain retention of the nanoparticles was greatest in the experimental mouse. Please see Appendix 10 for a table of DLU values.

7.2.2. Experiments in Transgenic (APP/PS1) Mice (sources: David Russell, Ph.D. and Jackson Laboratories)

1. ^{125}ICQ BCA NPs administered to 2 in-house transgenic (12 month old) mice, and 2 control mice (9 month old). 9/28/05; (n = 4)

In this experiment, each mouse was anesthetized by intramuscular injection with 100-150 μL Ketamine. The ID/mouse was approximately 7.81×10^5 CPM ^{125}ICQ in 1mg BCA NP (in 500 μL PBS). Post-injection of the nanoparticles, the mice were imaged simultaneously between 10 minutes and 90 minutes. Comparing the first 12 month in-house transgenic (TgA) mouse to the first 9 month control mouse (Control A) at 10 minutes, the TgA had a significantly

higher uptake of ^{125}ICQ BCA NPs (DLU/mm^2 = 1.60 x 10^5 ± 2.45 x 10^4 versus 1.29 x 10^5 ± 2.31 x 10^4). However, by 30 minutes, the Control A had a significantly higher brain uptake (DLU/mm^2 = 1.19 x 10^5 ± 9.77 x 10^3 ± 1.18 x 10^5 ± 2.81 x 10^4), although the DLU/mm^2 seems to have risen in the control mouse from 10-30 minutes. At both 60 and 90 minutes PI, there was no significant difference in the uptakes of ^{125}ICQ BCA NPs between the two mice. These trends suggest that the Control A experienced the highest uptake of the nanoparticles at 30 minutes PI, after which time the drug started to clear the brain. In the TgA brain, the maximum uptake was at 10 minutes, and clearance began by 30 minutes. Therefore, in this experiment, the NP retention was longest in the control brain.

Comparing TgA to Control B, at 10 minutes, the TgA had a significantly higher brain uptake of ^{125}ICQ BCA NPs (DLU/mm^2 = 1.60 x 10^5 ± 2.45 x 10^4 versus 1.35 x 10^5 ± 1.29 x 10^4). The results seem to be low for the TgA at 30 minutes (DLU/mm^2 = 1.19 x 10^5± 9.24 x 10^3), and indeed the Control B had the highest uptake at this time point (DLU/mm^2 = 1.47 x 10^5 ± 1.15 x 10^4). However, by 60 minutes the uptake in the TgA was significantly higher (DLU/mm^2 = 1.58 x 10^5 ± 1.98 x 10^4 versus 1.32 x 10^5 ± 1.23 x 10^4). The fluctuation in the transgenic mouse cannot be explained, except that perhaps the mouse moved during the experiment. There was no significant difference in the uptakes by the two brains at 90 minutes PI.

In comparison of TgB to Control A, the transgenic brain had a significantly higher uptake of ^{125}ICQ BCA NPs at all time points. Likewise, in comparison of TgB to Control B, the transgenic brain had a significantly higher uptake of ^{125}ICQ BCA NPs at all time points (please see appendix for table of DLU/mm^2 results).

2. ^{125}ICQ BCA NPs administered to transgenic (8 month old) and control (9 month old) mice. 12/02/05; n=2

The ID was approximately 403,557 CPM ^{125}ICQ in 1mg BCA NPs (in 500 µL PBS. Post-injection of the drug, the mice were imaged simultaneously from 10 minutes to 90 minutes. The transgenic mouse used in this experiment was bred in-house (laboratory of David Russell, Ph.D.). There was no significant difference in the brain uptakes of the two mice at 10 minutes PI, however, at 30 minutes PI, the transgenic brain had a significantly higher uptake than the control brain (DLU/mm^2 = 9.46 x 10^5 ± 1.278 x 10^4 versus 7.70 x 10^4 ± 1.05 x 10^4). There was no significant difference in the brain uptakes at 60 minutes, and at 90 minutes PI, the control brain had the highest uptake (please see table in Appendix 12).

3. ^{125}ICQ administered to 1 in-house transgenic (8 month old) and 2 aged matched controls (9 month old); n = 3

The intravenous injection dosage of the ^{125}ICQ was approximately 7.95 x 10^5 CPM in 500 µL PBS. Post injection (PI) of the ^{125}ICQ, the mice were imaged simultaneously over time from 10 minutes to 90 minutes. At 10 minutes PI, the 8 month transgenic had a significantly higher uptake of ^{125}ICQ, as compared with the first 9 month control mouse (control A) (DLU/mm^2 = 1.99 x 10^5 ± 2.79 x 10^4, versus 1.64 x 10^5 ± 1.75 x 10^4; p = .05). At 30 and 90 minutes PI, the transgenic brain had a higher brain uptake of the drug, although the difference in uptake was not significant.

This transgenic mouse was also simultaneously imaged with a second aged-matched control (control B). At 10 and 30 minutes PI, there was no significant difference in the brain uptake of the ^{125}ICQ by the transgenic mouse and the second aged-matched control. At 60 minutes PI, the second control mouse had a significantly higher brain uptake (1.13 x 10^5 ±1.75 x 10^4 versus 8.86 x 10^4 ± 1.27 x 10^4) than the transgenic mouse, suggesting that the radiolabel had begun to wash away from the transgenic brain by 30 minutes PI. At 90 minutes PI, there was no significant difference between the two brain uptakes. This data suggests that the radiolabel had begun to wash from the control brain by 90 minutes. In this experiment, it appears that the control brain had the longest retention of the ^{125}ICQ.

4. ^{125}ICQ administered to 2 commercial transgenic mice (7 month old) and 2 control mice (9 month old). 12/14/05; n = 4

This experiment was done in parallel with the experiment described in # 2, and therefore, each mouse received an injection dose (ID) of 7.95 x 10^5 CPM ^{125}ICQ in 500 μL PBS. All anesthetic and imaging controls were redundant. However, in this experiment the two transgenic mice were commercially purchased. When comparing the first transgenic (TgA) mouse and the first control (Control A) mouse, there was no significant difference at 10 minutes in the brain uptakes of ^{125}ICQ; at 30 and 60 minutes PI, the control mouse had a higher brain uptake than the transgenic mouse, suggesting that the transgenic brain experienced a wash-out of the drug by 30 minutes. This data is consistent with the wash-out rate of the in-house transgenic brain.

When comparing TgA to the second control (Control B), at 10, 30 and 60 minutes PI, the brain uptake was significantly higher in the control mouse, than in the transgenic mouse. At 90 minutes PI, there was no significant difference in the brain uptakes of the two mice.

When comparing TgB to Control A, at 10 minutes, the 7 month transgenic mouse had a significantly higher brain uptake of ^{125}ICQ (DLU/mm^2 = 2.26 x 10^5 ± 4.22 x 10^4 versus 1.64 x 10^5 ± 1.75 x 10^4), compared to the 9 month control. At 30 minutes, there was no significant difference. While this might suggest that the

radiolabel had begun to wash from the transgenic brain by 30 minutes, the results for the remaining time points are quite ambiguous. For example, the control had a higher uptake at 60 minutes PI ($DLU/mm^2 = 1.06$ x $10^5 \pm 1.57$ x 10^4 versus 7.07 x $10^4 \pm 1.14$ x 10^4), while at 90 min PI, the transgenic brain had the highest uptake ($DLU/mm^2 = 2.54$ x $10^5 \pm 5.31$ x 10^4 versus 1.98 x $10^5 \pm 2.22$ x 10^4). The DLU/mm^2 value is increased in both mice at 90 minutes, which seems to preclude standard clearance trends.

Comparing TgB to Control B, there was no significant difference in the uptake of ^{125}ICQ by the two mice at 10 and 30 minutes PI. At 60 minutes PI, the control mouse had the highest uptake ($DLU/mm^2 = 1.13$ x $10^5 \pm 1.75$ x 10^4 versus 7.94 x $10^4 \pm 6.98$ x 10^3), suggesting that the radiolabel had begun to wash from the transgenic brain. Finally, at 90 minutes PI, there was no significant difference in the uptake of ^{125}ICQ by the two mice. The transgenic mice in these experiments were 7 and 8 months old. Since both sources are known to develop amyloid plaques by 6 months of age, it is possible that the higher uptakes in the control mice may have been consequent of an age-related phenomenon of the amyloid deposition in the transgenic mice (please see table in Appendix 12).

5. ^{125}ICQ BCA NP administered to transgenic and control mice (8 months old)

The ID was approximately 7.54 x 10^6 CPM ^{125}ICQ in 1mg BCA NPs (in 500 μL PBS). Post-injection of the drug, the mice were imaged simultaneously from 12 minutes to 90 minutes. The transgenic mouse used in this experiment was bred in-house (laboratory of Dr. David Russell, Ph.D.). At each time point, the control mouse had a significantly greater brain uptake than the transgenic mouse (please see table of DLU/mm^2 values in Appendix 12). Again, the decreased activity in the transgenic brain may be explained by the animal's young age.

6. ^{125}ICQ and ^{125}ICQ BCA NPs administered to in-house transgenic mice (12 months old) and control mice (9 months old). 12/9/05; n = 5

In this experiment, the ID was approximately 7.58 x 10^5 CPM ^{125}ICQ in 1mg BCA NPs (in 500 μL PBS), or 8.06 x 10^5 CPM ^{125}ICQ in 500 μL PBS. Post-injection of the drug, the mice were imaged simultaneously from 14 minutes to 90 minutes. In comparing TgA NP (transgenic mouse A receiving nanoparticles) with Control NP (control mouse receiving nanoparticles) at 14 minutes, there is no significant difference in the uptake between the two brains. However, at 14 minutes the TgA NP had a significantly greater brain uptake (DLU/mm^2 = 2.02 x 10^5 ± 3.26 x 10^4 versus 7.14 x 10^4 ± 5.55 x 10^3) than did the Tg CQ (transgenic mouse receiving free drug). **This data suggests that the BCA NPs effectively**

delivered the ^{125}ICQ to the transgenic brain with greater efficiency than just the ^{125}ICQ (free drug). These results were reproducible when TgB NP was compared to Control NP, and when TgB NP was compared with TgCQ (DLU/mm^2 = 1.69 x 10^5 ± 4.74 x 10^4 versus 7.14 x 10^4 ± 5.55 x 10^3).

At 30 minutes PI, there was no significant difference in the uptakes between TgA NP and Control NP, while TgA NP had a significantly higher uptake of ^{125}ICQ than did TgCQ. (DLU/mm^2 = 1.30 x 10^5 ± 3.40 x 10^4 versus 7.62 x 10^4 ± 1.01 x 10^4). In comparison of TgB NP with Control NP and TgCQ, at 30 minutes, Control NP had a significantly greater uptake than TgB (DLU/mm^2 = 1.24 x 10^5 ± 3.64 x 10^4 versus 6.99 x 10^4 ± 6.46 x 10^3). There was no significant difference in the brain uptakes between TgB NP and TgCQ.

At 60 minutes PI, there was no significant difference in brain uptake between TgA NP and Control NP, however, TgA NP had a significantly greater uptake than did TgCQ (DLU/mm^2 = 121,680 ± 31,650 versus 69,852 ± 18,973). *Again, it appears that the nanoparticles are consistently delivering ^{125}ICQ to the transgenic brain more efficiently than just ^{125}ICQ alone.* These results were reproducible when TgB NP was compared with Control NP, and with TgCQ (107,018 ± 33,158 versus 69,852 ± 18,973). These data are consistent with the 90 minute time point (please see table of DLU/mm^2 values, Appendix 12).

7. Determination of nanoparticle retention time in (in-house) transgenic and control mice. 12/14/05; n = 8

In this experiment, the intravenous injection dosage of the ^{125}ICQ BCA NPs was approximately 1mg in 500 µL PBS (7.8 x 10^5 CPM ^{125}ICQ).   Post injection (PI) of the ^{125}ICQ BCA NPs, the mice were imaged simultaneously over time from 10 minutes to 90 minutes. The highest uptake in the transgenic mice occurs at 60 minutes PI, while the highest uptake in the control mice occurs at 30 minutes. **Therefore, the transgenic mice have a longer retention of the ^{125}ICQ BCA NPs.**

We want to define imaging parameters around the time when the radiolabel has washed away from the normal brain. The critical imaging window should be at a time when the drug has washed away from the normal brain, and there is a significant difference between the drug uptakes by plaques and normal brain. Ideally, at the time in which clearance has begun in the normal brain, localized activity can be seen in the image of the transgenic brain. This can occur if the transgenic brain retains the drug longer than the control brain. *Thus, the increased retention of the ^{125}ICQ BCA NPs in the transgenic group is the desired result.* (**It is hypothesized** that the metal binding properties of the ^{125}ICQ (to the histidine moiety and transitional metals of the amyloid plaque) is responsible for this phenomenon). Only then, can imaging parameters be defined. Of course, we

hoped for consistent imaging parameters throughout each trial, though it was recognized that biodistribution and *in vivo* imaging somewhat depended upon the animal under experiment.

In both groups (transgenic and control), there appeared different uptake patterns of the nanoparticles. For example, the control group could be sub-divided into mice whose uptakes increased at 30 minutes, and into mice whose uptakes decreased at 30 minutes. Likewise, the 30 minute time point was of interest in the transgenic group. For example, this cohort could also be subdivided, into mice whose uptakes decreased at 30 minutes, and into mice whose uptakes increased at 30 minutes. These inconsistencies can be explained by inherent artifacts of the imaging apparatus. However, the majority of transgenic mice showed a peak uptake at 60 minutes, while the majority of control mice showed a peak uptake at 30 minutes. Consequently, the variations may be explained by the individual biodistribution and health of the mice.

The transgenic mice ranged in age from 8 months to 21 months. From the data, it can be shown that the 12 month old mouse was the best model to image (please see Fig. 41 in Appendix 13). Likewise, the mice who are 8 months, 18 months, and 21 months gave images with the least activity. Since the transgenic mice are known to develop plaques at age 6 months, it may be that the density of the plaques in the 8 month mouse is not great enough for efficient imaging. The

same can be true of the 18- and 21 month old mice, if age plays a role in a decreased density of amyloid plaques and/or blood pool.

Lastly, it was important to recognize that our method of *in vivo* Phosphor screen imaging represented qualitative information; the resolution of the system is so low that it cannot be relied upon to represent accurate quantitative measurements. However, qualitatively speaking, the Perkin Elmer Cyclone *in vivo* Storage Phosphor imaging system is an adequate modality to prove increased brain activity of ^{125}ICQ BCA NPs in AD transgenic mice, and in mice intracranially injected with the aggregated Aβ_{42} peptide (as compared with control mice).

8. ^{124}ICQ administered to transgenic and control mice. 12/22/05; n = 2

In this experiment, each mouse was fitted with a nose cone and anesthetized with Isofluorane gas (1mL/min/25g). The transgenic mouse was then given an intravenous injection of 346 µCi ^{124}ICQ (in PBS), while the control mouse was injected with 260 µCi ^{124}ICQ. Unlike previous experiments where the mice were imaged via *in vivo* autoradiography on the Cyclone system, these mice were imaged via *in vivo* small animal microPET. However, at 2 hours PI, both brains were excised and placed upon the phosphor film for *ex vivo* autoradiography. The mouse brains were exposed to the phosphor film for approximately 45 minutes,

and 90 minutes. At both time points, the transgenic brain had a significantly higher uptake of ^{124}ICQ than the control brain, even after correcting for differences in administered activity.

9. ^{125}ICQ BCA NPs administered to (in-house) transgenic (10 mo) and control
(11 mo) mice. 2/10/06; n = 2

In this experiment APP/PS1 (n = 1) and control (n = 1) were injected with 1 mg NPs (2.24 x 10^6 CPM ^{125}I). The mice were anesthetized with 100 μL Ketamine and subjected to *in vivo* Storage phosphor autoradiography (5-90 minutes PI). There was no significant difference in the brain uptakes of the ^{125}ICQ BCA NPs by the two mice at 5 minutes PI, however, at every time point subsequent to 5 minutes, the transgenic mouse had a significantly higher brain uptake (please see table of DLU/mm^2 values, Appendix 12).

10. ^{125}ICQ BCA NPs administered to transgenic (15 mo, n = 1) and control
(12 mo, n = 2); 1 mg NPs (2.25 x 10^6 CPM ^{125}ICQ). 2/13/06; n = 3

In this experiment, one 15 month old AD transgenic mouse (courtesy of David Russell, Ph.D.), and two 12 month controls, were administered 1 mg BCA NPs (2.25 x 10^6 CPM ^{125}ICQ), by tail vein injection. Figure 18 represents the *in vivo* brain image of the mice, at 1 hour post injection of the nanoparticles. It is clearly

shown that the transgenic mouse had a greater brain uptake of the nanoparticles, as compared with the control mouse. Upon sacrifice, the brains of the transgenic and control mice were excised and harvested for histology. The AD transgenic brain was subjected to histological staining by Congo red (amyloid plaques), Prussian Blue (Fe^{3+} metal ion), Rubeanic acid (Cu^{2+} metal ion), and H&E (to show the normal cytoarchitecture). The AD transgenic brain was positive for amyloid plaques (throughout the brain space, including the hippocampus) and Fe^{3+}, although Cu^{2+} was not found. **Therefore, BCA NPs cross the BBB to deliver ^{125}ICQ to amyloid plaques in transgenic mice. Furthermore, the radiolabel associates with the plaques through metal ion interaction.** The control brain was negative for the above stains.

12 mo control   15 mo AD transgenic

1 hr post injection

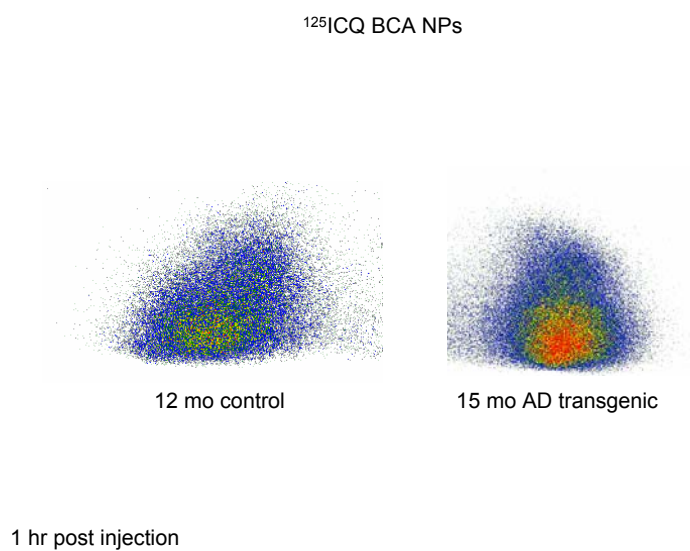**Fig. 14.** ^{125}ICQ BCA NP administration to a 15 mo AD transgenic mouse, and a 12 mo control. At one hour post injection, the AD transgenic mouse has an increased brain uptake of the nanoparticles, presumably due to the presence of amyloid plaques. The mice were sacrificed for histology, and the AD transgenic mouse was found positive for amyloid plaques and metal ions (please see Figs. 19-21).

Aggregated amyloid plaques: 15 mo AD transgenic mouse

10 µm
slice

Birefringence of Congo red
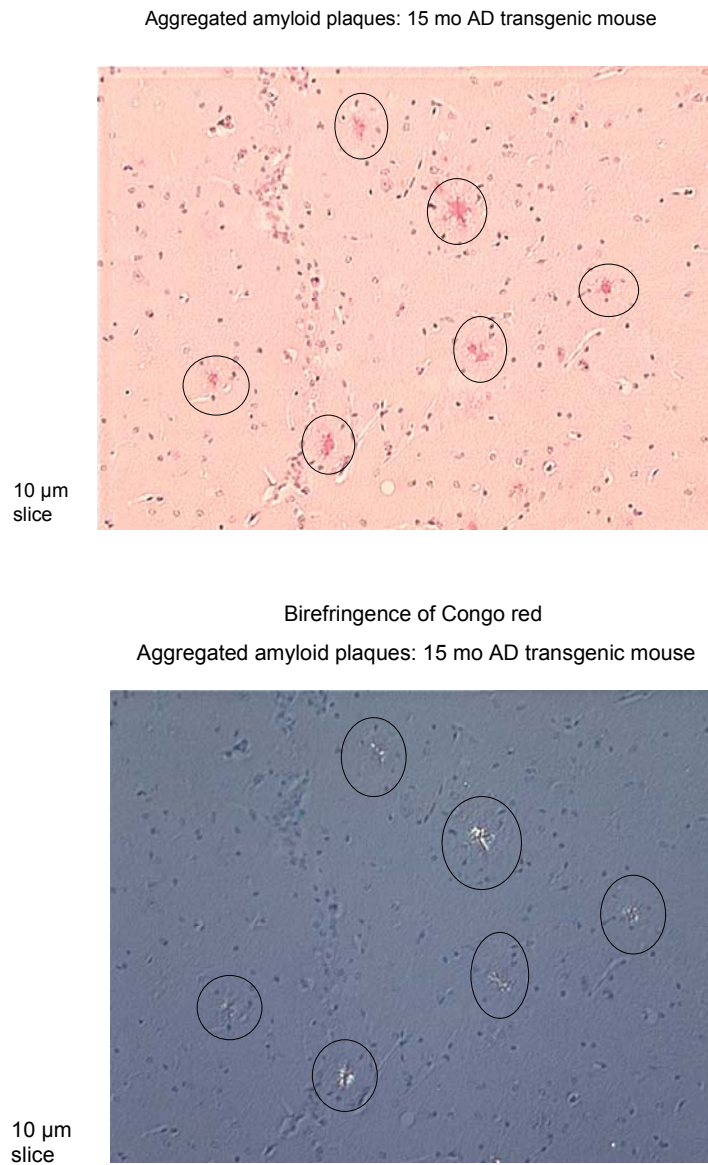Aggregated amyloid plaques: 15 mo AD transgenic mouse

10 µm
slice

Fig. 15. Congo red histological stain of brain slices extracted from a 15 mo AD transgenic mouse. The top image is a bright field image that shows the presence of aggregated amyloid plaques. The bottom image represents the brain slice, as viewed under polarized light, and shows the bifirengence of Congo red by the aggregated amyloid plaques.
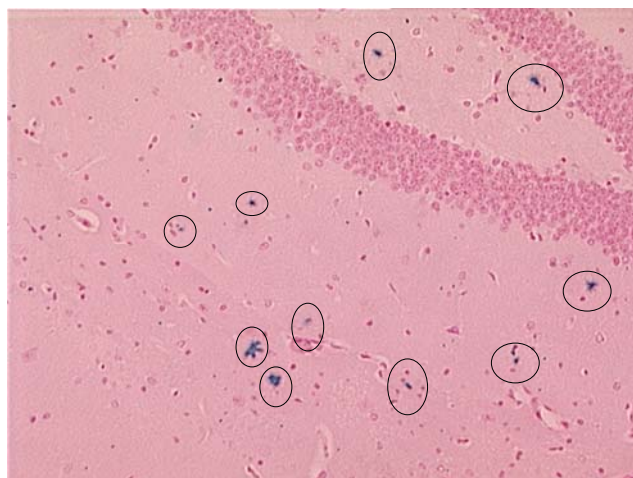
Hippocampal aggregates
15 mo AD transgenic

5 µm slice, bright field Congo red stain

Fig. 16. Additional amyloid aggregates were found in the 15 mo AD transgenic mouse throughout the hippocampus (image represents brain slice viewed under bright light)

15 mo AD transgenic:
Fe^{3+} staining of hippocampal amyloid aggregates

5 µm slice

Fig. 17. Iron staining of hippocampal amyloid aggregates in AD transgenic mouse. The hippocampal iron (Prussian Blue stain to identify Fe^{3+}) was found to correlate with the positive plaques that were identified in the hippocampus with Congo red. Therefore, BCA NPs deliver ^{125}ICQ to amyloid plaques. The radiolabel associates with the plaques through metal ion interaction.

11. ^{125}ICQ and ^{125}ICQ BCA NPs administered to transgenic mice (7 months old). 12/9/05; n = 2

In this experiment, each mouse was given approximately 7.58×10^5 CPM ^{125}ICQ in 1mg BCA NPs (in 500 µL PBS), or 8.06×10^5 CPM ^{125}ICQ in 500 µL PBS. Post-injection of the drug, the mice were imaged simultaneously from 15 minutes to 90 minutes. The transgenic mice used in this experiment were

commercially purchased from Jackson Laboratories. Both mice were seven months old at the time of the experiment. At 15 minutes PI, the brain uptake of TgNP was higher than that of TgCQ, although not significantly; however, at each subsequent time point, the TgNP brain uptake was significantly higher (please see table of DLU/mm^2 values) than the TgCQ brain uptake. **This suggests that in the transgenic mouse, the nanoparticles act as drug carriers of the ^{125}ICQ, and that the efficiency of the drug carriers is greater than when the ^{125}ICQ is delivered alone as a free drug. Subsequently, the ^{125}ICQ BCA NPs have a longer retention in the commercial transgenic mouse brain than does ^{125}ICQ.**

12. ^{125}ICQ BCA NPs administered to transgenic (8 mo) and control mice (12 mo). 04/27/06; n = 3

In this experiment, an 8 month old Jackson transgenic (APP/PS1) (n = 1) and two age-matched controls mice were administered ^{125}ICQ BCA NPs (1mg NPs, 3.55x10^6 CPM ^{125}ICQ) by tail vein injection. The mice were imaged by Storage phosphor autoradiography approximately 10 minutes post injection of the nanoparticles. Unfortunately, two mice (one transgenic and one control) died after the first image, so the data set for this experiment (10-90 minutes PI) was incomplete. However, at ten minutes post injection, the transgenic mouse had a significantly greater (p = 0.05) brain uptake of the nanoparticles than

both controls (mean DLU/mm^2 = 4.51 x 10^5 ± 6.18 x 10^4 versus 3.05 x 10^5 ± 2.1 x 10^4 and 4.04 x 10^5 ± 4.70 x 10^4).

7.2.3. Experiments in Triple Transgenic Mice (APP/PS1/Tau) Injected with ^{125}ICQ BCA NPs

1. ^{125}ICQ BCA NPs administered to triple transgenic and control (12 mo) mice. 02/10/06; n = 2

Triple transgenic (n = 1) (APP/PS1/Tau (3xTg); obtained in collaboration with Malu Tansey, Ph.D.), and control (n = 1) mice were anesthetized with 100 μL Ketamine, and imaged over the time interval 5-90 minutes post injection of ^{125}ICQ BCA NPs (1 mg NPs, 2.24 x 10^{6}CPM ^{125}ICQ). There was no significant difference between the mice at the initial time point of 5 minutes PI, however, the transgenic mouse had a significantly higher (p = 0.05) brain uptake of the nanoparticles versus the control mouse, at every other time interval (please see table of DLU/mm^2 values). **It appears that the nanoparticles carry the ^{125}ICQ across the BBB in the triple transgenic mouse; the radiochelator then proceeds in labeling the amyloid plaques by associating with an overabundance of metal ions.** This experiment was simultaneously carried out with a double transgenic (APP/PS1, (2xTg) Dr. Russell) mouse and control. It was noticed that the triple transgenic mouse did not have as much radioactive

uptake of the nanoparticles, when compared with the double transgenic mouse. This was a surprising result; it was expected that the 3xTg would have a greater brain uptake of the nanoparticles than the 2xTg (because the triple transgenic has the greater pathology). However, we have surmised that the 3xTg may not have had as great an amyloid burden as the 2xTg.

Aggregation of the tau protein is also associated with heavy metals (e.g. Cu^{2+}, Al^{3+}, Zn^{3+}). It is not known whether the brain uptake in the transgenic mouse was due to the presence of the tau or the amyloid plaques, however, the transgenic and control brains were extracted and stained with Congo red (Aβ), Prussian Blue (Fe^{3+}), Rubeanic acid (Cu^{2+}), and Bielschowski (Tau) to validate the imaging results. Histological verification of both metal ions validated the neuropathology of AD in the triple transgenic mouse, although it is still not known whether the ions associated with the plaques or the tangles. However, based on the appearance of the cells under stain with the metal ions, it was surmised that the metal ion association was due to the amyloid burden.
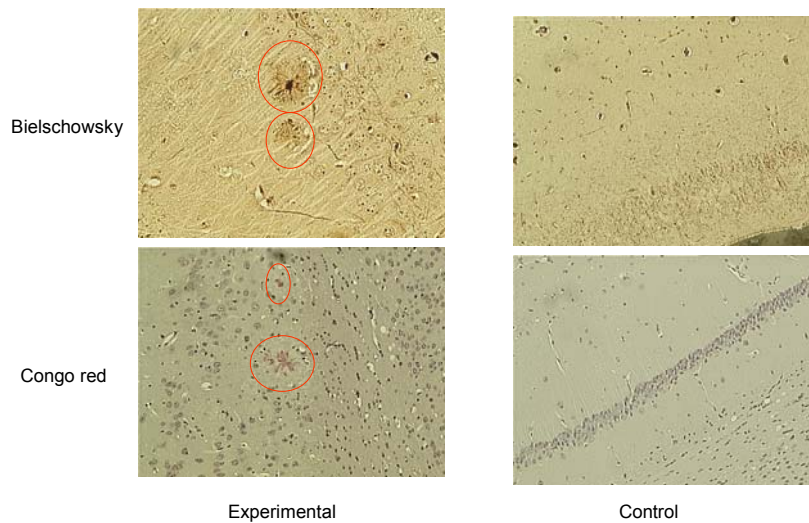
Triple transgenic histology

Fig. 18. Triple transgenic histology. The left panels represent positive amyloid plaques, found by Bielschowsky (top) and Congo red (bottom) stains. The right panels represent control brain slices, and are therefore, negative for Bielschowsky and Congo red.

Hippocampal pathology in 3xTg
Bielschowsky Stain
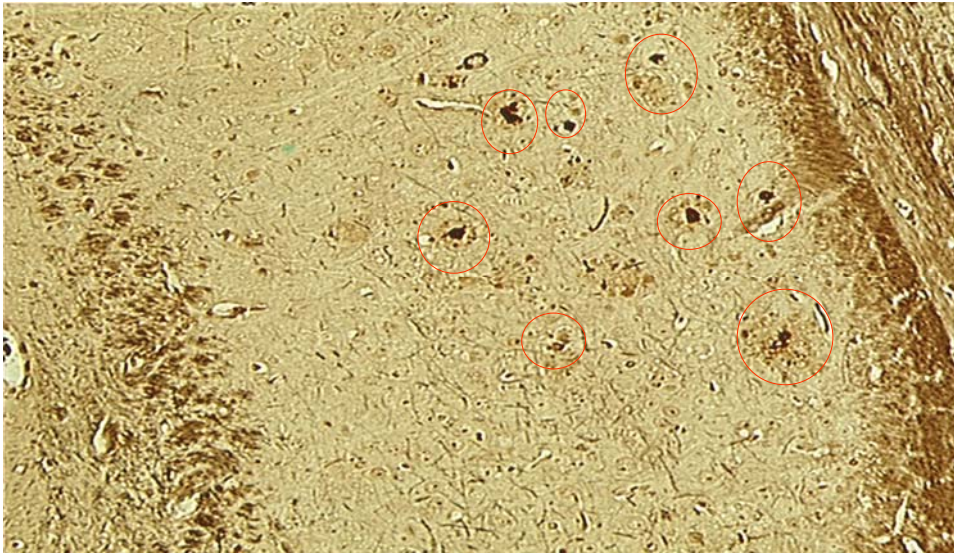
Fig, 19. Bielschowsky stain representing positive AD pathology in the hippocampus of a triple transgenic (APP/PS1/Tau) mouse.

Cu²⁺ staining of aggregates in 3xTg (APP/PS1/Tau) mouse
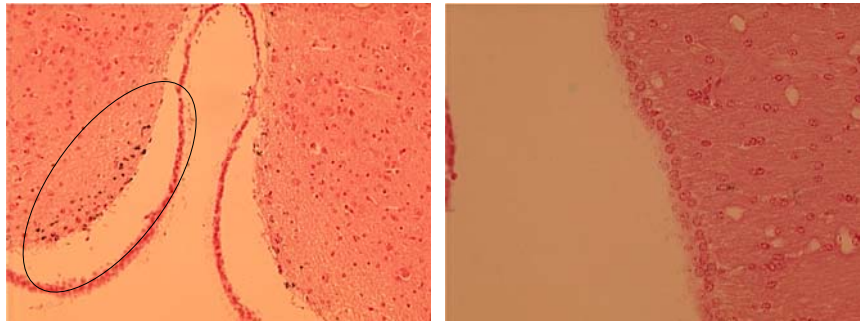
Transgenic brain   Control brain

5μm slice at level of fourth ventricle

Fig. 20. Cu^{2+} histological stain of AD 3xTg and control brain slices, at the level of the fourth ventricle. The positive copper stain in the transgenic mouse validates the AD neuropathology.

Fe^{3+} staining in 3xTg mouse
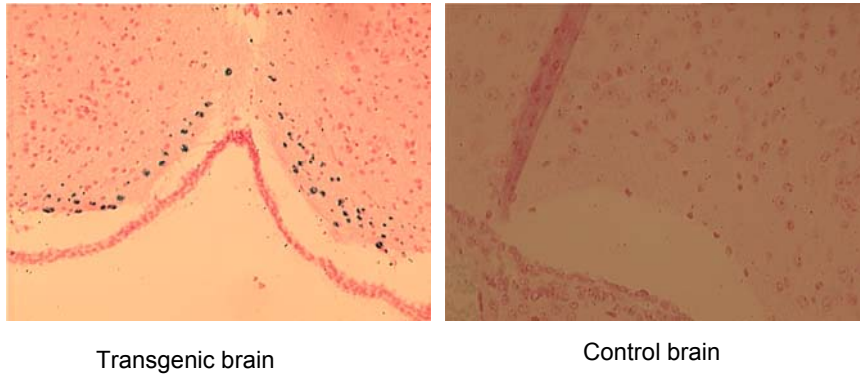

Transgenic brain   Control brain

5µm slice at level of fourth ventricle

Fig. 21. Fe^{3+} histological stain of AD 3xTg and control brain slices, at the level of the fourth ventricle. In addition to the positive copper stain (Fig. 24), the positive iron stain in the transgenic mouse further validates the AD neuropathology.

7.2.4. Chapter Seven Appendix (13)

Appendix 13. *IN VIVO* AUTORADIOGRAPHS of AD TRANSGENIC MICE

^{125}I CQ BCA NPs
1 hr post injection

9 mo control   12 mo Russell
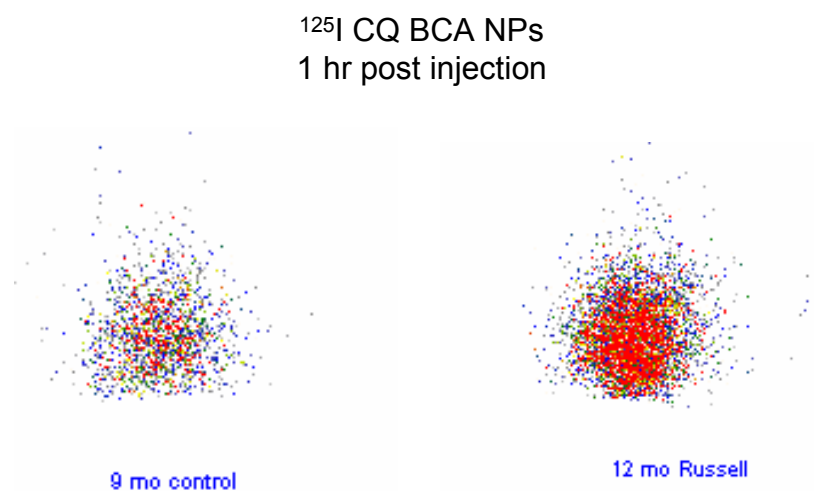
Fig. 41. ^{125}ICQ BCA NPs administered to AD transgenic (TgB) and control mice (Control B). The transgenic mouse has a significantly greater brain uptake of the nanoparticles, versus the control mouse. Increased brain uptake in the AD transgenic mouse indicates the presence of amyloid.
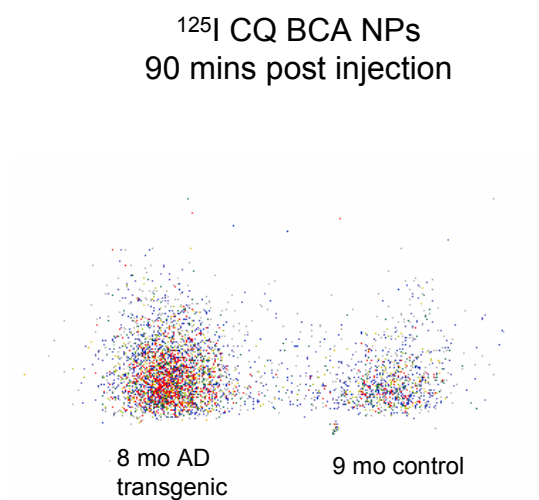
Fig. 42. ^{125}ICQ BCA NPs administered to AD transgenic (8 mo. Russell) and control mice (9 mo. Control A). The AD transgenic mouse has a significantly greater brain uptake of the ^{125}ICQ BCA NPs, as compared to the age-matched control mouse.
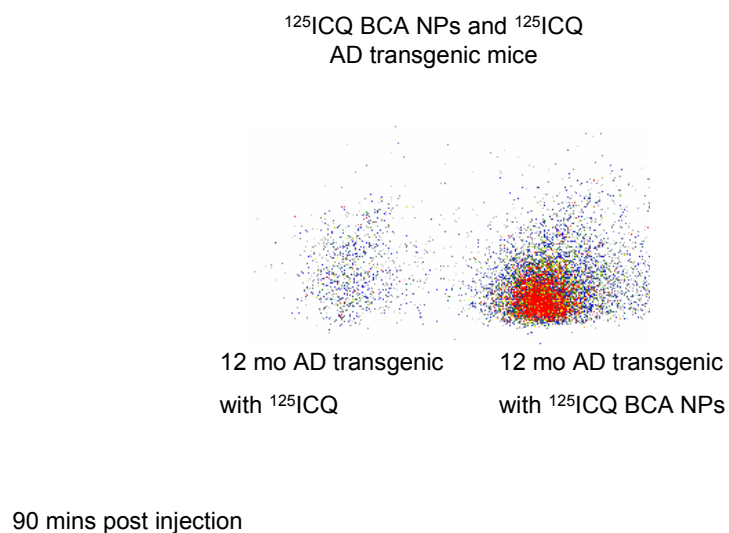
Fig. 43. ^{125}ICQ BCA NPs and ^{125}ICQ administered to AD transgenic mice. The transgenic mice have a significantly greater brain uptake of ^{125}ICQ BCA NPs, versus 125ICQ. **Therefore, the nanoparticles enhance ^{125}ICQ localization in AD transgenic mice**.
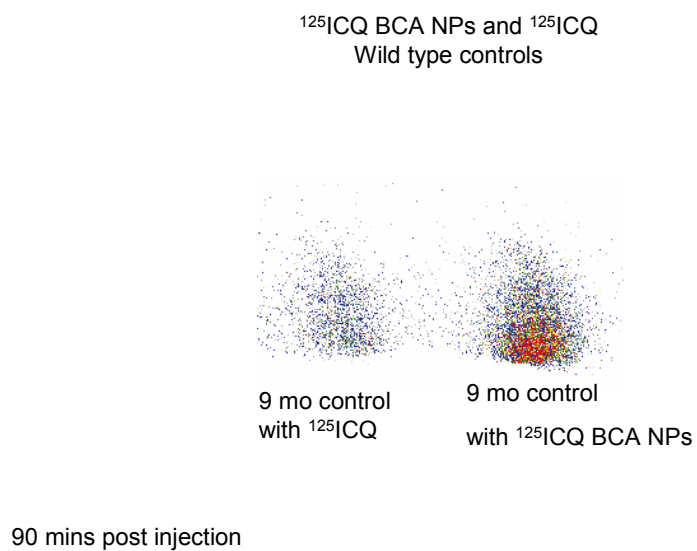
Fig. 44. ^{125}ICQ BCA NPs and ^{125}ICQ administered to wild type control mice. The control mice have a significantly greater brain uptake of the ^{125}ICQ BCA NPs. **Therefore, nanoparticles enhance BBB crossing of ^{125}ICQ in wild type mice.**

^{125}ICQ BCA NPs
AD transgenic mice

12 mo   9 mo
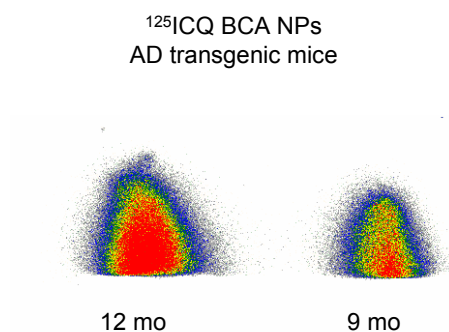
The brain uptake of 125ICQ BCA NPs is higher in the 12 mo versus
the 9 mo AD transgenic mouse; 60 mins post injection

Fig. 45. ^{125}ICQ BCA NPs administered to AD transgenic mice, aged 9 and 12 months old. This image shows a greater brain uptake of the nanoparticles in 12 month old mouse, versus the 9 month old mouse.
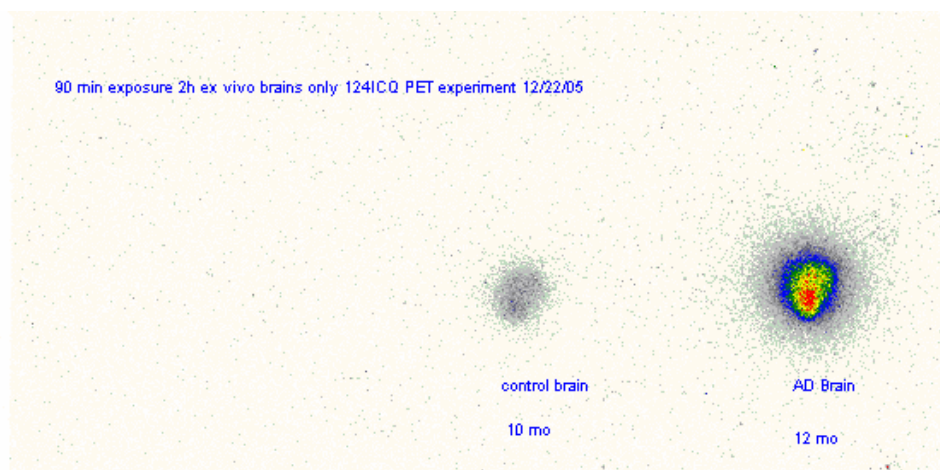
Fig. 46. *Ex vivo* autoradiograph of AD transgenic and control brains administered [124]ICQ by IV administration. *Note the area of localized activity in the AD transgenic brain.*
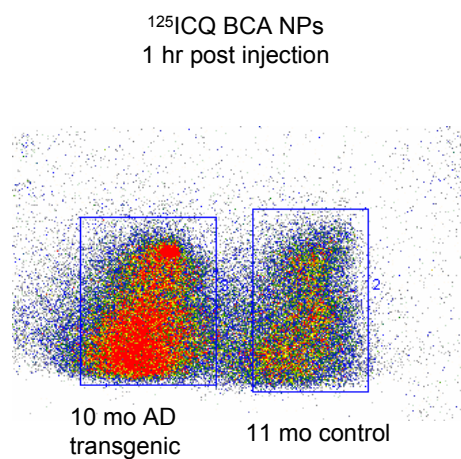
Fig. 47. [125]ICQ BCA NPs administered to AD transgenic and control mice. The transgenic mouse has a significantly greater brain uptake of the nanoparticles, versus the control mouse.

AD transgenic mice injected with ^{125}ICQ BCA NPs and ^{125}ICQ

AD transgenic mouse with
7.56x10^5 CPM ^{125}ICQ BCA NPs

AD transgenic mouse with
8.06x10^5 CPM ^{125}ICQ
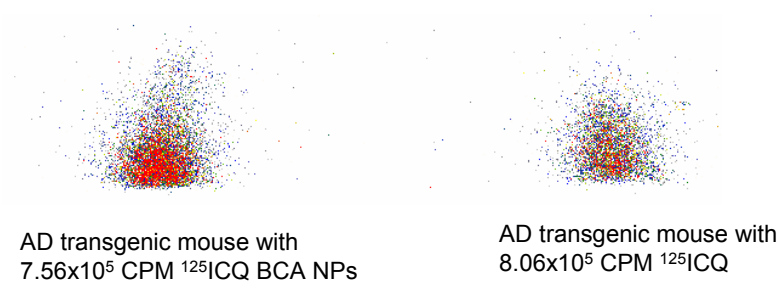
Mice aged 7 mo; 15 mins post injection

Fig. 48. ^{125}ICQ BCA NPs and ^{125}ICQ administered to commercially purchased AD transgenic mice. The AD transgenic mice have a greater brain uptake of the nanoparticles, as compared to the free ^{125}ICQ. **Therefore, nanoparticulate encapsulation of ^{125}ICQ enhances BBB crossing of the drug, in AD transgenic mice.**

AD transgenic mice injected with ^{125}ICQ BCA NPs
and ^{125}ICQ
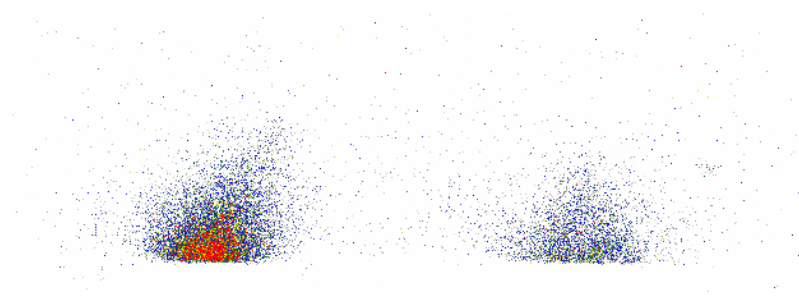
Mice aged 7 mo; 90 mins post injection

Fig. 49. ^{125}ICQ BCA NPs and ^{125}ICQ administered to commercially purchased AD transgenic mice. At 90 minutes post injection, the AD transgenic mice have a greater brain uptake of the nanoparticles (left), as compared to the free ^{125}ICQ (right). **Therefore, transgenic mice have a longer brain retention of the nanoparticles, as compared to the free drug.**

Commercial AD transgenic
10 mins post-injection of ^{125}ICQ BCA NPs

control   control   transgenic
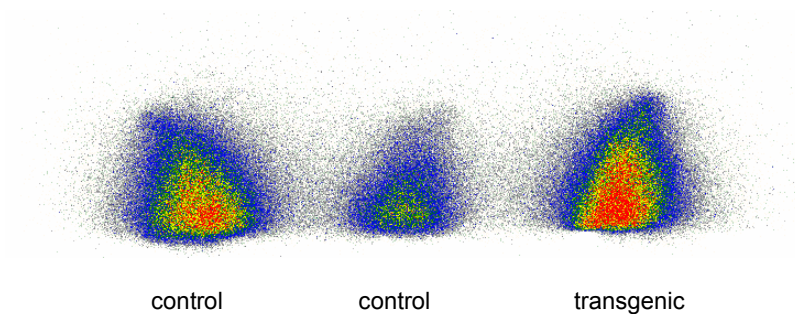
At ten minutes post injection of the nanoparticles, the AD transgenic
brain has a significantly greater brain uptake

Fig. 50. ^{125}ICQ BCA NPs administered to commercially purchased transgenic and control mice. The AD transgenic mouse has the highest brain uptake of the nanoparticles.

125ICQ BCA NPs
Triple transgenic mouse model

3xTg AD   control
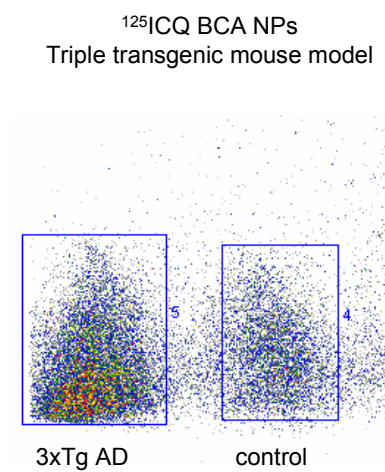
Mice aged 12 mo; 1 hr post injection

Fig. 51. *In vivo* brain image of 125ICQ BCA NP uptake of AD triple transgenic (APP/PS1/Tau) and control mice. At one hour post injection, the AD triple transgenic (left) mouse had the highest brain uptake of the nanoparticles.

Summary & Conclusions

Derivatives of cyanoacrylate monomers were polymerized into nanoparticles to deliver amyloid affinity drugs across the blood brain barrier in amyloid bearing mice, and in wild type littermates. Initially, an 8-length carbon chain (the octylcyanoacrylate derivative, OCA) and a 4-length carbon chain (the butylcyanoacrylate, BCA) were polymerized and encapsulated with the ^{125}I radioisotope [^{125}I]dU. The radio-encapsulated polymers or the [^{125}I]dU free drug were administered by venous injection to wild type control mice for *in vivo* biodistribution. Both polymer derivatives delivered the [^{125}I]dU to the brains of the wild type controls. In fact, the mice had a greater brain uptake (%ID/g) of both cyanoacrylate derivatives, compared to the brain uptake of [^{125}I]dU, when administered as a free drug. The mice that received the octylcyanoacrylates had the greatest brain uptake of the [^{125}I]dU, however, the synthesis of octylcyanoacrylate nanoparticles was not reproducible. Therefore, the butylcyanoacrylate derivative was chosen as the prototype nanoparticle. The BCA nanoparticles had a rapid brain upake and clearance form the normal brain.

Butylcyanoacrylate nanoparticles were synthesized with a mean diameter of 45nm, as shown by Dynamic Light Scattering. Polymerization was achieved with the optimum concentrations of the stabilizer (Dextran 70,000), surfactant (Tween-80), and the acid solvent (HCl). For example, the smallest sized particles

202

were obtained when both the surfactant and stabilizer concentrations were each at 1% of the volume of solution. The smallest sized particles were also obtained when the pH of solution was 1. Each criterion is important for a number of reasons. For example, nanoparticles do not polymerize without the presence of a steric stabilizer. Secondly, the surfactant is essential because it forms the micellar shell into which the polymer chain grows. The surfactant also has other important duties. It lowers the surface tension of the micelles in solution, thereby allowing the monomer into the micellar shell, it prevents aggregation of the nanoparticles in solution, and it increases the lipophilicity of the particles. Lipophilic nanoparticles have an increased chance of crossing the Blood Brain Barrier (BBB). In fact, it was found that nanoparticles, whose surfaces were not coated by surfactant, did not significantly cross the BBB of wild type mice. Scanning and Transmission Electron Microscopy verified that the butylcyanoacrylate nanoparticles had a spherical morphology and a uniform distribution in solution.

The nanoparticles were polymerized with the steric stabilizer Polyethylene Glycol (PEG) to increase the circulatory time of particles in the *in vivo* system. When these PEGylated nanoparticles were introduced to the wild type mice by venous injection, the spleen and liver had a decreased uptake (%ID/g organ) of the nanoparticles, compared to the organ uptakes of NPs polymerized with Dextran-70. Therefore, the nanoparticles had a decreased recognition by the Reticuloendothelial System (RES); however, decreased recognition by the RES

did not correlate with an increased brain uptake of the PEGylated nanoparticles. Thus, Dextran-70 was chosen as the standard stabilizer in the nanoparticle polymerizations.

In an effort to show that amyloid affinity drugs could be encapsulated within the matrices of butycyanoacrylates, the nanoparticles were polymerized with common histological dyes, namely Thioflavin-S (ThS), Thioflavin-T (ThT) and Congo red (CR). Dynamic Light Scattering of the dye encapsulated nanoparticles showed that loading of the dyes (0.1 %) did not appreciably increase the radii of the nanoparticles. The *in vitro* effect of uploading the drugs should not appreciably impact the *in vivo* effect of percentage brain uptake. Therefore, the BCA NPs maintained stability upon drug loading in the *in vitro* system.

Amyloid affinity dyes are charged molecules, and so, a caveat to their encapsulation within BCA NPs is that they do not significantly cross the BBB. The dye encapsulated NPs were, thus, used only as an *in vitro* demonstration that drugs with an affinity for amyloid plaques could be encapsulated within the matrix of the nanoparticles. The dye encapsulated nanoparticles were not used in the *in vivo* system.

Amyloid plaques are overloaded with redox active ions, namely Cu^{2+} and Fe^{3+}. The Cu/Fe chelator Clioquinol (CQ) was chosen as the prototype amyloid affinity drug because it freely crosses the BBB and it associates with the metals

found in the plaques. The CQ was radiolabelled with ^{125}I to quantitatively test the labeling efficiency of the drug *in vitro*, and to test the distribution of the drug in the *in vivo* system.

In vitro labeling studies showed that ^{125}ICQ labeled human post-mortem AD brain homogenates and paraffin-fixed slices with a greater efficiency than the labeling of control brain homogenates and slices. When the ^{125}ICQ was encapsulated within BCA NPs, the same trend was true. *In vivo* biodistribution studies in the wild type mouse showed that ^{125}ICQ crosses the BBB, however, the brain uptake of the drug was minimal (%ID/g was 1, at two minutes). Therefore, nanoparticles were chosen as drug delivery agents to enhance the brain uptake of ^{125}ICQ. The butylcyanoacrylates delivered the ^{125}ICQ to the brains of wild type mice at a %ID/g of 2.3 (at two minutes). Thus, encapsulation of ^{125}ICQ into BCA NPs enhanced the brain uptake of the drug. Likewise, ^{125}ICQ brain retention was longest in transgenic mice that received the drug encapsulated within the polymeric nanoparticles.

Experiments were designed with amyloid bearing mice to test the *in vivo* labeling efficiency of ^{125}ICQ. In the first design, wild type mice were intracranially injected with the aggregated Aβ_{42} peptide, and challenged with a maze test to study the cognitive effects of the peptide. These artificially produced mice did not show any signs of cognitive decline when compared to normal mice that were not injected with the aggregated peptide. The artificial Aβ_{42} mice were

typically challenged through the maze before the injection of the peptide, and again at 3 and 7 days post surgery. They were sacrificed after seven days, and thus, the life span of the disease may have been too short to properly assess the challenge of the maze on the cognitive behavior, namely the working spatial memory (short term memory).

However, the $A\beta_{42}$ mice were imaged by *in vivo* autoradiography, and it was found that the experimental mice experienced a greater brain labeling efficiency by the ^{125}ICQ when it was encapsulated within the polymeric nanoparticles, as opposed to the brain labeling by the free ^{125}ICQ. The labeling efficiency of the ^{125}ICQ was also greater in the experimental mice, versus control mice (no amyloid). The assumption was that the brains of the $A\beta_{42}$ mice had the greatest labeling by ^{125}ICQ because of the presence of the aggregated peptide.

The artificially produced $A\beta_{42}$ mice were sacrificed for neurohistology. Positive Congo red stains of harvested brain slices verified the presence of the aggregated peptide throughout the brain space, and most importantly, in the hippocampus. The hippocampus is of extreme importance because this is the origin of AD in human subjects. In addition, hippocampal brain slices were stained for the presence of metal ions to correlate the interaction of CQ with the peptide; aggregated amyloid deposits were found in relation to positive deposits of Fe^{3+} on Prussian blue stains. The stains were negative in the control brain

slices. Thus, the mechanism of CQ interaction with the peptide is via metal association, in artificially produced $A\beta_{42}$ mice.

In the second experimental design, the radiolabel was administered to AD transgenic mice as a free drug (^{125}ICQ), and as the drug encapsulated within polymeric nanoparticles (^{125}ICQ BCA NPs). *In vivo* auto radiography verified the labeling efficiency of ^{125}ICQ in the transgenic system. Double transgenic mice, mutant for the APP and PS1 transgenes, had a greater radiolabelling efficiency by ^{125}ICQ when it was encapsulated within the matrix of the nanoparticles. For example, brain washout of the free ^{125}ICQ was experienced in the control mice by 90 minutes post-injection of the drug. However, brain *retention* of ^{125}ICQ was experienced by the transgenic mice when the radiolabel was encapsulated within the nanoparticles. Therefore, the NPs enhanced retention of ^{125}ICQ in the AD transgenic mouse model, presumably due to the presence amyloid plaques. Finally, imaging of the amyloid plaques was also demonstrated in the APP/PS1 mouse model by *ex vivo* autoradiography, using ^{124}ICQ.

The APP/PS1 transgenic mice were sacrificed for histology. Cortical and hippocampal brain slices harvested from these animals were positive for Congo red, which denoted the presence of amyloid. In addition, harvested slices were also positive for Prussian blue, denoting the presence of Fe^{3+}. The stains were negative in the control brain slices. The amyloid was found in association with the iron; thus, the mechanism of CQ interaction was correlated to the relationship

between the plaques and endogenous metals. Finally, the cognitive behavioral skills of the APP/PS1 AD transgenic mice were challenged using a Y maze. It was found that 5 month old AD transgenic mice had the equivalent short term memory of 18 month old wild type mice.

Lastly, triple transgenic mice, mutant for the APP, PS1 and Tau transgenes, were imaged by *in vivo* autoradiography after intravenous administration of ^{125}ICQ BCA NPs. The labeling efficiency of the ^{125}ICQ was greatest in the experimental mouse, compared to the littermate control, presumably because of the AD pathology. Finally, the labeling efficiency of the ^{125}ICQ was greater in the double transgenic mice, as compared with the triple transgenic mice. These labeling differences may be due to a greater amyloid burden in the double transgenic mouse model.

The triple transgenic and control mice were sacrificed for histology to verify the presence of the amyloid plaques. In the transgenic mouse, a Bielschowsky stain denoted the presence of amyloid plaques and neurofibrillary tangles, while a Congo red stain verified the presence of amyloid plaques. Both stains were negative in the control. In addition, the transgenic and control brain slices were stained for Fe^{3+} (with Prussian blue), and for Cu^{2+} (with Rubeanic acid). In the experimental mouse, amyloid deposits were found in association with deposits of both metals; therefore, CQ interaction with amyloid plaques is correlated with the chelator's affinity for Fe^{3+} and Cu^{2+}.

These results are extremely significant for the future prospects of *in vivo* imaging in Alzheimer's disease. The tight junctions of the BBB restricts the passage of many molecules into the brain parenchyma, however, polymeric nanoparticles freely cross the BBB and deliver imaging agents such as ^{125}ICQ, that only cross with a minimal passage. In addition to enhancing the BBB crossing of amyloid affinity drugs, the NPs also enhanced the brain retention of the drugs, thus providing a feasible platform for *in vivo* imaging. Imaging of the amyloid plaques was demonstrated in three mouse models using the ^{125}ICQ BCA NPs as an *in vivo* imaging vector. All *in vivo* imaging results were verified for the presence of amyloid by histology. The correlation of amyloid association with ^{125}ICQ, via metal interaction, was also verified by histology. Thus, ^{125}ICQ BCA NPs demonstrate an effective method of *in vivo* and *ex vivo* detection of amyloid plaques in mouse models of Alzheimer's disease.

BIBLIOGRAPHY

1.   Gutman, R., G. Peacock, and D. Lu, *Targeted drug delivery for brain cancer treatment.* J Contr Rel, 2000. **65**: p. 31-41.

2.   Zhuang, Z., et al., *Radioiodinated styrylbenzenes and thioflavins as probes for amyloid aggregates.* J Med Chem, 2001. **44**: p. 1905-1914.

3.   Smith, Q., *A review of blood brain barrier transport techniques.* The Blood Brain Barrier: Biology and Research Protocols, ed. S. Sag. Vol. 89. 2003, Totowa, NJ: Humana Press, Inc. 193-205.

4.   Huang, X., et al., *The AB peptide of Alzheimer's disease directly produces hydrogen peroxide through metal ion reduction.* Biochemistry, 1999. **38**: p. 7609-16.

5.   Ritchie, C., et al., *Metal-protein attenuation with iodochlorhydorxyquin (clioquinol) targeting AB amyloid deposition and tozicity in Alzheimer disease.* Arch Neurol, 2003. **60**: p. 1685-1691.

6.   Olson, M. and C. Shaw, *Presenile dementia and Alzheimer's disease in mongolism.* Brain, 1969. **92**: p. 147.

7.   Selkoe, D.J., *Alzheimer's Disease.* Physiol Rev, 2001. **81**(2): p. 741-766.

8.   Patrick, G.N., et al., *Conversion of p35 to p25 deregulates Cdk5 activity and promotes neurodegeneration.* Nature, 1999. **402**: p. 615-622.

9.   Terry, R.D., et al., *Senile dementia of the Alzheimer type without neocortical neurofibrillary tangles.* J Neuropath Exp Neurol, 1987. **46**: p. 262-268.

10.   Hansen, L.A., et al., *Plaque-only Alzheimer disease is usually the Lewy body variant, and vice versa.* J Neuropath Exp Neurol, 1993. **52**: p. 648-654.

11.   Oltersdorf, T., et al., *The Alzheimer amyloid precursor protein.* J Biol Chem, 1990. **265**: p. 4492-4497.

12.   Walter, J., et al., *Ectodomain phosphorylation of B-amyloid precursor protein at two distinct cellular locations.* J Biol Chem, 1997. **272**: p. 1896-1903.

13.   Slunt, H.H., et al., *Expression of a ubiquitous, cross-reactive homologue of teh mouse B-amyloid precursor proteing (APP).* J Biol Chem, 1994. **269**: p. 2637-2644.

14.   Selkoe, D.J., et al., *B-Amyloid precursor protein of Alzheimer disease occurs as 110-135 kilodalton membrane-associated proteins in neural and nonneural tissues.* Proc Natl Acad Sci USA, 1998. **85**: p. 7341-7345.

15.   Haas, C., A.Y. Hung, and D.J. Selkoe, *Processing of B-amyloid precursor protein in microglia and astrocytes favors a localization in internal vesicles over constitutive secretion.* J Neurosci, 1991. **11**: p. 3783-3793.

16. Esch, F.S., et al., *Cleavage of amyloid B-peptide during constitutive processing of its precursor.* Science, 1990. **248**: p. 1122-1124.

17. Seubert, P., et al., *Secretion of B-amyloid precursor protein cleaved at the amino-terminus of the B-amyloid peptide.* Nature, 1993. **361**: p. 260-263.

18. Haas, C., et al., *Amyloid B-peptide is produced by cultured cells during normal metabolism.* Nature, 1992. **359**: p. 322-325.

19. Sisodia, S.S., et al., *Evidence that B-amyloid protein in Alzheimer's disease is not derived by normal processing.* Science, 1990. **248**: p. 492-495.

20. Selkoe, D.J., *Translating cell biology into therapeutic advances in Alzheimer's disease.* Nature, 1999. **399**: p. A23-A31.

21. Perez, R.G., et al., *Mutagenesis identifies new signals for B-amyloid precursor protein endocytosis, turnover and the generation of secreted fragments, including A42.* J Biol Chem, 1999. **274**: p. 18851-18856.

22. Scheuner, D., et al., *Secreted amyloid B-protein similar to that in the senile plaques of Alzheimer's disease is increased in vivo by the presenilin 1 and 2 and APP mutations linked to familial Alzheimer's disease.* Nature Med, 1996. **2**: p. 864-870.

23. Motter, R., et al., *Reduction of beta-amyloid peptide 42 in the cerebrospinal fluid of patients with Alzheimer's disease.* Ann neurol, 1995. **38**: p. 643-648.

24. Yamazaki, T., D.J. Selkoe, and E.H. Koo, *Trafficking of cell surface B-amyloid precursor protein: retrograde and transcytotic transport in cultured neurons.* J Cell Biol, 1995. **129**: p. 431-442.

25. Lemere, C.A., et al., *Sequence of deposition of heterogeneous amyloid B-peptides and Apo E in Down syndrone.* Neurobiol Dis, 1996. **3**: p. 16-32.

26. Sherrington, R., et al., *Cloning of a novel gene bearing missense mutations in early onset familial Alzheimer disease.* Nature, 1995. **375**: p. 754-760.

27. Levy-Lahad, E., et al., *Candidate gene for the chromosome 1 familial Alzheimer's disease locus.* Science, 1995. **269**: p. 973-977.

28. Hardy, J., *The Alzheimer family of diseases.* Proc Natl Acad Sci USA, 1997. **94**: p. 2095-2097.

29. Strittmatter, W.J., et al., *Apolipoprotein E: high-avidity binding to B-amyloid and increased frequency of type 4 allele in late-onset familial Alzheimer disease.* Proc Natl Acad Sci USA, 1993. **1993**: p. 1977-1981.

30. Corder, E.H., et al., *Protective effect of apolipoprotein E type 2 allele for late onset Alzheimer's disease.* Nature Genet, 1994. **7**: p. 180-184.

31. Betram, L., et al., *Evidence for genetic linkage of Alzheimer's disease to chromosome 10q.* Science, 2001.

32. Blacker, D., et al., *Alpha-2 macroglobulin is genetically associated with Alzheimer disease.* Nature Genet, 1998. **19**: p. 357-360.

33. Pericak-Vance, M.A., et al., *Evidence for a new locus on chromosome 12.* J. A. M. A., 1997. **278**: p. 1237-1241.

34. Tomita, T., et al., *The presenilin 2 mutation (N141I) linked to familial Alzheimer disease (Volga German families) increases the secretion of amyloid B protein ending at the 42nd (or 43rd) residue.* Proc Natl Acad Sci USA, 1997. **94**: p. 2025-2030.

35. Duff, K., et al., *Increased amyloid B42(43) in brains of mice expressing mutant presenilin 1.* Nature, 1996. **383**: p. 710-713.

36. Holcomb, L., et al., *Accelerated Alzheimer-type phenotype in transgenic mice carrying both mutant amyloid precursor protein and presenilin 1 transgenes.* Nature Med, 1998. **4**: p. 97-100.

37. Lemere, C.A., et al., *The E280A presenilin 1 Alzheimer mutation produces increased AB42 deposition and severe cerebellar pathology.* Nature Med, 1996. **2**: p. 1146-1150.

38. Gearing, M., H. Mori, and S.S. Mirra, *AB-peptide length and apolipoprotein E genotype in Alzheimer's disease.* Ann neurol, 1996. **39**: p. 395-399.

39. Namba, Y., et al., *Apolipoprotein E immunoreactivity in cerebral deposits and neurofibrillary tangles in Alzheimer's disease and kuru plaque amyloid in Creutzfeldt-Jacob disease.* Brain Res, 1991. **541**: p. 163-166.

40. Polvikoski, T., et al., *Apolipoprotein E, dementia, and cortical deposition of B-amyloid protein.* N. Engl. J. Med., 1995. **333**: p. 1242-1247.

41. Ma, J., et al., *The amyloid associated proteins alpha-1 antichymotrypsin and apolipoprotein E promote the assemply of teh Alzheimer B-protein into filaments.* Nature, 1994. **372**: p. 92-94.

42. Bales, K.R., et al., *Lack of apolipoportein E dramatically reduces amyloid B-peptide deposition.* Nature Genet, 1997. **17**: p. 263-264.

43. Holtzman, D.M., et al., *Expression of human apolipoprotein E reduces amyloid-beta deposition in a mouse model of Alzheimer's disease.* J Clin Invest, 1999. **103**: p. R15-R21.

44. Gouras, G.K., et al., *Intraneuronal AB42 accumulation in human brain.* Am J Pathol, 2000. **156**: p. 15-20.

45. Iwatsubo, T., et al., *Visualization of A beta 42(43) and A beta 40 in senile plaques with end-specific A beta monoclonals.* Neuron, 1994. **13**: p. 45-53.

46. Harper, J.D., et al., *Observation of metastable AB amyloid protofibrils by atomic force microscopy.* Chem Biol, 1997. **4**: p. 119-125.

47. Hsia, A.Y., et al., *Plaque-independent disruption of neural circuits in Alzheimer's disease mouse models.* Proc Natl Acad Sci USA, 1999. **96**: p. 3228-3233.

48. Itagaki, S., et al., *Relationship of microglia and astrocytes to amyloid deposits of Alzheimer disease.* J Neuroimmunol, 1989. **24**: p. 173-182.

49. Rogers, J., et al., *Complement activation by B-amyloid in Alzheimer disease.* Natl Acad Sci USA, 1992. **89**: p. 10016-10020.

50. Griffin, W.S.T., et al., *Brain interleukin 1 and S-100 immunoreactivity are elevated in Down syndrome and Alzheimer disease.* Proc Natl Acad Sci USA, 1989. **86**: p. 7611-7615.

51. Abraham, C.R., D.J. Selkoe, and H. Potter, *Immunochemical identification of the serine protease inhibitor, alpha-1-antichymotrypsin in the brain amyloid deposits of Alzheimer's disease.* Cell, 1988. **52**: p. 487-501.

52. Behl, C., et al., *Hydrogen peroxide mediates amyloid B toxicity.* Cell, 1994. **77**: p. 817-827.

53. Harris, M.E., et al., *Direct evidence of oxidative injury produced by the Alzheimer's beta-amyloid peptide (1-40) in cultured hippocampal neurons.* Exp Neurol, 1995. **131**: p. 193-202.

54. Matson, M.P., et al., *B-Amyloid peptides destabilize calcium homeostasis and render human cortical neurons vulnerable to excitotoxicity.* J Neurosci, 1992. **12**: p. 379-389.

55. Bush, A.I., *Metal complexing agents as therapies for Alzheimer's disease.* Neurobiol of Aging, 2002. **23**: p. 1031-1038.

56. Atwood, C.S., et al., *Dramatic aggregation of Alzheimer AB by Cu(II) is induced by conditions representing physiological acidosis.* J Biol Chem, 1998. **273**: p. 12817-26.

57. Bush, A.I., et al., *A novel zinc (II) binding site modulates the function of the BA4 amyloid protein precursor of Alzheimer's disease.* J Biol Chem, 1993. **268**: p. 16109-12.

58. Hesse, L., et al., *The betaA4 amyloid precursor protein binding to copper.* FEBS Lett, 1994. **349**: p. 109-16.

59. Bush, A.I., et al., *Rapid induction of Alzheimer AB amyloid formation by zinc.* Science, 1994. **256**: p. 1464-7.

60. Yates, C.M., et al., *Enzyme activities in relation to pH and lactate in postmortem brain in Alzheimer-type and other dementia.* J Neurochem, 1990. **55**: p. 1624-30.

61. Moir, R.D., et al., *Differential effects of apolipoprotein E isoforms on metal-induced aggregation of AB using physiological concentrations.* Biochemistry, 1999. **38**: p. 4595-603.

62. Atwood, C.S., et al., *Characterization of copper interactions with Alzheimer AB peptides - identification of an attomolar affinity copper binding site on AB1-42.* J Neurochem, 2000. **75**: p. 1219-33.

63. Vaughan, D.W. and A. Peters, *The structure of neuritic plaques in the cerebral cortex of aged rats.* J Neuropathol Exp Neurol, 1981. **40**: p. 472-87.

64. Bush, A.I., et al., *Modulation of AB adhesiveness and secretase site cleavage by zinc.* J Biol Chem, 1994. **269**: p. 12152-8.

65. Curtin, C., et al., *Alzheimer's disease amyloid binds Cu and Zn to generate an allosterically-ordered membrane-penetrating structure containing SOD-like subunits.* J Biol Chem, 2001. **276**: p. 20466-73.

66. Cherney, R.A., et al., *Aqueous dissolution of Alzheimer's disease AB amyloid deposits by biometal depletion.* J Biol Chem, 1999. **274**: p. 23223-8.

67. Huang, X., M. Cuajungco, and C. Atwood, *Cu (II) potentiation of Alzheimer AB neurotoxicity.* J Biol Chem, 1999. **274**: p. 37111-37116.

68. Sayre, L.M., et al., *In situ oxidative catalysis by neurofibrillary tangles and senile plaques in Alzheimer's disease: a central role for bound transition metals.* J Neurochem, 2000. **74**: p. 270-9.

69. Nunomura, A., et al., *RNA oxidation is a prominent feature of vulnerable neurons in Alzheimer's disease.* J Neurosci, 1999. **19**: p. 1959-64.

70. Sayre, L.M., et al., *4-Hydroxynonenal-derived advanced lipid peroxidation end products are increased in Alzheimer's disease.* J Neurochem, 1997. **68**: p. 2092-7.

71. Smith, M.A., et al., *Oxidative damage in Alzheimer's disease.* Nature, 1996. **382**: p. 120-1.

72. Cuajungco, M.P., et al., *Evidence that the beta-amyloid plaques of Alzheimer's disease represent the redox-silencing and entombment of AB by zinc.* J Biol Chem, 2000. **275**: p. 19439-42.

73. Opazo, C., et al., *Metalloenzyme-like activity of Alzheimer's disease B-amyloid: Cu-dependent catalytic conversion of dopamine, cholesterol and biological reducing agents to neurotoxic H2O2.* J Biol Chem, 2002. **277**: p. 40302-8.

74. Lee, J.-Y., et al., *Contribution by synaptic zinc to the gender-disparate plaque formation in human Sweedish mutant APP trnasgenic mice.* Proc Natl Acad Sci USA, 2002. **99**: p. 7705-10.

75. Howell, G.A., M.G. Welch, and C.J. Frederickson, *Stimulation-induced uptake and release of zinc in hippocampal slices.* Nature, 1984. **308**: p. 736-8.

76. Hartter, D.E. and A. Barnea, *Brain tissue accumulates 67 copper by two ligand-dependent saturable processes.* J Biol Chem, 1988. **263**: p. 799-805.

77. Hartter, D.E. and A. Barnea, *Evidence for release of copper in the brain: depolarization-induced release of newly taken-up 67 copper.* Synapse, 1988. **2**: p. 412-5.

78. Frederickson, C.J., *Neurobiology of zinc and zinc-containing neurons.* Int Rev Neurobiol, 1989. **31**: p. 145-328.

79. Cole, T.B., et al., *Elimination of zinc from syaptic vesicles in the intact mouse brain by disruption of the ZnT3 gene.* Proc Natl Acad Sci USA, 1999. **96**: p. 1716-21.

80. Cherney, R.A., et al., *Treatment with a copper-zinc chelator markedly and ragidly inhibits B-amyloid accumulation in Alzheimer's disease transgenic mice.* Neuron, 2001. **30**: p. 665-76.

81. Lovell, M., et al., *Copper, iron and zinc in Alzheimer's disease senile plaques.* J Neurol Sci, 1998. **158**: p. 47-52.

82. Suh, S.W., et al., *Histological evidence implicating zinc in Alzheimer's disease.* Brain Res, 2000. **852**: p. 274-8.

83. Huang, X., et al., *Zinc-induced Alzheimer's AB1-40 aggregation is mediated by conformational factors.* J Biol Chem, 1997. **272**: p. 26464-70.

84. Wu, S.M., C.M. Boyer, and S.V. Pizzo, *The binding of receptor-recognized alpha2-macroglobulin to the low density lipoprotein receptor-related protein and the alpha2M signaling receptor is decoupled by oxidation.* J Biol Chem, 1997. **272**: p. 20627-35.

85. DeMattos, R.B., et al., *Peripheral anti-A beta antibody alters CNS and plasma A beta clearance and decreases brain A beta burden in a mouse model of Alzheimer's disease.* Proc Natl Acad Sci USA, 2001. **98**: p. 8850-5.

86. Yassin, M.S., et al., *Changes in uptake of vitamin B(12) and trace metals in brains of mice treated with clioquinol.* J Neurol Sci, 2000. **173**: p. 40-4.

87. Kontush, A., et al., *Amyloid-beta is an antioxidant for lipoproteins in cerebrospinal fluid and plasma.* Free Radic Biol Med, 2001. **30**: p. 119-28.

88. Duff, K. and F. Suleman, *Transgenic mouse models of Alzheimer's disease: How helpful have they been for therapeutic development?* Brief in Funct Genom Proteom, 2004. **3**: p. 47-59.

89. Sisodia, S.S., et al., *Cellular and molecular biology of Alzheimer's disease and animal models.* Neuroimaging Clin N Am, 1995. **5**: p. 59-68.

90. Link, C.D., *Transgenic invertebrate models of age-associated neurodegenerative diseases.* Mech Ageing Dev, 2001. **122**: p. 1639-1649.

91. Lamb, B.T., K.A. Bardel, and L.S. Kulnane, *Amyloid production and deposition in mutant amyloid precursor protein and presenilin-1 yeast artificial chromosome transgenic mice.* Nat Neurosci, 1999. **2**: p. 695-697.

92. Guo, Q., W. Fu, and B.L. Sopher, *Increased vulnerability of hippocampal neurons to excitotoxic necrosis in presenilin-1 mutant knock-in mice.* Nat Med, 1999. **5**: p. 101-106.

93. Duff, K., H. Knight, and L.M. Refolo, *Characterization of pathology in transgenic mice over-expressing human genomic and cDNA tau transgenes.* Neurobiol Dis, 2000. **7**: p. 87-98.

94. Games, D., D. Adams, and R. Alessandrini, *Alzheimer-type neuropathology in transgenic mice overexpressing V717F beta-amyloid precursor protein.* Nature, 1995. **373**: p. 523-527.

95. Chen, G., et al., *A learning deficit related to age and B-amyloid plaques in a mouse model of Alzheimer's disease.* Nature, 2000. **408**: p. 975-9.

96. Hsiao, K., P. Chapman, and S. Nilsen, *Correlative memory deficits, Abeta elevation, and amyloid plaques in transgenic mice.* Science, 1996. **274**: p. 99-102.

97. Calhoun, M.E., K.H. Wiederhold, and D. Abramowski, *Neuron loss in APP transgenic mice.* Nature, 1998. **395**: p. 755-6.

98. Chishti, M.A., D.S. Yang, and C. Janus, *Early-onset amyloid deposition and cognitive deficits in transgenic mice expressing a double mutant form of amyloid precursor protein 695.* J Biol Chem, 2001. **276**: p. 21562-21570.

99. Dodart, J.C., H. Mexiane, and C. Mathis, *Behavioral disturbances in transgenic mice overexpressing hte V717F beta-amyloid precursor protein.* Behav Neurosci, 1999. **113**: p. 982-990.

100. Morgan, D., et al., *AB peptide vaccination prevents memory loss in an animal model of Alzheimer's disease.* Nature, 2000. **408**: p. 982-5.

101. Borchelt, D.R., et al., *Accelerated Amyloid Deposition in the Brains of Transgenic Mice Coexpressing Mutant Presenilin 1 and Amyloid Precursor Proteins.* Neuron, 1997. **19**(4): p. 939-945.

102. Borchelt, D.R., et al., *Familial Alzheimer's Disease-Linked Presenilin 1 Variants Elevate A[beta]1-42/1-40 Ratio In Vitro and In Vivo.* Neuron, 1996. **17**(5): p. 1005-1013.

103. Janus, C., et al., *A[beta] peptide immunization reduces behavioural impairment and plaques in a model of Alzheimer's disease.* Nature, 2000. **408**(6815): p. 979-982.

104. Moechars, D., et al., *Expression in brain of amyloid precursor protein mutated in the alpha-secretase site causes disturbed behavior, neuronal degeneration and premature death in transgenic mice.* EMBO J, 1996. **15**: p. 1265-1274.

105. Moechars, D., K. Lorent*, and F. Van Leuven, *Premature death in transgenic mice that overexpress a mutant amyloid precursor protein is preceded by severe neurodegeneration and apoptosis.* Neuroscience, 1999. **91**(3): p. 819-830.

106. Dewachter, I., D. Reverse, and N. Caluwaerts, *Neuronal deficiency of presenilin 1 inhibits amyloid plaque formation and corrects hippocampal long-term potentiation but not a cognitive defect of amyloid precursor protein [V717I] transgenic mice.* J Neurosci, 2002. **22**: p. 3445-3453.

107. Wolfe, M.S., *Presenilin and gamma-secretase: Structure meets function.* J Neurochem, 2001. **76**: p. 1615-1620.

108. Holtzman, D.M., K.R. Bales, and T. Tenkova, *Apolipoprotein E isoform-dependent amyloid deposition and neuritic degeneration in a mouse model of Alzheimer's disease.* Proc Natl Acad Sci USA, 2000. **97**: p. 2892-2897.

109. Burns, M. and K. Duff, *Use of in vivo models to study the role of cholesterol in the etiology of Alzheimer's disease.* Neurochem Res, 2003. **28**: p. 979-986.

110. Yamamoto, A., et al., *Iron (III) induces aggregation of hyperphosphorylated tau and its reduction to iron (II) reverses the aggregation: implications in the formation of neurofibrillary tangles of Alzheimer's disease.* J Neurochem, 2002. **82**(5): p. 1137-47.

111. Ma, Q.F., et al., *Binding of copper (II) ion to an Alzheimer's tau peptide as revealed by MALDI-TOF MS, CD, and NMR.* Biopolymers, 2005. **79**(2): p. 74-85.

112. Gotz, J., A. Probst, and A. Spillantini, *Somatodendritic localization and hyperphosphorylation of tau protein in transgenic mice expressing the longest human brain tau isoform.* EMBO J, 1995. **14**: p. 1304-1313.

113. Lewis, J., et al., *Neurofibrillary tangles, amyotrophy and progressive motor disturbance in mice expressing mutant (P301L) tau protein.* Nat Gen, 2000. **25**: p. 402-5.

114. Andorfer, C., et al., *Hyperphosphorylation and aggregation of tau in mice expressing normal human tau isoforms.* J Neurochem, 2003. **86**: p. 582-90.

115. Lewis, J., et al., *Enhanced neurofibrillary degeneration intransgenic mice expressing mutant tau and APP.* Science, 2001. **293**: p. 1487-91.

116. Götz, J., et al., *Formation of neurofibrillary tangles in P301l tau transgenic mice induced by Abeta 42 fibrils.* Science, 2001. **293**: p. 1491-95.

117. Lau, L.F., et al., *Tau protein phosphorylation as a therapeutic target in Alzheimer's disease.* Curr Top Med Chem, 2002. **2**: p. 395-415.

118. Oddo, S., et al., *Triple-transgenic model of Alzheimer's disease with plaques and tangles: intracellular Abeta and synaptic dysfunction.* Neuron, 2003. **39**: p. 409-21.

119. Oddo, S., et al., *Amyloid deposition precedes tangle formation in a triple transgenic model of Alzheimer's disease.* Neurobiol of Aging, 2003. **24**: p. 1063-1070.

120. Hardy, J. and D. Selkoe, *The amyloid hypothesis of Alzheimer's disease: progress and problems on the road to therapeutics.* Science, 2002. **297**: p. 353-6.

121. DeKosky, S.T. and S.W. Scheff, *Synapse loss in frontal cortex biopsies in Alzheimer's disease: correlation with cognitive severity.* Ann Neurol, 1990. **27**(5): p. 457-64.

122. Skovronsky, D.M., et al., *In vivo detection of amyloid plaques in a mouse model of Alzheimer's disease.* Proc Natl Acad Sci U S A, 2000. **97**(13): p. 7609-14.

123. Okamura, N., et al., *Styrylbenzoxazole derivatives for in vivo imaging of amyloid plaques in the brain.* J Neurosci, 2004. **24**(10): p. 2535-41.

124. Higuchi, M., et al., *19F and 1H MRI detection of amyloid beta plaques in vivo.* Nat Neurosci, 2005. **8**(4): p. 527-33.

125. Klunk, W.E., et al., *Imaging brain amyloid in Alzheimer's disease with Pittsburgh Compound-B.* Ann Neurol, 2004. **55**(3): p. 306-19.

126. Klunk, W.E., et al., *Binding of the positron emission tomography tracer Pittsburgh compound-B reflects the amount of amyloid-beta in Alzheimer's disease brain but not in transgenic mouse brain.* J Neurosci, 2005. **25**(46): p. 10598-606.

127. Bacskai, B.J., et al., *Four-dimensional multiphoton imaging of brain entry, amyloid binding, and clearance of an amyloid-beta ligand in transgenic mice.* Proc Natl Acad Sci U S A, 2003. **100**(21): p. 12462-7.

128. Wadghiri, Y., et al., *Detection of Alzheimer's amyloid in transgenic mice using magnetic mice using magnetic resonance microimaging.* Mag Res Med, 2003. **50**: p. 293-302.

129. Vanhoutte, G., et al., *Noninvasive in vivo MRI detection of neuritic plaques associated with iron in APP[V717I] transgenic mice, a model for Alzheimer's disease.* Magn Reson Med, 2005. **53**(3): p. 607-13.

130. Vymazal, J., et al., *T1 and T2 of ferritin at different field strengths: effect on MRI.* Magn Reson Med, 1992. **27**(2): p. 368-74.

131. Hintersteiner, M., et al., *In vivo detection of amyloid-beta deposits by near-infrared imaging using an oxazine-derivative probe.* Nat Biotechnol, 2005. **23**(5): p. 577-83.

132. Reese, T. and M. Karnovsky, *Fine structural localization of a blood-brain barrier to exogenous peroxidase.* J Cell Biol, 1967. **34**: p. 207-217.

133. Nag, S., *Morphology and molecular properties of cellular componenets of normal cerebral vessels.* Methods in Molecular Medicine: The Blood Brain Barrier, ed. S. Nag. Vol. 89. 2003, Totowa, NJ: Humana Press. 1-34.

134. Yan, Q. and E. Sage, *Transforming growth factor-beta 1 induces apoptotic death in cultured retinal endothelial cells but not in pericytes: Association with decreased expression of p21 wafl/cip1.* J Cell Biochem, 1998. **70**: p. 70-83.

135. Hirshi, K. and P. D'Armore, *Control of angiogenesis by pericytes: molecular mechanisms and significance.* EXS, 1997. **79**: p. 419-428.

136. Johanson, C., *Permeability and vascularity of the developing brain: Cerebellum vs. cerebral cortex.* Brain Res, 1980. **190**: p. 3-16.

137. Pardridge, W., *Molecular biology of the blood-brain barrier.* Methods in molecular medicine: The blood brain barrier, ed. S. Nag. 2003, Totowa, NJ: Humana Press. 385-399.

138. Crone, C. and S. Olesen, *Electrical resistance of brain microvascular endothelium.* Brain Res, 1982. **241**: p. 49-55.

139. Krause, D., et al., *Correlation of zonua occludens ZO-1 antigen and transendothelial resistance in porcine and rat cultured cerebral endothelial cells.* Neurosci Lett, 1991. **128**: p. 301-304.

140. Smith, Q. and S. Rapoport, *Cerebrovascular permeability coefficients to sodium, potassium and chloride.* J Neurochem, 1986. **46**: p. 1732-1742.

141. Furuse, M., T. Hirase, and M. Ito, *Occludin: A novel integral membrane protein localizing at tight jucntions.* J Cell Biol, 1993. **123**: p. 1777-1788.

142. Wolburg, H. and A. Lippoldt, *Tight junctions of the blood-brain barrier: Development, composition and regulation.* Vasc Pharma, 2002. **38**: p. 323-337.

143. Wolburg, H., et al., *Localization of claudin-3 in tight junctions of the blood-brain barrier is selectively lost during experimental autoimmune encephalomyelitis and human glioblastoma multiforme.* Acta Neuropathol, 2003. **105**: p. 586-92.

144. Martin-Padura, I., S. Lostaglio, and M. Schneemann, *Junctional adhesion molecule, a novel member of the immunoglobulin superfamily that distributes at intercellular junctions and modulates monocyte transmigration.* J Cell Biol, 1998. **142**: p. 117-127.

145. Morita, K., et al., *Endothelial claudin: claudin-5/TMVCF constitutes tight junction strands in endothelial cells.* J Cell Biol, 1999. **147**: p. 185-194.

146. Mitic, L., C.v. Itallie, and J. Anderson, *Molecular physiology and pathophysiology of thight junctions.* Amer J Physiol Gastrointest Liver Physiol, 2000. **279**: p. G250-G254.

147. Furuse, M., et al., *Overexpression of occludin, a tight junction integral membrane protein, induces the formation of intracellular multilamellar bodies bearing tight junction-like structures.* J Cell Sci, 1996. **109**: p. 429-435.

148. Mitic, L. and J. Anderson, *Molecular artchitecture of tight junctions.* Annu Rev Physiol, 1998. **60**: p. 121-142.

149. Reichel, A., D. Begley, and N. Abbott, *An overview of in vitro techniques for blood brain barrier studies*, in *Methods in molecular medicine: The blood-brain barrier: Biology and research protocols*, S. Nag, Editor. 2003, Humana Press, Inc: Totowa, NJ. p. 307-325.

150. Ring, A., J. Weiser, and E. Tuomanen, *Pneumococcal trafficking across the blood brain barrier: Molecular analysis of a novel bidirectional pathway.* J Clin Invest, 1998. **102**: p. 347-360.

151. Pron, B., et al., *Interaction of Neisseria meningitidis with the components of the blood brain barrier correlates with an increased expression of PilC.* J Infect Dis, 1997. **176**: p. 1285-1292.

152. Neuwelt, E., *Mechanisms of disease: The blood brain barrier.* Neurosurgery, 2004. **54**: p. 131-141.

153. Huber, J., et al., *Inflammatory pain alters blood brain barrier permeablility and tight junctional protein expression.* Amer J Physiol, 2001. **280**: p. H1241-H1248.

154. Smith, Q., *Quantitation of blood-brain barrier permeability*, in *Implications of the blood brain barrier and its manipulation*, E. Neuwelt, Editor. 1989, Plenum Press: New York. p. 85-118.

155. Lee, G., et al., *Drug transporters in the central nervous system: brain barriers and brain parenchymal considerations.* Pharmacol Rev, 2001. **53**: p. 569-596.

156. Kabanov, A. and E. Batrakova, *New technologies for drug delivery across the blood brain barrier.* Curr Pharma Des, 2004. **10**: p. 1355-1363.

157. Kreuter, J., *Nanoparticles*, in *Encyclopedia of Pharma Tech*, J.B. J. Swarbrick, Editor. 1994, Marcel Dekker: New York. p. 165-190.

158. Agnihotri, S.A., N.N. Mallikaujuana, and T.M. Aminabhavi, *Recent advances on chitosan-based micro and nanoparticles in drug delivery.* J Contr Rel, 2001. **100**: p. 65-81.

159. Aminabhavi, T.M., et al., *Biodebradable polymeric nanoparticles as drug delivery devices.* J Contr Rel, 2001. **70**: p. 1-20.

160. Behan, N., C. Birkinshaw, and N. Clarke, *Poly n-butyl cyanoacrylate nanoparticles: A mechanistic study of polymerization and particle formation.* Biomat, 2001. **22**: p. 1335-1344.

161. Fessi, H., et al., *Nanocapsule formation by interfacial polymer deposition following solvent displacement.* Int J Pharm, 1989. **55**: p. R1-R4.

162. Gubha, S. and B. Mandal, *Dispersion polymerization of acrylamide.* J Colloid Interf Sci, 2004. **271**: p. 55-59.

163. Leroux, J., et al., *New approach for the preparation of nanoparticles by an emulsification-diffusion method.* Eur J Pharm Biopharm, 1995. **41**: p. 14-18.

164. Li, Y., et al., *PEGylated polycyanoacrylate nanoparticles as tumor necrosis factor-alpha carriers.* J Contr Rel, 2001: p. 287-296.

165. Lobenberg, R., et al., *Body distribution of azidothymidine bound to hexyl-cyanoacrylate nanoparticles after i.v. injection to rats.* J Contr Rel, 1998. **50**: p. 21-30.

166. Murakami, H., et al., *Preparation of poly(D,L-lactide-co-glycolide) latex for surface modifying material by a double coacervation method.* Proced Intern Symp Control Rel Bioact Mater, 1996. **23**: p. 361-362.

167. Niwa, T., et al., *Preparations of biodegradable nanospheres of water-soluble and insoluble drugs with D,L-lactide / glycolide copolymer by a novel spontaneous emulsification solvent diffusion method and the drug release behavior.* J Contr Rel, 1993. **25**.

168. Peracchia, M., et al., *PEGylated nanoparticles from a novel MePEGcyanoacrylate hexadecylcyanoacrylate amyphiphilic copolymer.* Pharm Res, 1998. **15**: p. 548-554.

169. Quintanar, G., et al., *Influence of the stabilizer coating layer on the purification and freexe drying of poly (D,L-lactic acid) nanoparticles prepared by the emulsification-diffusion technique.* J Microencap, 1998. **15**: p. 107-119.

170. Scholes, P., et al., *The preparation of sub-500 nm poly(lactide-co-glycolide) microspheres for site-specific drug delivery.* J Contr Rel, 1993. **25**: p. 145-153.

171. Wehrle, P., P. Magenheim, and S. Benita, *Influence of process parameters on the PLA nanoparticle size distribution evaluated by means of factorial design.* J Pharm Biopharm, 1995. **41**: p. 19-26.

172. Zambaux, M., et al., *Influence of experimental paramenters on the characteristics of poly(lactic acid) nanoparticles prepared by double emulsion method.* J Contr Rel, 1998. **50**: p. 31-40.

173. Kreuter, J., *Nanoparticulate systems for brain delivery of drugs.* Adv Drug Del Rev, 2001. **47**: p. 65-81.

174. Kreuter, J., et al., *Passage of peptides through the blood brain barrier with collodial polymer particles (nanoparticles).* Brain Res, 1995. **674**: p. 171-174.

175. Schroeder, U., P. Sommerfeld, and B. Sabel, *Efficacy of oral dalargin-loaded nanoparticle delivery across the blood brain barrier.* Peptides, 1998. **19**: p. 777-780.

176. Schroeder, U., B. Sabel, and H. Schroeder, *Diffusion enhancement of drugs by loaded nanoparticles in vitro.* Prog Neuro Psychopharmacol Bio Psychiat, 1999. **23**: p. 941-949.

177. Vauthier, C., et al., *Drug delivery to resistant tumors: the potential of poly(alkyl cyanoacrylate) nanoparticles.* J Contr Rel, 2003. **93**: p. 151-160.

178. Munk, P. and T.M. Aminabhavi, *Introduction to macromolecular science.* 2002, New York: John Wiley & Sons, Inc. 95-164.

179. Cui, Z., et al., *Novel D-penicillamine carrying nanoparticles for metal chelation therapy in Alzheimer's and other CNS diseases.* Eur J Pharm Biopharm, 2005. **59**: p. 263-272.

180. Hartig, W., et al., *Electron microscopic analysis of nanoparticles delivering thioflavin-T after intrahippocampal injection in mouse: implications for tafrgeting b-amyloid in Alzheimer's disease.* Neurosci Lett, 2003. **338**: p. 174-176.

181. Dong, J., et al., *Metal binding and oxidation of amyloid-beta within isolated senile plaque cores: Raman microscopic evidence.* Biochemistry, 2003. **42**: p. 2768-2773.

182. Roney, C., et al., P. communication, Editor.

183. Koziara, J., et al., *In situ blood brain barrier transport of nanoparticles.* Pharm Res, 2003. **20**: p. 1772-1778.

184. Klunk, W.E., et al., *Uncharged thioflavin-T derivatives bind to amyloid-beta protein with high affinity and readily enter the brain.* Life Sci, 2001. **69**(13): p. 1471-84.

185. Ahi, J., J. Radulovic, and J. Spiess, *The role of hippocampal signaling cascades in consolidation of fear memory.* Behav Brain Res, 2004. **149**(1): p. 17-31.

186. Blank, T., et al., *Priming of long-term potentiation in mouse hippocampus by corticotropin-releasing factor and acute stress: implications for hippocampus-dependent learning.* J Neurosci, 2002. **22**(9): p. 3788-94.

187. Maurice, T., B.P. Lockhart, and A. Privat, *Amnesia induced in mice by centrally administered beta-amyloid peptides involves cholinergic dysfunction.* Brain Res, 1996. **706**(2): p. 181-93.

VITAE

Celeste Anita Roney was born in Augusta, Georgia, on September 16, 1977, the daughter of Carrie Winfrey Roney and Claude Roscoe Roney, Sr. After completing her work at Redan High School, Stone Mountain, Georgia in 1995, she entered Spelman College at Atlanta, Georgia. She received the degree of Bachelor of Science with a major in Chemistry from Spelman in May, 1999. During the following year she entered Harvard University at Cambridge, Massachusetts, where she took additional courses in biology. In February, 2001 she entered the Graduate School of Biomedical Sciences at the University of Texas Southwestern Medical Center at Dallas. She was awarded the degree of Doctor of Philosophy in Radiological Sciences in 2006. She hopes to pursue a career as a physician-scientist.

Permanent Address: 4207 Bowser Avenue
                     Apartment 205
                     Dallas, Texas 75219